A numerical study of peristaltic flow

By

MinSu Yun

Submitted for the degree of

Master of Engineering (Research)

Faculty of Engineering and Information Technology

University of Technology, Sydney (UTS)

Australia

2009

CERTIFICATE

I certify that this thesis has not already been submitted for any degree and is not being submitted as part of candidature for any other degree.

I also certify that the thesis has been written by me and that any help that I have received in preparing this thesis, and all sources used, have been acknowledged in this thesis.

Signature of Candidate

.....

Acknowledgements

I would like to thank Dr Phuoc Huynh for his valuable advice and encouragement during the course of this work. Dr Huynh has provided important insights and has been flexible, patient and a valuable source of knowledge.

I also thank Phyllis Agius who helped me greatly in concentrating on this research. I want to thank her for all her support, expertise and general trouble shooting.

I would like to dedicate this work to my parents, Choi, Eunna and Yun, Yunsik for their support throughout the course of this study.

Abstract

Peristaltic flow is a transport mechanism primarily used in the human body to transport fluids. This form of transport is characterised by the contraction and relaxation of flexible tubes. Many studies have been undertaken to investigate this phenomenon. Factors such as amplitude ratio, wave number and the Reynolds number have been studied to identify their effects on peristaltic flow.

In this work, the peristaltic flow of power-law fluids under non-isothermal conditions is investigated using the Computation Fluid Dynamics (CFD) methodology. The effect of temperature on peristaltic flow will be investigated in various conditions, for example, in Newtonian fluid (a special case of power-law fluids), non-Newtonian fluid of power-law type and different values of coefficient a_1 (a_1 being exponential coefficient of the temperature dependent viscosity).

Peristaltic flow for possible industrial applications will be considered, with fluid properties thus corresponding to those of an oil and a wider range of the Reynolds numbers (1-1000) than for biological applications. Comparison of isothermal versus non-isothermal flow shall also be shown.

Flow will be studied in the reference frame which moves with the wave (the wave frame). In this reference frame, the flow becomes steady. Firstly, isothermal flow models are shown to produce comparable results with previous works from the literature, therefore proving the validity of the present computational methodology. These conditions were then applied to non-isothermal models.

After this confidence has been established, non-isothermal flow is then investigated. This in turn affects whole flow field including factors such as change of viscosity and shear stress due to temperature change.

Streamline patterns, velocity profiles and pressure drop per wavelength are presented to show the effect of temperature in peristaltic flow. Pressure drop in non-isothermal flow is shown to be significantly less than that for isothermal case. Thus, for example, in the case of isothermal Newtonian flow, pressure drop per wavelength is 6305.2 Pa with conditions of the Reynolds number Re=10, wave number $(\alpha) = 0.25$ and amplitude ratio $(\phi) = 0.5$. On the other hand, in the case of non-isothermal flow, pressure drop per wavelength becomes 2054.7 Pa with the same conditions.

Influence of temperature is then considered in flow of non-Newtonian fluids of the power-law type. Consistent flow conditions are modelled to give a reasonable comparison. It is found that Newtonian and shear-thickening fluids are influenced by temperature strongly. However, in the case for shear thinning fluid, the effect of temperature is relatively small. Thus, for example, in table 5.2 (chapter 5), pressure drop per wavelength in a case for shear thinning fluids is very similar, at 49.153 Pa and 55.892 Pa corresponding to viscosity exponential coefficient $a_1 = -0.034\,°C^{-1}$ and $a_1 = 0\,°C^{-1}$ respectively.

The role of coefficient a_1 in power-law fluid is clarified in this research. Different values of a_1 are used and the corresponding results presented. They show that a_1 has stronger influence on the flow at regions adjacent to walls.

Vorticity patterns are also presented to show the effect of temperature. Especially, for Newtonian fluids, temperature affects vorticity differently at the crest and trough sections.

The effect of temperature on peristatic flow in different geometry is shown by streamline patterns, pressure drops and velocity profile. The variable, h (the mean distance of the wall from the axis of symmetry) is utilised to produce a model that shows the effect of the geometry in isothermal

flow. After the geometry is changed and resulting effect plotted, non-isothermal flow model is considered to prove the presence of thermal effects. The results gained by the models indicate that the temperature effect is stronger at the region adjacent to the wall in different geometries and the effect of temperature reduced the effect of geometry in pressure drop.

The above study was carried out in order to simulate realistic peristaltic flow. The addition of temperature by modelling non-isothermal flow has been shown to reduce the impact of the Reynolds number therefore changing the streamline pattern. This effect has been visualised in a number of special fluid applications to give a variety of results. The effects shown visually by CFD represent what peristaltic flow in industrial applications could look like.

TABLE OF CONTENTS

CHAPTER 3 METHODOLOGY

CHAPTER 4 ISOTHERMAL FLOW

Nomenclature

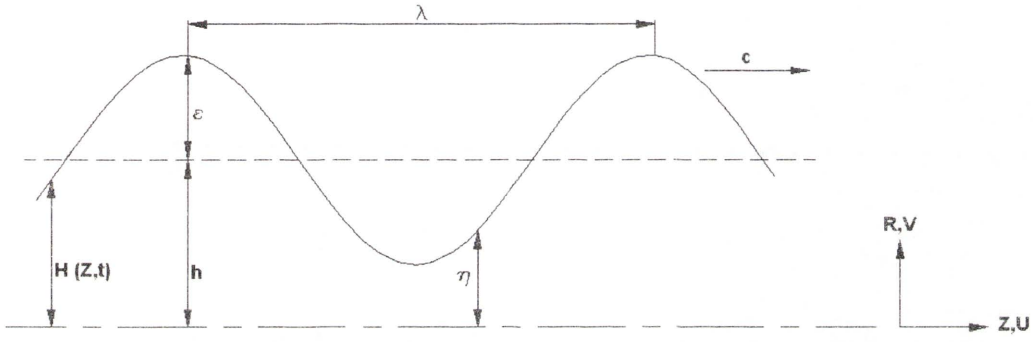

Configuration of peristaltic flow

c = the wave speed (m/s)

C_p = specific heat capacity ($J\,g^{-1}K^{-1}$)

F = non-dimensional volume flow rate in the wave frame ($\frac{q}{ch}$)

h = mean distance (m)

$\bar{\ell}$ = the dimensionless time-average flow rate in the laboratory frame

n = power-law index

$\Delta \bar{p}_{\lambda}$ = the dimensionless pressure rise per wavelength

q = the rate of fluid flow in the wave frame (m^3/s)

$\bar{Q}$ = the time-average rate of volume flow in the laboratory frame (m^3/s)

R = the radial coordinate in laboratory frame (m)

r = the radial coordinate in wave frame (m)

Re = Reynolds number

T = temperature ($°C$)

t = time (sec)

U = the axial velocity in Laboratory frame (V_z) (m/s)

u = the axial velocity in wave frame (v_z) (m/s)

V = the radial velocity in laboratory frame (V_r) (m/s)

v = the radial velocity in wave frame (v_r) (m/s)

Z = the axial coordinate in laboratory frame (m)

z = the axial coordinate in wave frame (m)

α = wave number ($\frac{h}{\lambda}$)

$\dot{\gamma}$ = the local calculated shear rate (s^{-1})

$\dot{\gamma}_0$ = the cut off shear rate (s^{-1})

ε = the wave amplitude (m)

$\eta_{(r)}$ or η = the displacement of wall (m)

λ = the wavelength (m)

μ = dynamic fluid viscosity ($Kg/(m \cdot s)$)

μ_0 = the zero-shear-rate viscosity ($Kg/(m \cdot s)$)

ν = kinematic fluid viscosity (m^2/s)

v_s = mean fluid velocity (m/s)

ρ = fluid density (kg/m^3)

ϕ = amplitude ratio ($\frac{\varepsilon}{h}$)

List of Units

Angle	=	deg	(degree)
Energy	=	J	(joule)
Force	=	N	(newton)
Length	=	m	(meter)
Mass	=	Kg	(kilogram)
Time	=	s	(second)
Temperature	=	$°C$	(degree Celsius)

List of Figures

List of Tables

CHAPTER 1

INTRODUCTION

1.1 Introduction

Peristaltic flow has been investigated by many studies during the past few decades and most of these studies have focused on physiological science. This chapter will briefly introduce the previous studies to provide an understanding of the history of peristaltic flow. The problem and objectives that are considered in this research will be stated with an outline of the thesis.

Many studies have investigated the peristaltic flow and factors like amplitude ratio, wave number and the Reynolds number have been shown to be important in describing peristaltic flow. Most of studies have only focused upon biological applications therefore, in this study, the possible use of peristaltic flow in industry with fluids having oil properties and a wide range of the Reynolds numbers (from 1-1000) is investigated. The main objective of this work is to investigate the effect of temperature on peristaltic flow.

Finally, the outline of this research is given in order to present a good understanding for the structure and direction of this work.

1.2 Brief history of peristaltic flow study

Peristalsis is a progressive wave resulting from area contraction and expansion of an extensible tube, and propagates a fluid along the length of the tube (Ayukawa et al [11]). As it propagates, it has a capability of affecting the motion for the fluid contained in the tube. It was described by Bayliss and Starling [1] as a type of movement where there is contraction and relaxation.

Yih and Fung [24] speculated that peristalsis may be involved in the vasomotion of small blood vessels which change their diameters periodically.

In 1971, Jaffrin and Shapiro [9] introduced the basic mechanism of a peristaltic pumping system.

Takabatake and Ayukawa [19] investigated the effect of the amplitude ratio and the wave number, which are determined by the geometry of the peristaltic wave. They also studied that the effect of the Reynolds number on peristaltic flow and the velocity and pressure fields were obtained and the relationship between the pressure rise per wave number were discussed.

Ayukawa and Takabatake [11] studied the characteristics of a peristaltic flow such as the periodicity of the flow pattern and effects of the Reynolds number in range of 0.01-1000.

Takabatake, Ayukawa and Mori [20] investigated peristaltic reflux, trapping phenomenon and pumping efficiency. The effect of the Reynolds number on trapping phenomenon was investigated.

Flow structure, pressure and shear stress distribution for zero flow rates were investigated by Xiao and Damodaran [23]. The effect of Reynolds number on the conditions of different values of wave number (α =0.01 and α 〉 0.01) was studied.

In 2006, the effect of power-law on the peristaltic flow was studied by Hayat and Ali [5]. They investigated the distribution of velocity and pressure in three conditions, in Newtonian, shear thinning and shear thickening fluids on peristaltic flow. However, their work is for isothermal flow only.

1.3 Problem statements and research objectives

Peristaltic flow is a primary transport mechanism inherent in many tubular organs of the human body, for example, the ureter, the gastro-intestinal tract and the urethra. It is also used in material handling systems in industry. The peristaltic pumping system is also used in medical applications like the blood pump in which the Reynolds number has a moderately high value. Currently the peristaltic pumping system is one of the most important instruments to transport material.

Many studies have developed the understanding of fluid phenomenon on peristaltic flow and its characteristics. However, the effect of temperature on the peristaltic flow has not been fully investigated yet. It is believed that peristaltic flow is deemed to be significantly dependent on viscosity. Any change in this property would therefore affect the flow characteristics. Since viscosity in turn is often dependent on temperature, any changes in thermal condition (for example by viscous heating) can therefore affect peristaltic flow.

In this work, the effect of temperature on peristaltic flow through an axi-symmetric tube will be investigated numerically using a commercial Computational Fluid Dynamics (CFD) software package. The fluid is assumed to be of a power-law type whose viscosity is also temperature dependent.

The power-law index will cover the range of fluid behaviour, for shear thinning, through Newtonian, to shear thickening type.

Various geometries (characterised by different wave numbers and amplitude ratios) will also be considered under both isothermal and non-isothermal conditions.

1.4 Thesis outline

In chapter 2, a literature review showing previous studies that have investigated aspects of this flow is provided. The backgrounds such as definition of peristaltic flow, the Reynolds number and governing equations is introduced to provide an understanding of this flow phenomenon. The governing equations that are used in numerical calculations for modelling and representing this flow phenomenon are presented in this chapter along with the relevant boundary conditions.

Chapter 3 describes the methodology which is utilised in this research. This chapter introduces the use of Computation Fluid Dynamics (CFD) to produce a model that simulates isothermal and non-isothermal flow. The specific software used in this work is introduced along with the hardware. The discussion of boundary conditions in the wave frame is shown in this chapter. The parameters such as axial velocity, radial velocity, reference pressure and reference temperature that have to be applied on the inlet, outlet, wall and axis of symmetry to obtain the steady-flow results are introduced. Grid convergence which is a technique to ensure accurate results produced in CFD, is also presented.

Chapter 4 presents the initial steps used to produce an isothermal flow model. Results from this model are compared to previous works from the literature and provide a benchmark for future investigations. Maximum and minimum velocities with three parameters, amplitude ratios, wave numbers and the Reynolds numbers were obtained and compared with the results from Xiao et al [23]. Streamline patterns with various values of the Reynolds number were plotted. The effect of

the Reynolds number in condition of $\alpha = 0.01$ and $\phi = 0.7$ were plotted and compared to the results from Xiao et al [23]. The dimensionless time mean flow ($\bar{Q}/\pi h^2 c$) was also utilised and its streamline patterns were plotted. The results for this work are shown in this chapter.

In Chapter 5, simulations of the effect of temperature on peristaltic flow with various conditions, is discussed. The first case for Newtonian fluid with a wide range of the Reynolds number is used to show the effect of temperature on peristaltic flow. The effects of temperature on Newtonian and non-Newtonian fluids are compared. Additionally in this chapter, the influence of viscosity exponential coefficient a_1 of in a Newtonian fluid is investigated. The effect of temperature on the vorticity in peristaltic flow is numerically found for the conditions of a Newtonian and shear thinning fluid. The temperature effect on different geometries is also discussed in this chapter.

Chapter 6 provides the conclusions and recommendations from this work. The results of this research are summarised and a comparison of this work with other results are shown. This chapter will also provide ideas for further development, better techniques and unsolved problems.

CHAPTER 2

LITERATURE REVIEW

2. Literature review

2.1. Introduction

This literature review will discuss some previous works by other researchers related to peristaltic flow and the current understanding of this phenomenon. Many research groups have studied peristaltic flow in different directions. .

In order to investigate peristaltic flow, the effects of the amplitude ratio, wave number and the Reynolds number on peristaltic flow need to be investigated. These factors affect the fluid flow properties in the form of velocity, pressure and shear change. The studies of the effects of these factors on peristaltic flow are discussed.

2.1.1 Peristaltic pumping (Shapiro et al [9])

2.1.1.1) Basic mechanism of peristaltic pumping

The basic mechanism of a peristaltic pump can be seen below in Figure 2.1 (Shapiro et al [9]).

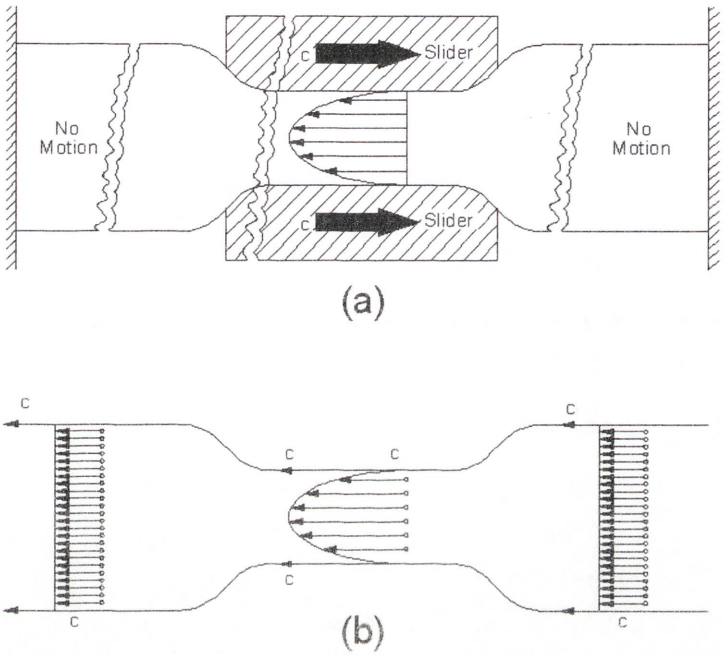

Figure 2.1 Conceptual illustration of the basic mechanism in peristaltic pumping. (a) : unsteady flow as seen in a laboratory frame, (b) : steady flow as seen in a wave frame (Shapiro et al [9]).

In Figure 2.1, (a) in the laboratory frame, shows a long tube closed at both ends, where a peristaltic wave of contraction is produced by moving a sliding cuff to the right at speed c. Part (b) of the same figure shows a wave frame of reference which moves towards the right with the speed c, relative to the laboratory frame; in this wave frame, the waveform appears stationary.

However, in the wave frame, the walls move towards the left with the speed c, and there is a uniform flow of speed $-c$ in the two large cross-sections. The average leftwards velocity in the contracted section must exceed c to conserve volume flow of an incompressible fluid. The velocity profile in this contraction section must be parabolic, assuming for the moment that the

flow is viscous and inertia-free with velocity of $-c$ at the walls. There is pressure drop from right to left in the contracted section, due to viscous losses.

Two conclusions can be drawn from the physics in this example.

1) Dissipation is an essential feature of peristaltic pumping. Without this viscous effect, the flow in the contracted section would have no associated pressure drop.
2) The fluid in the minimum section (trough) moves opposite to the wave direction as seen in the laboratory frame, while the fluid in the enlarged sections moves in the same direction as the wave frame (Shapiro et al [9]).

Figure 2.2 shows the configuration of the peristaltic flow which was utilised in the work conducted by Shapiro et al [9].

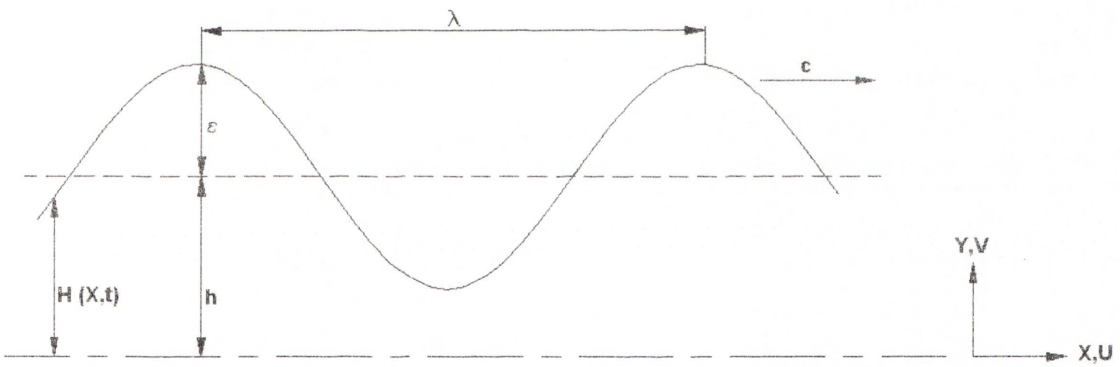

Figure 2.2 Nomenclature for 2-dimensional periodic sine wave.

Four important dimensionless parameters are introduced as following,

$$\alpha = \frac{h}{\lambda},\quad \phi = \frac{\varepsilon}{h},\quad \mathrm{Re} = \frac{hc\alpha}{\nu} \quad \text{and} \quad \bar{\ell} = \frac{\bar{Q}}{ch} \tag{2.1}$$

2.1.1.2) Parameters of the problem

Identifying the problem parameters for peristaltic pumping

There are four dimensionless parameters (Shapiro et al [9]).

1) The amplitude ratio, $\phi = \frac{\varepsilon}{h}$ which determine the relative degree of geometric occlusion or squeeze.
2) The wave number, $\alpha = \frac{h}{\lambda}$, is related to the slope and curvature of the wall.
3) The Reynolds number, defined as $\mathrm{Re} = \frac{hc}{v}\alpha$, is the correct ratio of inertial to viscous terms when inertial effects are relatively small and when peristalsis acts as a pump (Shapiro et al [18]).
4) The dimensionless time-mean flow ($\bar{\ell} = \frac{\bar{Q}}{ch}$) for 2 dimensional flow indicates the dimensionless mean-volume flow per unit area.

The first two (amplitude ratio and wave number) are determined by geometry; the Reynolds number gives partial description of the flow nature and flow rate is often given as imposed boundary condition.

2.1.1.3) Trapping

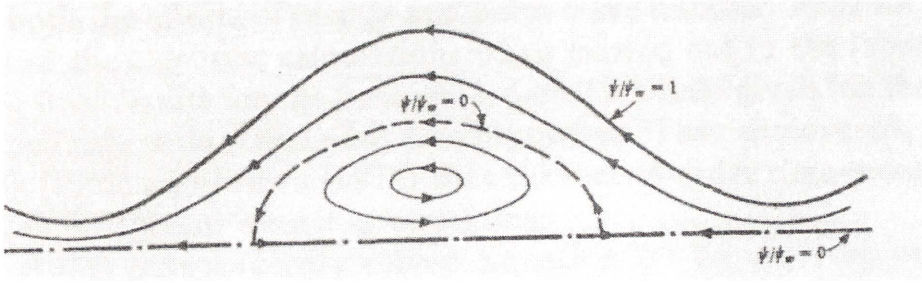

Figure 2.3 Streamlines in a wave frame when a trapped bolus exists in the laboratory frame (Shapiro et al [9])

In the wave frame, the streamlines are generally similar in shape to the wall but with lesser amplitude as the axis is approached. An interesting exception to this situation is that, under certain condition (identified by Shapiro et al [9]) as $\bar{Q} > \frac{(2-\phi)}{3}$; where $\bar{Q}$ is the time mean flow rate and ϕ is amplitude ratio), the central streamline splits to enclose a bolus of fluid particles describing closed streamlines in the wave frame. This bolus is centered under the crest of the wave as shown in Figure 2.3.

2.1.2 Numerical Analysis of Two-Dimensional Peristaltic Flow

(Ayukawa et al [11])

An investigation was made to determine the influence of wave amplitude, wave number and the Reynolds number on the flow pattern. They presented the characteristics of a peristaltic flow such as the periodicity of the flow pattern and effects of the Reynolds number in range of 0.01-1000.

2.1.2.1) Periodicity of the flow pattern

The periodicity of the flow pattern is judged from the velocity profiles on sections at the crests and the troughs.

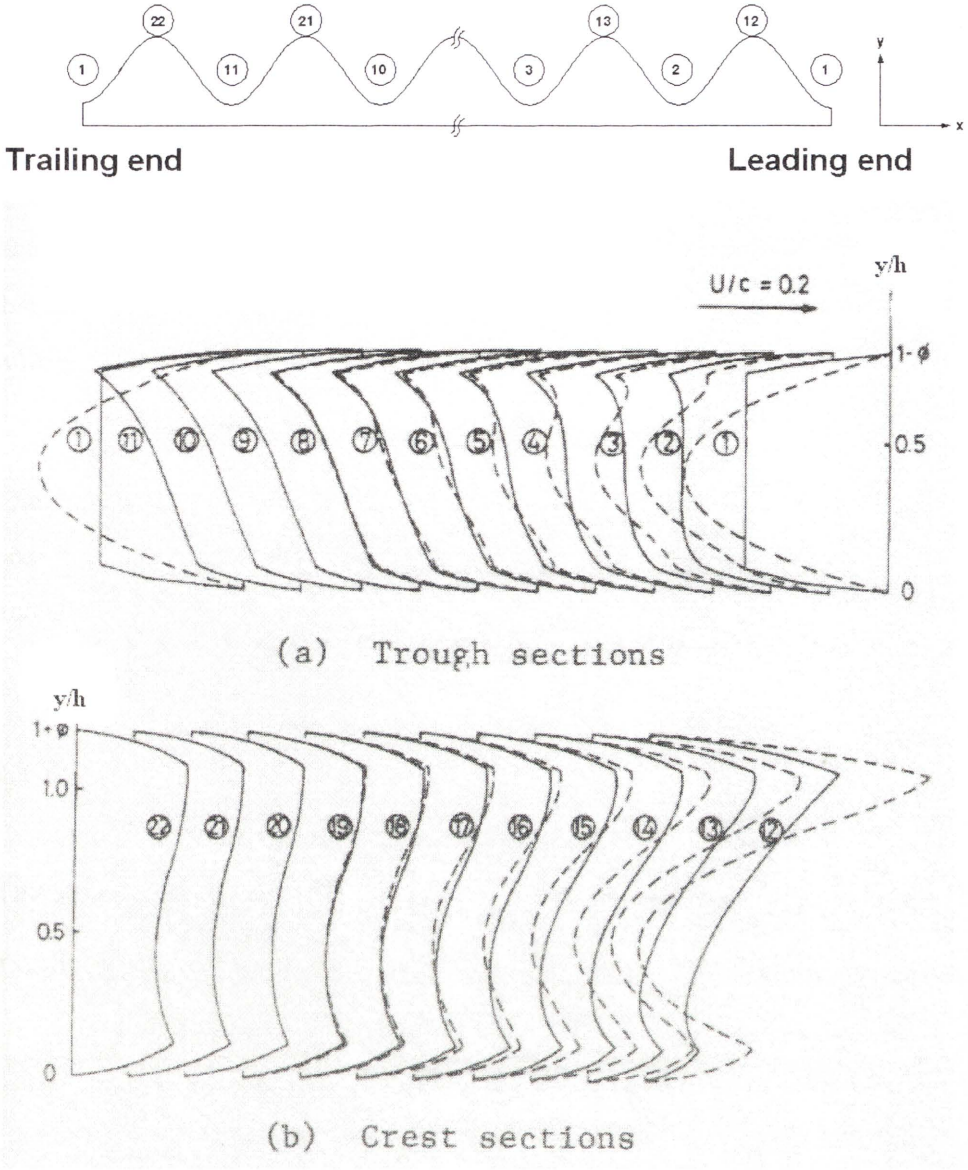

Figure 2.4 Velocity profiles ; $\phi = 0.19$, $\alpha = 0.21$, Re=210 and $\bar{Q} = 0$, Dashed lines are profiles when a parabolic wave is imposed at leading and trailing ends, solid lines are profiles when a trapezoidal wave is imposed (Ayukawa et al [11])

Figure 2.4 presents the longitudinal velocity profiles at eleven locations in the laboratory frame. The figure shows the trough and the crest sections in the finite region which are gained by imposing different velocity profiles (via stream function) at inlet. When the velocity profiles on the sections at the crest and the trough are compared with the next one, the flow is regarded as periodic if the absolute values of different turn out to be smaller than 10^{-6}.

The solid curves present the results obtained by imposing a trapezoidal velocity profile at the leading and trailing ends, while the dashed curves are the ones obtained for parabolic velocity profile.

The velocity profile imposed at the leading end influences the velocity profiles at the crest and the trough sections in the inner part of the flow region but this influence becomes gradually weaker as the distance from the leading end increases, becoming negligible after 8 wavelengths.

The regular profiles which are independent of the imposed velocity profiles on the ends are observed in the central part of the flow region (9^{th} and 10^{th} wavelength region from the leading ends).

2.1.2.2) Effect of the geometrical shape of the peristaltic wave

The geometrical shape of the peristaltic wave is governed by two dimensionless parameters, the amplitude ratio ($\phi = \frac{\varepsilon}{h}$) the wave number ($\alpha = \frac{h}{\lambda}$).

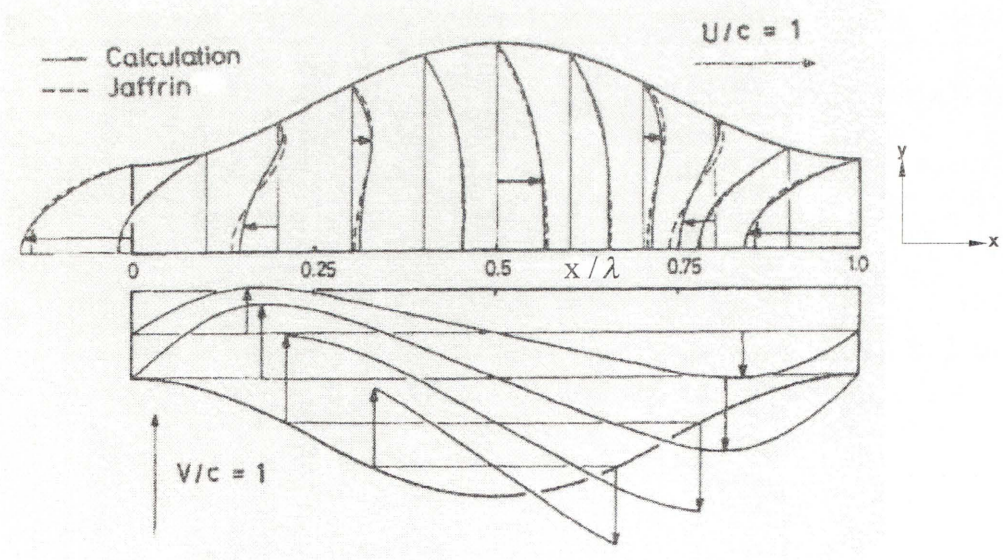

Figure 2.5 Velocity profiles ; $\phi = 0.4$, $\alpha = 0.3$, Re=0.01 and $\bar{Q} = 0$ (Ayukawa et al [11]) ; Reference to Jaffrin is Reference [8] in this work

Figure 2.5 presents the profiles of U and V for $\phi = 0.4$ and $\alpha = 0.3$. For the limit in $\alpha \to 0$, Shapiro et al [18] pointed out that the profile of U was parabolic at each cross section of the channel but the profiles (Ayukawa et al [11]) are seen to be slightly deformed from the parabolic profiles because of the finite value of α. It is thus seen that α is a significant geometric factor which dominates the flow field in the peristaltic channel.

2.1.2.3) The effect of the Reynolds number

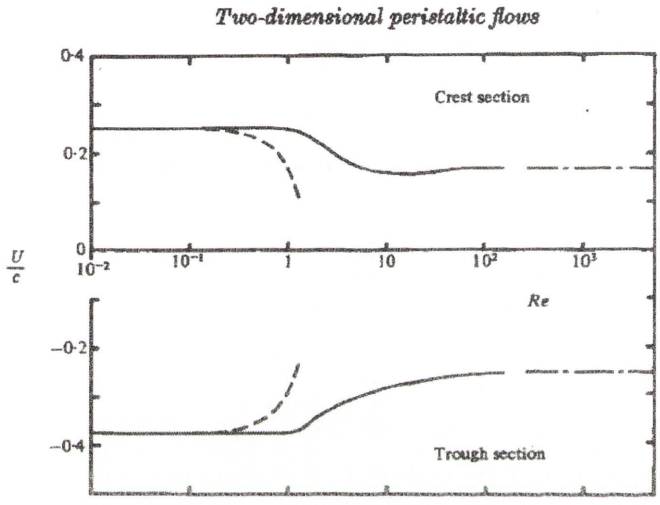

Figure 2.6 Velocities on the centre axis at the crest and the trough sections for $\phi = 0.2, \alpha = 0.01$ and $\bar{Q} = 0$ (Ayukawa et al [11])

When $\mathrm{Re} < 1$, both velocities on the centre axis at the crest and the trough sections are constant independently of the Reynolds number. On the other hand, for $\mathrm{Re} > 1$, the absolute values of velocity on the centre axis decrease and asymptotically approach the solution of a potential flow as the Reynolds number increases (Ayukawa et al [11]).

2.1.3 Numerical study of Two-Dimensional Peristaltic Flow (Takabatake et al [19])

The influences of amplitude ratio, wave number and Reynolds number on the flow were investigated through numerical calculations. The velocity and pressure fields were obtained and the relationship between the pressure rise per wave number were discussed. Takabatake et al [19] introduced the idea of stagnation points, which are the locations where the direction of flow motion is reversed. The dimensionless time-average flow rate ($\bar{\ell} = \frac{\bar{Q}}{ch}$) for 2 dimensional flow in the laboratory frame is defined in this study, Takabatake et al [19]. It indicates the dimensionless mean-volume flow per unit area.

2.1.3.1) Velocity field

The peristaltic flow has four significant dimensionless parameters, the amplitude ratio $\phi = \frac{\varepsilon}{h}$, wave number $\alpha = \frac{h}{\lambda}$, the Reynolds number and the dimensionless time-mean flow ($\bar{\ell} = \frac{\bar{Q}}{ch}$) for 2 dimensional (and axi-symmetric) flow; The amplitude ratio and the wave number are determined by the geometry of the peristaltic wave.

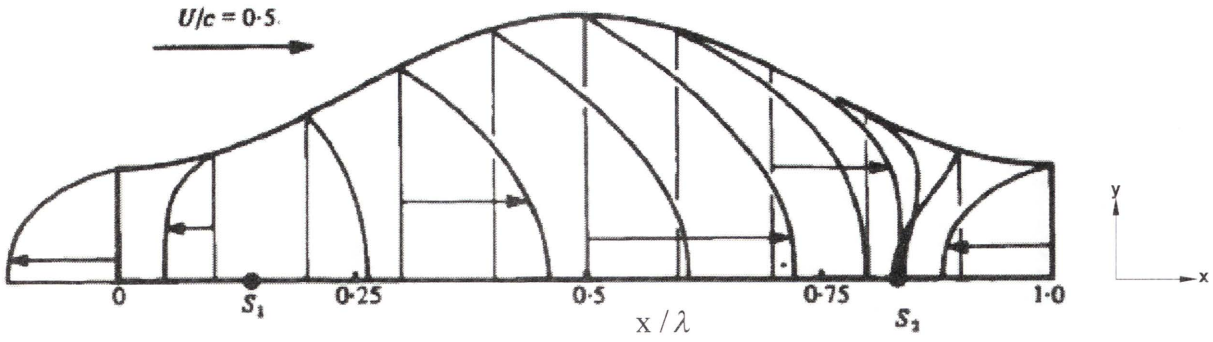

Figure 2.7 Longitudinal velocity profiles ϕ=0.4, α=0.2, Re=1, $\Delta p_\lambda = 0$ and $\bar{\ell}(=\frac{\bar{Q}}{ch}) = 0.239$ for 2 dimensional flow (Takabatake et al [19])

When the dimensionless time mean flow ($\bar{\ell}$) is zero, the forward-flow region and the retrograde-flow region equally occupy half of the one wavelength region but in Figure 2.7, the forward-flow region is predominant because of the finite value of the time mean flow.

In Figure 2.7, two stagnation points S_1 and S_2 appear along the axis near the trailing and the leading end respectively, separating the central region of a forward flow from two retrograde flow regions (where flow direction is reversed)

The longitudinal velocity profiles at the sections near the leading stagnation point S_2 are shown to be deformed slightly from the parabolic profiles because of the effects of fluid inertia and wall slope, due respectively to the finite values of Re and α.

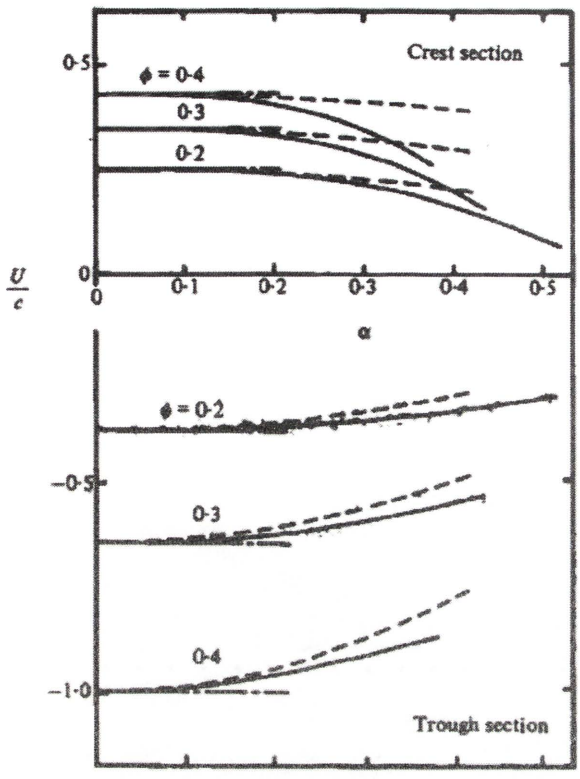

Figure 2.8 Velocities on the centre axis at the crest and the trough section for Re=0.01 and $\bar{\ell}\ (=\frac{\bar{Q}}{ch}) = 0$ (Takabatake et al [19])

Figure 2.8 shows the effects of ϕ and α on the velocities on the axis at the crest and the trough. When α is small, velocities on the axis are constant for all values of ϕ (Takabatake et al [19])

2.1.3.2) Pressure field

The effects of the Reynolds number on the pressure contours were identified in this investigation [19]. Figure 2.9 shows the effect of the Reynolds number on pressure **distribution** along peristaltic wall when the dimensionless pressure rise per wavelength $\Delta \bar{P}_\lambda = \frac{h^2 \Delta P_\lambda}{\mu c \lambda}$ is zero (where Δp_λ is pressure rise per wavelength). The dimensionless pressure rise per wavelength $\Delta \bar{P}_\lambda$ at zero time mean flow ($\bar{\ell} = 0$) is plotted in Figure 2.10.

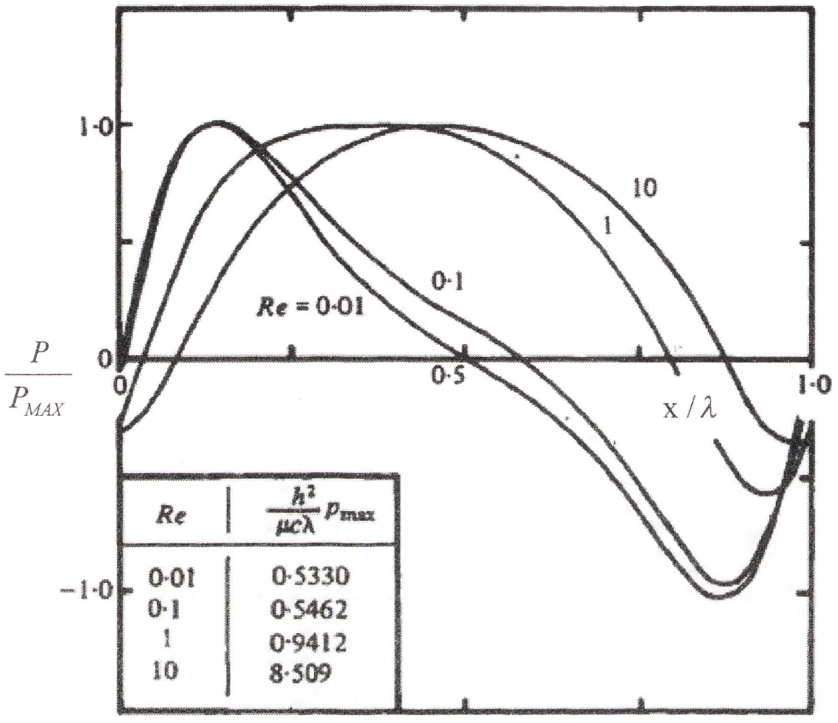

Figure 2.9 Pressure distribution along peristaltic wall for ϕ=0.4, α=0.2, $\bar{\ell}\ (=\frac{\bar{Q}}{ch}) = 0.239$ for 2 dimensional flow and ΔP_λ=0; (here p is pressure) (Takabatake et al [19])

Pressure distributions along the wall for various values of the Reynolds number were investigated. When Re is extremely small, the pressure on the wall is positive at the contracting part of the channel and is negative at the expansion part.

The distribution along the wall is closely antisymmetric about the midsection. As Re increases, the positions of the maximum and the minimum pressure move forward (positive x-direction) and a nearly symmetrical distribution along the wall is found.

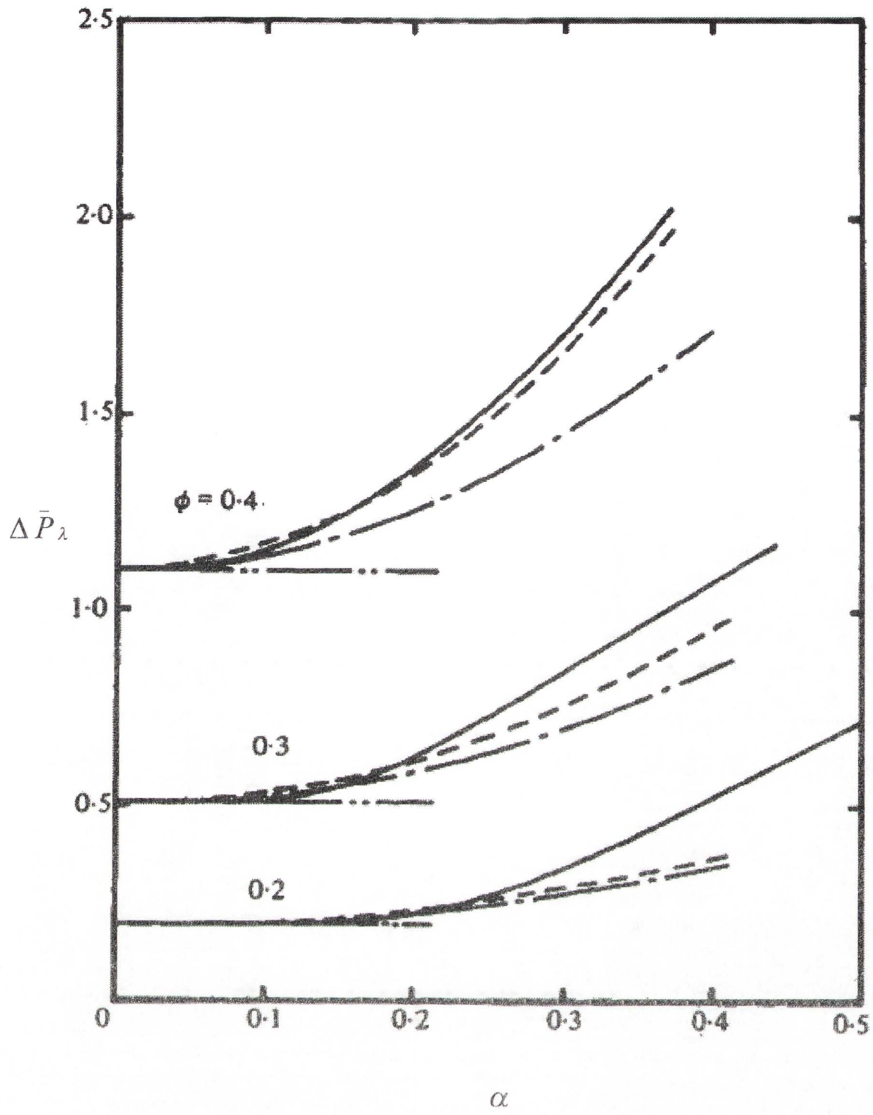

Figure 2.10 Pressure rise per wave number for Re=0.01, $\bar{\ell}(=\frac{\bar{Q}}{ch})=0$ for 2 dimensional flow (Takabatake et al [19])

Figure 2.10 (Takabatake et al [19]) shows variation in terms of amplitude ratio and wave number. This contribution appears at smaller α as ϕ increase.

2.1.4 A numerical investigation of peristaltic waves in circular tubes (Xiao et al [23]).

In the work by Xiao et al [23], the computational model developed covered a wide range of Reynolds numbers (0.01-100), wave amplitudes (0-0.8) and wavelengths (0.01-0.4). Some results pertaining to the distribution of velocity, pressure and shear stress for different peristaltic flow conditions characterising flow at moderately higher Reynolds number have been obtained.

2.1.4.1) Flow structure, pressure, shear stress distribution for zero time mean flow

Their paper presented computational results pertaining to the Reynolds number effect on the flow structure for the case corresponding to the geometric condition of $\alpha = 0.01$. Figure 2.11 and 2.12 shows the variation of the computed streamlines with the Reynolds number in both the wave frame and laboratory frame for the case of $\alpha = 0.01$ and $\bar{Q}/\pi ch^2 = 0, \phi = 0.2$ and $\phi = 0.7$ respectively.

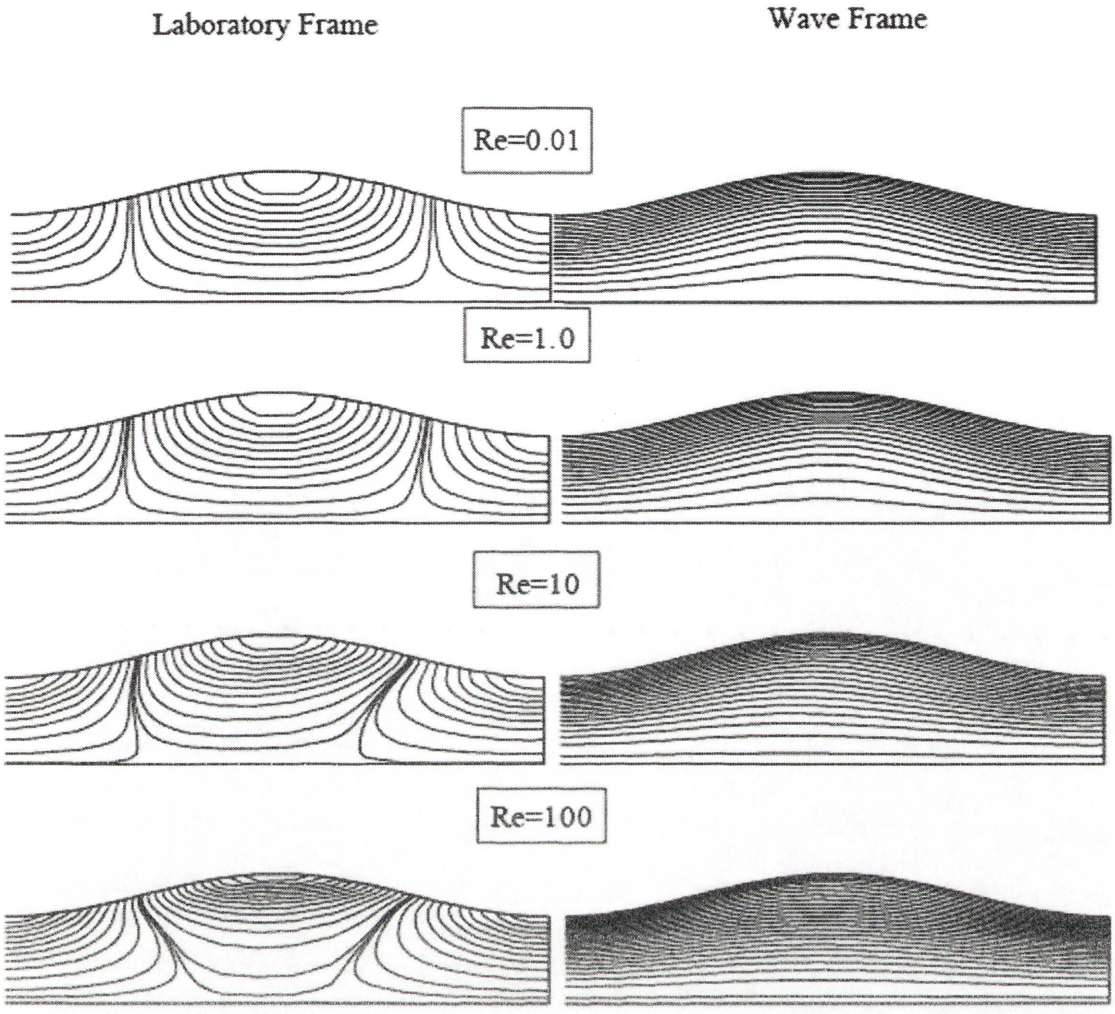

Figure 2.11 The effect of the Reynolds number on the streamline patterns in the wave frame and laboratory frame for $\alpha = 0.01$, $\bar{Q}/\pi ch^2 = 0$, $\phi = 0.2$ (Xiao et al [23])

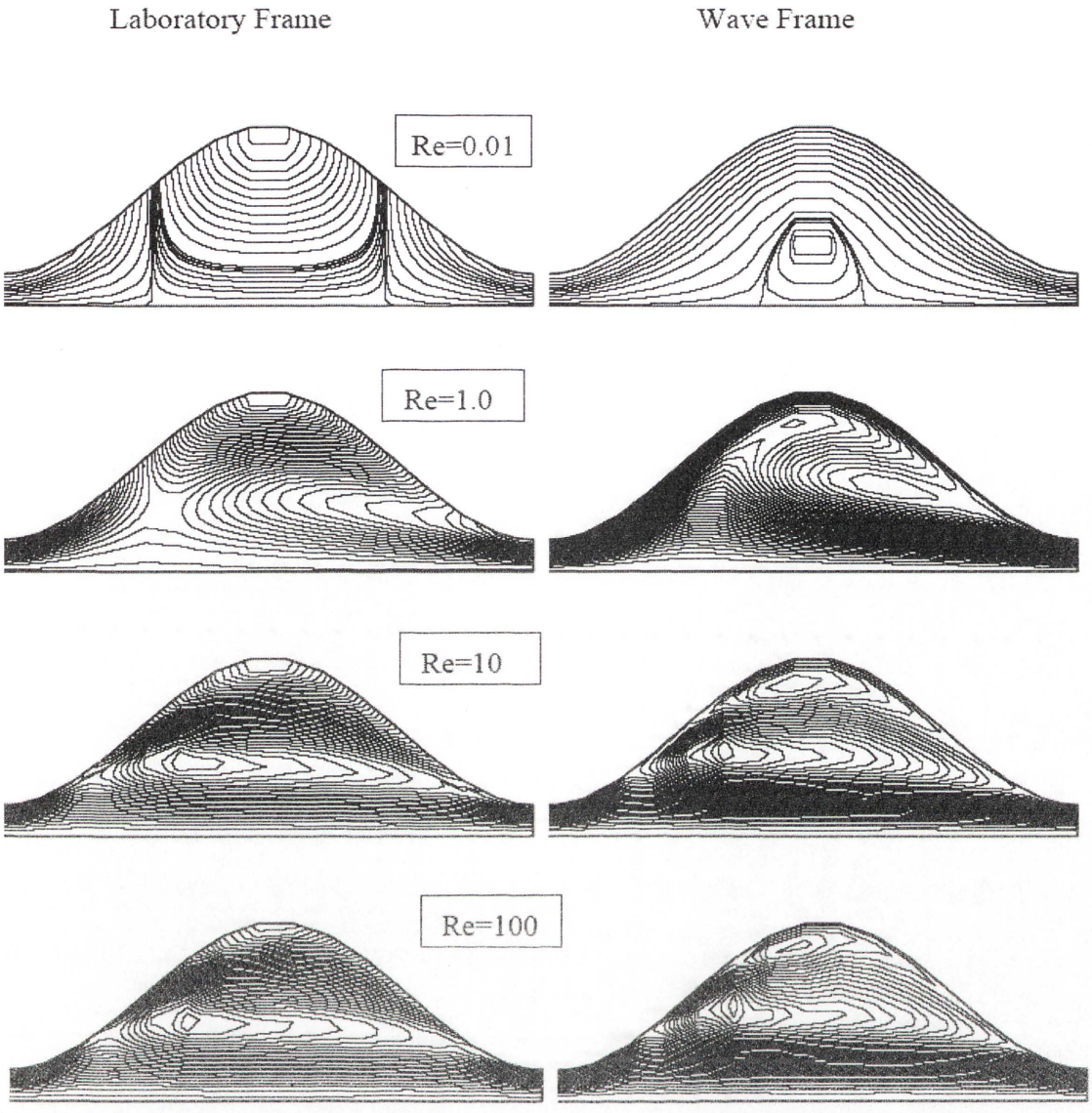

Figure 2.12 The effect of the Reynolds number on the streamline patterns in the wave frame and laboratory frame for $\alpha = 0.01$, $\bar{Q}/\pi ch^2 = 0$, $\phi = 0.7$ (Xiao et al [23])

As it can be seen by comparing the two figures(Fig 2.11 and 2.12), the effect of the Reynolds number on the flow structure can be seen ; the Reynolds number can be seen to have strong effect on the flow pattern where amplitude ratio ϕ is larger ; the comparison shown is between $\phi = 0.2$ and $\phi = 0.7$ and the stronger effect of the Reynolds number is discovered in the case corresponding to $\phi = 0.7$ in Figure 2.12 than the case corresponding to $\phi = 0.2$ in Figure 2.11. This result implies that inertial force effect on the peristaltic flow is stronger for the case with a larger amplitude ratio.

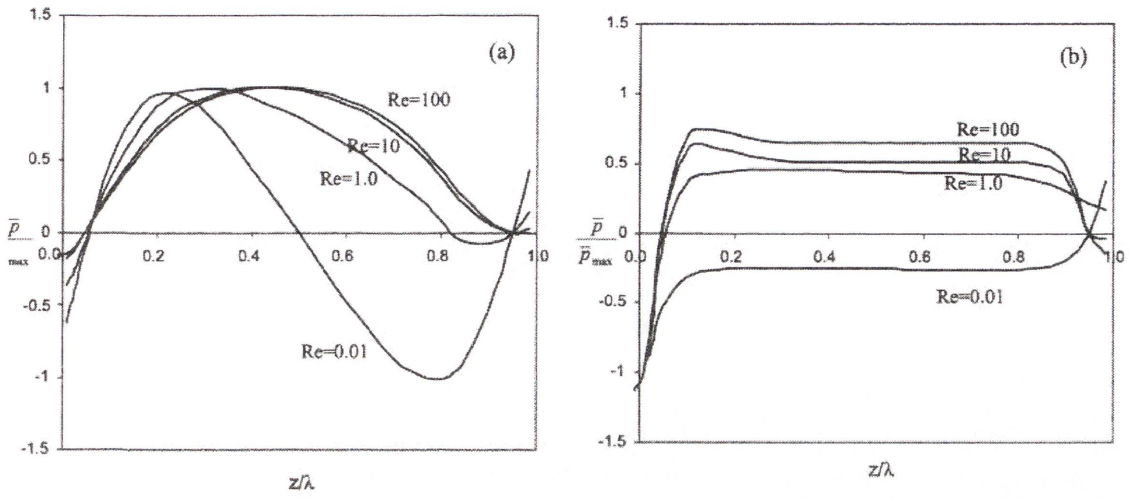

Figure 2.13 The effect of the Reynolds number on the normalised non-dimensional pressure distribution for $\alpha = 0.01$ and $\bar{Q}/\pi ch^2 = 0, (a)\ \phi = 0.2 \quad (b)\ \phi = 0.7$ (Xiao et al [23])

The effect of the Reynolds number on the normalised, non-dimensional pressure distribution corresponding to flow cases where the amplitude ratio $\phi = 0.2$ and $\phi = 0.7$ respectively is shown in Figure 2.13. For $\phi = 0.7$, the pressure distribution remains a constant in the central part of one wavelength (i.e $0.2 < z/\lambda < 0.8$) with the sudden rise in $\bar{p}$ near the two boundaries of the wave cycle. Whereas the pressure distribution in the case for $\phi = 0.2$ varies with the z/λ during the whole wave cycle and as the Reynolds number increases the maximum non-dimensional pressure approaches the middle point of the wave cycle.

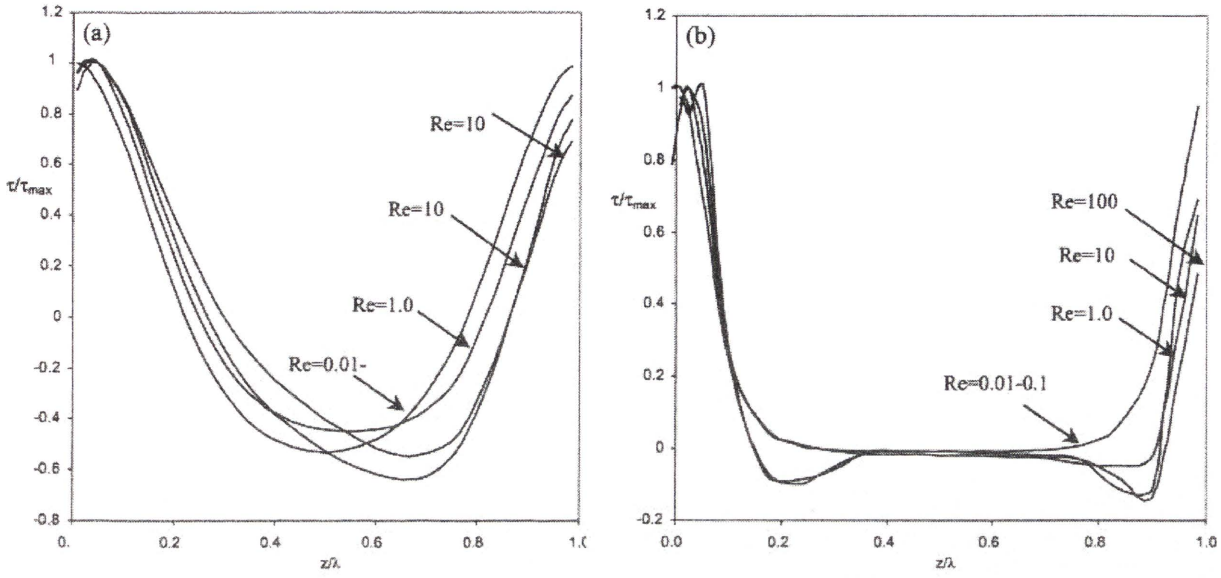

Figure 2.14 The effect of the Reynolds number on the shear stress distribution for $\alpha = 0.01$ and $\bar{Q}/\pi ch^2 = 0, (a)\ \phi = 0.2 \quad (b)\ \phi = 0.7$ (Xiao et al [23])

The variation of the non-dimensional shear stress (τ/τ_{max}) distribution along the peristaltic wall corresponding to the two cases for $\phi = 0.2$ *and* $\phi = 0.7$ are presented respectively. For the range of the Reynolds number from 0.01 to 1.0, the effect of the Reynolds number on the shear stress distribution is small for both cases although the variation of shear stress is much sharper for $\phi = 0.2$ than $\phi = 0.7$.

Both figures present a symmetric feature about the midsection. However, the symmetric feature is broken if the Reynolds number increase to 10 and 100 and the location for the minimum shear stress moves downstream. In the case for $\phi = 0.7$, the symmetry is maintained for the entire range with two locations for minimum shear stress appear around $z/\lambda = 0.2$ *and* 0.9.

2.1.4.2) Reynolds number effect corresponding to the case when α〉0.01

In order to study the effect on the flow structure by relaxing the assumption of $\alpha = 0.01$, computations for cases when $\alpha = 0.1$, 0.2 and 0.4 was investigated.

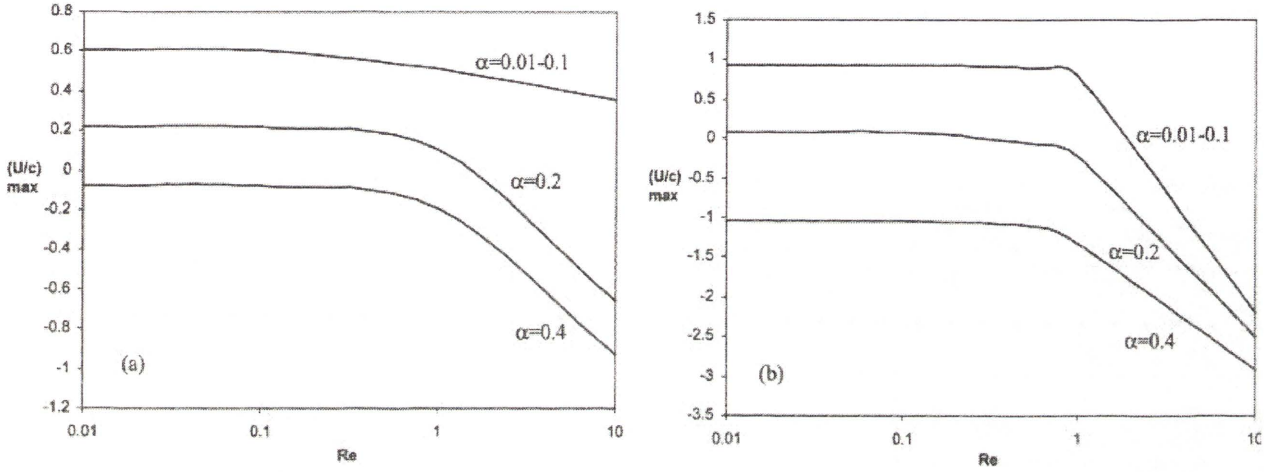

Figure 2.15 The effect of the Reynolds number on the maximum axial velocity for different wave number α . (a) $\phi = 0.2$ (b) $\phi = 0.4$ (Xiao et al [23])

The effect of the Reynolds number on the maximum axial velocity in the laboratory frame for different values of wave number corresponding to $\phi = 0.2$ and $\phi = 0.4$ is plotted in Figure 2.15. Figure 2.15 shows a similar trend with maximum axial velocity associating with the Reynolds number. When Re < 1.0, $(U/c)_{max}$ remains a constant (which is a function of α) irrespective of the Reynolds number. On the other hand, when Re>1.0, $(U/c)_{max}$ decreases with Reynolds number.

2.1.5 On mechanism of the peristaltic flow for Power-law fluid (Hayat et al [5]),

These researchers presented a mathematical model for flow induced by peristaltic waves through a deformable tube, considering an incompressible power-law fluid. The main goal of this work was the stream function, axial velocity and pressure gradient for power-law fluid.

2.1.5.1) Pressure drop per wavelength with power-law fluid

Table 2.1 Pressure drop per wavelength along flow direction ΔP_λ (in Pa) for different values of total flux F ($=\frac{q}{ch}$), wave amplitude ϕ and non-Newtonian parameter m.

F	-1			-2			-3		
ϕ	0.2	0.3	0.4	0.2	0.3	0.4	0.2	0.3	0.4
m=0	69.46	100.79	164.16	192.34	259.47	393.59	315.22	418.14	623.02
m=0.2	136.18	242.15	493.62	545.55	866.36	1605.5	1081.5	1672.1	3021.2
m= -0.2	36.82	44.47	57.97	69.33	81.34	102.61	93.59	109.02	136.29

(In this case, m = n-1 ; n is the power-law index)

The total flux F is defined in the works of Hayat et al [4, 5], as non-dimensional volume flow rate ($\frac{q}{ch}$) in the wave frame for their two dimensional model.

Table 2.1 presents the value of ΔP_λ (Pa) for Newtonian, and non-Newtonian, shear thickening and shear thinning fluids for different values of F and ϕ. It can be seen from Table 2.1, the value of ΔP_λ (Pa) increases as the increase of F and the amplitude ratio (ϕ).

The value of ΔP_λ (Pa) has large magnitude in the case for shear thickening fluid in comparison with those of Newtonian and shear thinning fluids.

Table 2.2 Axial velocities (u/c) at the center of the cylindrical tube listed for various values of m and total flux F ($=\frac{q}{ch}$) (In this case, m = n-1 ; n is the power-law index)

m	F=-1	F=-2	F=-3	F=-5	F=-10
-0.2	-2.75	-6.25	-9.75	-16.75	-34.25
-0.1	-2.88	-6.66	-10.44	-18	-36.88
0	-3	-7	-11	-19	-39
0.1	-3.09	-7.27	-11.45	-19.81	-40.72
0.2	-3.16	-7.50	-11.83	-20.50	-42.16

In Table 2.2, the axial velocity (u/c) at the center of cylindrical tube is listed for various values of m and F. It is evident that an increase in F increases the magnitude of axial velocity for fixed values of m.

2.1.5.2) The behaviour of axial velocity (u/c) for three values of m

(In this case, m = n-1 ; n is the power-law index)

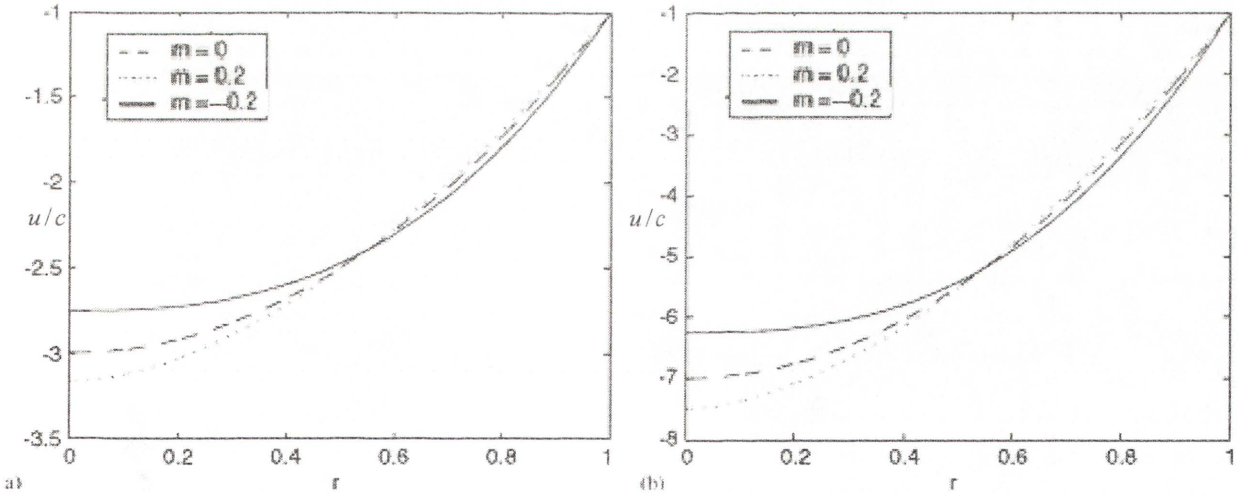

Figure 2.16 Radial distribution of the axial velocity (u/c) for a position with dimensionless tube radius of h=1 for three different values of m when F=-1 (a) and F=-2 (b) (Hayat et al [5])

Figure 2.16 a) presents the behaviour of axial velocity (u/c) for three values of m. The axial velocity (u/c) for shear thickening fluid near the center of the tube is greater in magnitude as compared with Newtonian and shear thinning fluids.

Figure 2.16 b) describes that increase of total flux F($=\frac{q}{ch}$) as the magnitude of axial velocity (u/c) near the center of wall increase for all three values of m.

2.1.6.3) The effect of ϕ, F and m on dp/dz

(In this case, m = n-1 ; n is the power-law index)

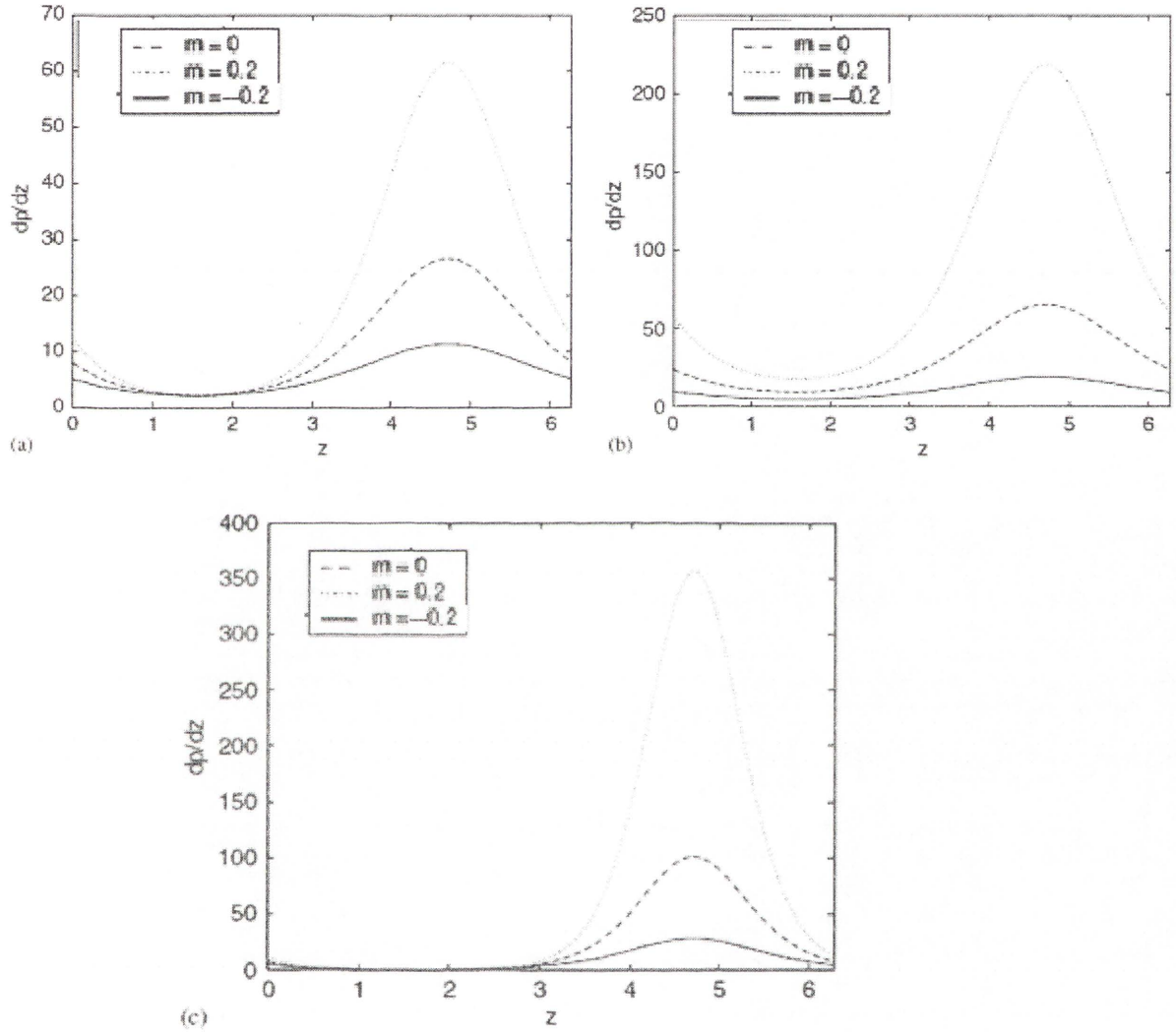

Figure 2.17 Distribution of the pressure gradient dp/dz within a wavelength $z \in [0, 2\pi]$ for F=-1 and $\phi = 0.2$ (a), F=-2 and $\phi = 0.2$ (b) and F=-1 and $\phi = 0.4$ (c) (Hayat et al [5])

Figure 2.17 shows the effects of ϕ ,F ($=\frac{q}{ch}$) and m on dp/dz . In figure 2.20 a) dp/dz against z for three different values of m with F=-1 and ϕ =0.2 is plotted. It is clear from Fig. 2.17 a) that smaller values of axial pressure gradient are required to maintain the same flux in the narrow part of the tube for shear thinning fluids when compared with Newtonian and shear thickening fluids.

Figure 2.17 b) and c) state that an increase in total flux F ($=\frac{q}{ch}$) and amplitude ratio ϕ results in the increase in dp/dz for all three values of m.

Their paper presented analytical solutions for the axial velocity (m/s) and axial pressure gradient obtained in closed form under long wavelength assumption. The expressions for power-law fluid were then compared to the results of Newtonian fluid and the agreement between the results of two fluids. Flow analysis is strongly dependent upon F and m.

2.2 Background

2.2.1 Introduction

This chapter introduces the definition of peristaltic flow and governing equations. Peristaltic flow is the flow generated in the fluid contained in a distensible tube when a progressive wave travels along the tube's wall.

The Reynolds number utilised in peristaltic flow has been investigated in previous studies and the general Reynolds number and the Reynolds number in peristaltic flow will be introduced.

Peristaltic flow has a feature of the periodic wave that has situations where the wave is iterated at regular intervals. The periodic wave is described in this chapter to provide a better understanding of a characteristic peristaltic flow.

The governing equations, continuity equation, conservation of momentum, balance of energy and boundary conditions utilised in numerical calculations are introduced to understand the fluid behaviour in peristaltic flow. Power-law fluid shall be introduced to provide the understanding of temperature effect on viscosity in this study.

2.2.2 Definition of peristaltic flow

Peristalsis was described by Bayliss and Starling [1] as a type of movement where there is contraction and relaxation. Peristaltic pumping is well defined by Jaffrin and Shapiro [9].

This fundamental mechanical event, called peristalsis, can be described as a composition of a wave of contraction rings that propel contents such as foodstuffs. This peristaltic phenomenon is exhibited by the oesophagus, stomach, and intestines within animals and humans. The relaxation and contraction sequence is generated with intestinal sphincters and specific areas with increased muscle tone to control the forward and backward movement of fluids and solids. Contraction is followed by relaxation followed by contraction as part of the peristaltic sequence.

Fig 2.18 shows that the gastrointestinal tract consists of a series of hollow tubes and compartments. Peristaltic fluid occurs in digestive organ in a human body.

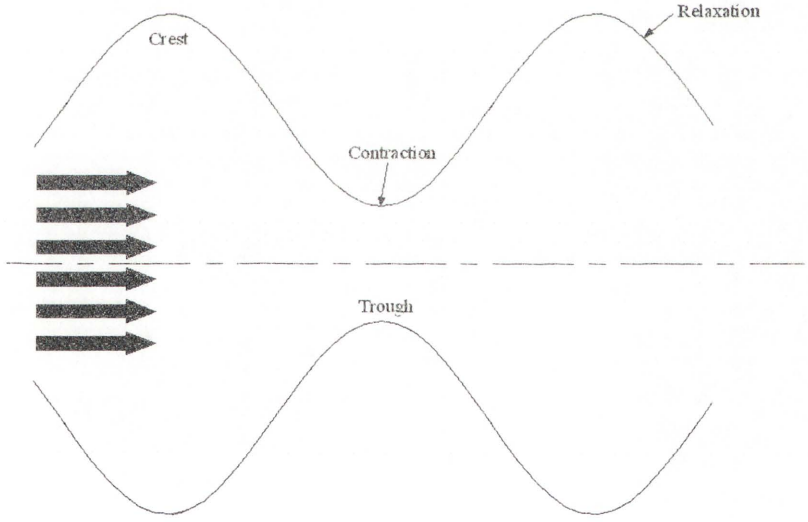

Figure 2.18 Movement of fluid by contraction and relaxation sequence

2.2.3 Reynolds number

In peristaltic flow calculations and modelling, the Reynolds number is one of the most important parameters used and the effect of the Reynolds number in peristaltic flow has been widely studied. A wide range of the Reynolds number is often implemented in order to prove its effect on the peristaltic flow when undergoing changes in temperature.

In general, the Reynolds number is defined as

$$\text{Reynolds number} = \frac{\rho v_s L}{\mu} = \frac{v_s L}{\nu} = \frac{\text{Inertial force}}{\text{Viscous force}}$$

- v_s - mean fluid velocity,
- L - characteristic length (equal to diameter ($2r$) if a cross-section is circular),
- μ - dynamic fluid viscosity,
- ν - kinematic fluid viscosity: $\nu = \mu / \rho$,
- ρ - fluid density

In fluid mechanics, the Reynolds number is the ratio of inertial forces $(v_s \rho)$ to viscous forces (μ / L) and is used to determine whether a flow will be laminar or turbulent. It is the most important dimensionless number in fluid dynamics and provides a criterion to determine dynamic similitude.

At low Reynolds numbers, laminar flow exists where viscous forces are dominant and are classified by smooth, constant fluid motion. The opposite to this is when turbulent flow occurs at high Reynolds number because inertial forces dominate, producing random eddies, vortices and other flow fluctuations.

The transition between laminar and turbulent flow is often indicated by a critical Reynolds number Re_{crit} which depends on the exact flow configuration and must be determined experimentally.

For fluid flow over a flat plate, the characteristic length is the length of the plate and the characteristic velocity is the free stream velocity. In a boundary layer over a flat plate the local regime of the flow is determined by the Reynolds number based on the distance measured from the leading edge of the plate. In this case, the transition to turbulent flow occurs at a Reynolds number of the order of 10^5 or 10^6.

In peristaltic flow, the Reynolds number is defined as $\mathrm{Re} = \left(\frac{hc}{\nu}\right)\alpha$ and should be noted the different notation to the previous definition above. This Reynolds number is the correct ratio of inertial to viscous term when inertial effects are relatively small. This definition was described by Shapiro et al [18].

2.2.4 Definition of periodic waves

A periodic wave has situations in which wave iterated at regular intervals is used in this work. The period is the time between successive cycles of a repeating sequence of events. Many numerical studies use periodic waves in order to define applications. The length scale, wavelength, the time scale and period are used to characterise a periodic wave.

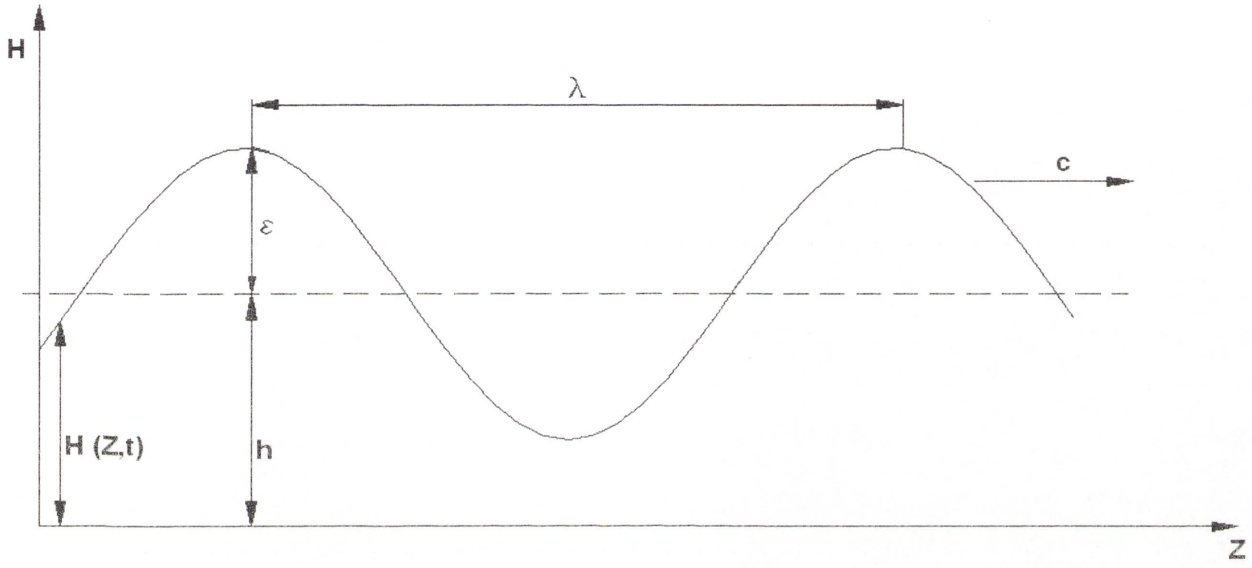

Figure 2.19 An example of periodic waves

$$H(Z,t) = h - \varepsilon \cos\left\{\frac{2\pi}{\lambda}(Z - ct)\right\} \tag{2.2}$$

The term $(\frac{2\pi}{\lambda})$ is simply called as the wave number determining the scale of the wave and the amplitude, ε, represents the magnitude of maximum value (and minimum) of the position of the wall relative to the mean position.

2.2.5 Governing equations

The peristaltic model is in the form of the sine curve which is described in periodic waves. Fluid motion is governed by the equations of continuity (mass conservation), conservation of momentum and balance of energy equation. The fluid is a temperature dependant power-law type.

These equations in this thesis are used under these specific circumstances: steady, axi-symmetric and incompressible.

2.2.5.1 Power-law fluid

A power-law fluid is a fluid for which the shear stress is a function of shear rate at the particular time, but not dependent upon the history of deformation.

$$\tau = K\mu_0 e^{(a_1 T)}\left(\frac{\partial u}{\partial r}+\frac{\partial v}{\partial z}\right)^n \tag{2.3}$$

where:

K is the flow consistency index

n is power-law index

r is the radial coordinate in wave frame

z is the axial coordinate in wave frame

u is the axial velocity

v is the radial velocity

$\frac{\partial u}{\partial r}+\frac{\partial v}{\partial z}$ is the shear rate

T is temperature.

μ_0 is the zero shear rate viscosity ($Kg/(m \cdot s)$).

a_1 ($^{\circ}C^{-1}$) is a coefficient.

The quantity

$$\tau = K\mu_0 e^{(a_1 T)}\left[\frac{\partial u}{\partial r}+\frac{\partial v}{\partial z}\right]^{n-1} \times \left(\frac{\partial u}{\partial r}+\frac{\partial v}{\partial z}\right) \Rightarrow \tau = \mu_{eff} \times \left(\frac{\partial u}{\partial r}+\frac{\partial v}{\partial z}\right) \tag{2.4}$$

$$\mu_{eff} = K\mu_0 e^{(a_1 T)}\left[\frac{\partial u}{\partial r}+\frac{\partial v}{\partial z}\right]^{n-1} \tag{2.5}$$

represents an apparent or effective viscosity that is a function of the shear rate.

If n were to be less than one, the power-law predicts that the effective viscosity would decrease with an increasing shear rate, requiring a fluid with infinite viscosity at rest and zero viscosity as the shear rate approaches infinity. It is named as a shear-thinning fluid that has a lower apparent viscosity at higher shear rates.

If n is equal to 1, the power-law predicts that its shear rate or strain curve is linear and its constant of proportionality would be known as the viscosity. The shear stress is directly proportional to the shear rate. Water is considered to be Newtonian, because it continues to exemplify fluid properties no matter how fast it is stirred or mixed.

If n is larger than 1, it is called a shear-thickening fluids as apparent viscosity increase at higher shear rates. Shear-thickening fluids are rarely encountered.

It is known that temperature affects the viscosity of a fluid. Therefore, the effective viscosity (2.5) of the fluid will be needed to be considered to demonstrate the effect of temperature on peristaltic flow.

A power-law module (2.7) for fluid viscosity is used with an exponential dependence on temperature for non-isothermal flow.

$$\tau = \text{Viscosity} \times \text{Shear rate}$$

$$\tau = K\mu_0 e^{(a_1 T)}\left[\frac{\partial u}{\partial r} + \frac{\partial v}{\partial z}\right]^{n-1}\left(\frac{\partial u}{\partial r} + \frac{\partial v}{\partial z}\right) \tag{2.6}$$

$$\text{Viscosity} = K\mu_0 e^{(a_1 T)}\left[\frac{\partial u}{\partial r} + \frac{\partial v}{\partial z}\right]^{n-1} \tag{2.7}$$

$$\text{shear rate} = \left(\frac{\partial u}{\partial r} + \frac{\partial v}{\partial z}\right) \tag{2.8}$$

2.2.5.2) Conservation of mass

See Appendix part 1.

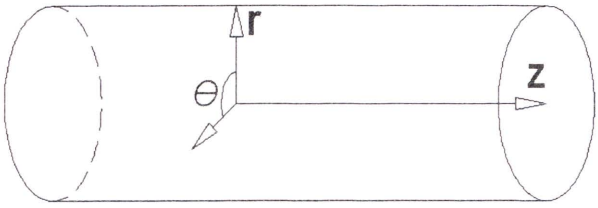

Figure 2.20 Cylindrical Coordinate for equations below

The form of the Continuity equation in an incompressible flow is

$$\frac{1}{r}\frac{\partial}{\partial r}(v_r r)+\frac{1}{r}\frac{\partial v_\theta}{\partial \theta}+\frac{\partial v_z}{\partial z}=0 \quad \text{in Cylindrical coordinates} \qquad (2.9)$$

It represents that conservation law by equating a net flux over a surface with a loss or gain of material within the surface and stats conservation of mass.

2.2.5.3) Conservation of momentum.

See Appendix part 2.

r - component

$$\rho\left(\frac{\partial v_r}{\partial t}+v_r\frac{\partial v_r}{\partial r}+\frac{v_\theta}{r}\frac{\partial v_r}{\partial \theta}-\frac{v^2{}_\theta}{r}+v_z\frac{\partial v_r}{\partial z}\right)=-\frac{\partial P}{\partial r}-\left(\frac{1}{r}\frac{\partial}{\partial r}(r\tau_{rr})+\frac{1}{r}\frac{\partial \tau_{r\theta}}{\partial \theta}-\frac{\tau_{\theta\theta}}{r}+\frac{\partial \tau_{rz}}{\partial z}\right)+\rho g_r \tag{2.10}$$

θ - component

$$\rho\left(\frac{\partial v_\theta}{\partial t}+v_r\frac{\partial v_\theta}{\partial r}+\frac{v_\theta}{r}\frac{\partial v_\theta}{\partial \theta}+\frac{v_r v_\theta}{r}+v_z\frac{\partial v_\theta}{\partial z}\right)=-\frac{1}{r}\frac{\partial P}{\partial \theta}-\left(\frac{1}{r^2}\frac{\partial}{\partial r}(r^2\tau_{r\theta})+\frac{1}{r}\frac{\partial \tau_{\theta\theta}}{\partial \theta}+\frac{\partial \tau_{\theta z}}{\partial z}\right)+\rho g_\theta \tag{2.11}$$

z – component

$$\rho\left(\frac{\partial v_z}{\partial t}+v_r\frac{\partial v_z}{\partial r}+\frac{v_\theta}{r}\frac{\partial v_z}{\partial \theta}+v_z\frac{\partial v_z}{\partial z}\right)=-\frac{\partial P}{\partial z}-\left(\frac{1}{r}\frac{\partial}{\partial r}(r\tau_{rz})+\frac{1}{r}\frac{\partial \tau_{\theta z}}{\partial \theta}+\frac{\partial \tau_{zz}}{\partial z}\right)+\rho g_z \tag{2.12}$$

2.2.5.4) Balance of energy

An energy balance equation is the direct result of the momentum balance equation. An energy balance is a systematic explanation of energy flows and transformations in a system, based on the first law of thermodynamics.

In an incompressible flow, density (ρ) is constant. The balance of energy is defined by

$$\rho C_p \left(\frac{\partial T}{\partial t} + v_r \frac{\partial T}{\partial r} + \frac{v_\theta}{r}\frac{\partial T}{\partial \theta} + v_z \frac{\partial T}{\partial z}\right) = k\left[\frac{1}{r}\frac{\partial}{\partial r}\left(r\frac{\partial T}{\partial r}\right) + \frac{1}{r^2}\frac{\partial^2 T}{\partial \theta^2} + \frac{\partial^2 T}{\partial z^2}\right]$$
$$+ 2\mu\left\{\left(\frac{\partial v_r}{\partial r}\right)^2 + \left[\frac{1}{r}\left(\frac{\partial v_\theta}{\partial \theta} + v_r\right)\right]^2 + \left(\frac{\partial v_z}{\partial z}\right)^2\right\}$$
$$+ \mu\left\{\left(\frac{\partial v_\theta}{\partial z} + \frac{1}{r}\frac{\partial v_z}{\partial \theta}\right)^2 + \left(\frac{\partial v_z}{\partial r} + \frac{\partial v_r}{\partial z}\right)^2 + \left[\frac{1}{r}\frac{\partial v_r}{\partial \theta} + r\frac{\partial}{\partial r}\left(\frac{v_\theta}{r}\right)\right]^2\right\}$$

(2.13)

Where,

- ρ is the fluid density
- μ is dynamic viscosity
- C_p is specific heat
- k is thermal conductivity
- T is temperature.

2.2.5.5) Boundary conditions-general consideration

The boundary is utilized to create the peristalsis motion in order to investigate peristaltic flow with the thermal effect in this work. The flow problem at hand is shown graphically in Figure 2.1. The flow in the channel is unsteady by a moving boundary in the fixed coordinate frame (Z,R) (the laboratory frame).

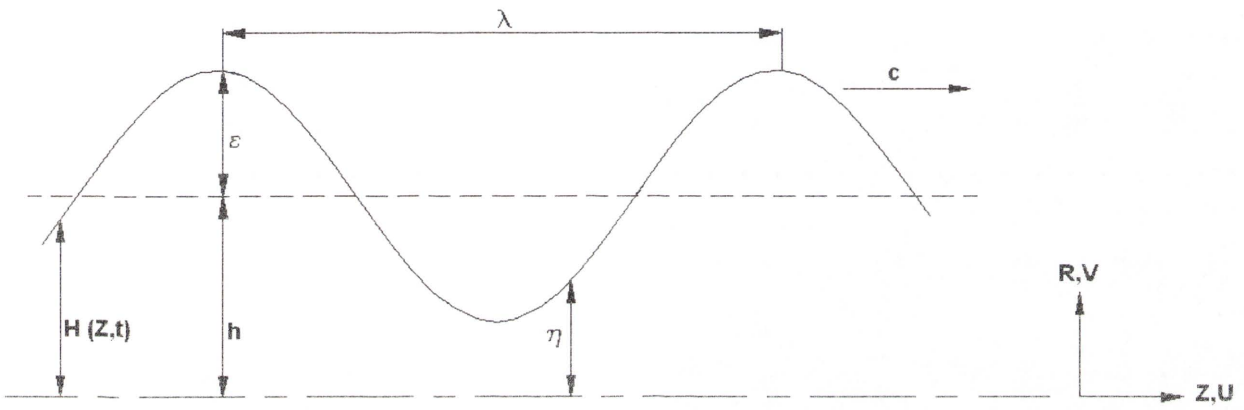

Figure 2.21 Configuration of peristaltic flow in two-dimensional axi-symmetric tube

Figure 2.21 shows the propagation of an infinite sine curve wave which travels along the walls of an axi-symmetric channel. Equation 2.17 would define peristaltic moving boundary according to the periodic wave. In the time-dependent laboratory frame

$$H(Z,t) = h - \varepsilon \cos(\frac{2\pi}{\lambda})(Z - ct) \qquad (2.14)$$

Where

- t is the time.
- h is the mean distance of the wall from the symmetric axis (m).
- ε is the wave amplitude (m).
- λ is the wavelength (m).
- c is the wave speed (m/s).

In the fixed coordinates (Z,R) (the laboratory frame) the flow in the channel is unsteady with a moving boundary as explained above. However, in this work, a new reference frame (z,r) that moves with the wave will be used. This is wave frame. The following transformation formulas relating the two reference frames are

$$z = Z - ct,\ \ r = R, u = U - c, v = V \quad \text{(Transformation formula)} \tag{2.15}$$

In this new reference frame (z,r), the wave frame, the flow will be then steady and travels in the negative z-direction at inlet; the boundary will also be time independent (Xiao et al [23] and Takabatake et al [19])

Here (U, V) and (u,v) identify the velocity component in the laboratory and the wave frame respectively.

The fluid is subjected to a boundary condition formed by the motion of the flexible walls. However, the boundary will be steady, in a non time dependent status.

In the wave frame (now time-independent), the shape of peristaltic wall ($r = \eta(z)$) can be represented by :

$$\eta(z) = h - \varepsilon \cos\frac{2\pi z}{\lambda} \tag{2.16}$$

Horizontal displacement in the laboratory frame is assumed as zero and the fluid velocity components on the wall are

$$u = -c,\ \ v = \frac{\partial \eta(z)}{\partial z} \tag{2.17}$$

Therefore, the boundary conditions on $r = \eta(z)$ for the fluid is derived as

$$u = -c,\ v = \frac{\partial \eta}{\partial z} = -\frac{2\pi\varepsilon}{\lambda} c \sin\frac{2\pi z}{\lambda} \tag{2.18}$$

At the centre line : axi-symmetric conditions are imposed.

CHAPTER 3

METHODOLOGY

3.1 Introduction

Computation Fluid Dynamics (CFD), utilised in this research is a computation tool for simulating fluid dynamics. An isothermal flow model was produced using CFD to replicate previous studies to demonstrate the validity of CFD applications in chapter 4. A non-isothermal flow model will then be utilised to investigate the effect of temperature on peristaltic flow in chapter 5.

This chapter introduces the commercial software package CFD-ACE from the ESI group and its model. The solutions with residual reduction of 4 orders of magnitude and those with residual reduction of 5 orders of magnitude are compared to show the validation of 4-order convergence. The model representing an axi-symmetric steady flow fluid in the wave frame and its boundary conditions imposed at inlet, wall, outlet and axis of symmetry are presented.

In order to obtain accurate data from CFD, grid convergence is used to help ensure that the solutions are valid. The newly generated model was simulated repeatedly with different numbers of grid points in both cases of isothermal and non-isothermal flow. This process is essential to identify an appropriate quantity of grid points in the model.

3.2 Computation Fluid Dynamics (CFD)

Computational Fluid Dynamics, or CFD, uses the commercial software package CFD-ACE from the ESI Group to model the flow of fluids through a processing facility. The package is quite well known, and its validity is assumed to have been adequate. In addition, results from some isothermal cases of this study will be compared with previous work from the literature for validity in chapter 4. The numerical scheme is the Finite Volume Method, and the coupled system of the governing equations is solved iteratively for the two velocity components, temperature and pressure.

4-order convergence is adapted (iteration residuals decrease by 4 orders of magnitude). This is deemed adequate; a comparison of the solutions with residual reduction of 4 orders of magnitude and those with residual reduction of 5 orders of magnitude shows very small difference. Table 3.1 below shows that there are very small changes between results from 4-order convergence and 5-order convergence.

Table 3.1 Comparison of changes in axial velocity and pressure drop with different numbers of order convergence.

	$\alpha = 0.25,\ \phi = 0.5,\ a_1 = -0.034\ ^{\circ}C^{-1}$ (Non-isothermal flow) Residual decrease		
	by 3-orders of magnitude	by 4-orders of magnitude	by 5-orders of magnitude
ΔP (Pa)	26.916	26.760	26.707
u (m/s)	-0.224295	-0.224214	-0.224208

* ΔP (Pa) per wavelength, u (m/s) at located in 6.5 wavelengths from inlet on the centre line

3.2.1 Modelling

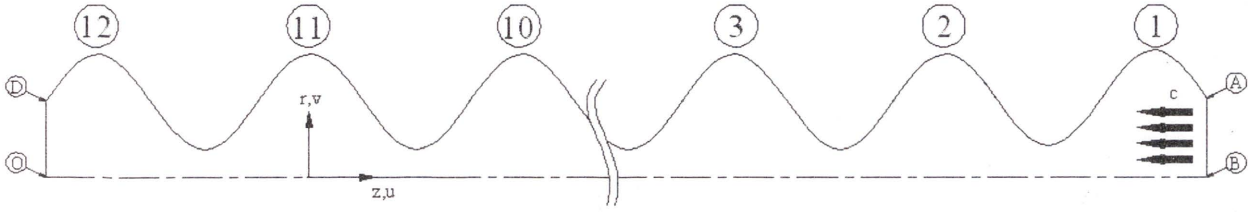

Figure 3.1 Computational model of the peristaltic flow.

The model represents an axi-symmetric steady flow fluid in the wave frame, consisting of 12 cycles of peristaltic waves. Key dimensions of the flow field are shown in Figure 3.2.

The boundary conditions in the wave frame are follows:

- At inlet AB: uniform negative axial velocity u = -c; zero radial velocity v = 0; uniform temperature T = 30 °C . This gives a zero flow rate in the laboratory frame. The exception is in section 5.2.1.2 where a non-zero flow rate in the laboratory wave is prescribed; then a non uniform u-profile will be imposed at the inlet.
- Along the wall: constant negative axial velocity u = -c; radial velocity is prescribed as function of z, $v=-\frac{2\pi\varepsilon}{\lambda}c\sin\frac{2\pi z}{\lambda}$ (see (2.20)); uniform temperature T = 30 °C .
- At outlet OD: uniform pressure P = 0 (Pa) and temperature are imposed , namely P=0 (gauge) and T = 30 °C . However, the thermal condition here applies only on those sections of the boundary where there is inflow; if there is outflow, the constant temperature condition will be ignored, and the software calculates the temperature instead.
- At the centre line: axi-symmetric conditions are imposed , namely $\frac{\partial u}{\partial r}=0,\frac{\partial T}{\partial r}=0$ and $\frac{\partial v}{\partial r}=0$.

All results in this thesis are from the middle part of the flow domain (around section number 7). Periodicity has been obtained in this middle part of the flow domain; in other words, flow pattern is no longer affected by the velocity profile imposed at the inlet.

A geometry in CFD software package designed as a form of a sine curve is built corresponding to values of α , ϕ .

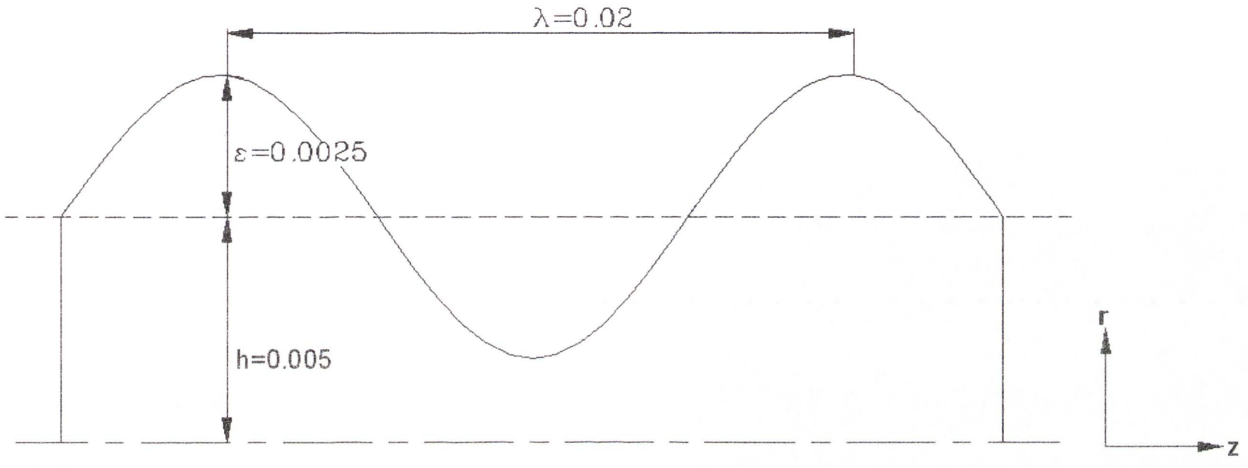

Figure 3.2 Dimension for the geometry (unit: m): $\alpha = 0.25, \phi = 0.5$.

Figure 3.2 shows the dimensions for the geometry utilised in this research.

In chapter 4, the comparison with isothermal results from the literature is presented. The amplitude ratio ϕ and wave number α are varied but the flow rate (in the laboratory frame) is kept constant at zero.

The flow velocity imposed at the inlet is obtained from the desired value of the Reynolds number ($\mathrm{Re} = \left(\frac{hc}{v}\right)\alpha$).

3.2.2 CFD-ACE applications

For the implementation of a model simulating peristaltic flow with power-law fluid, two modules, Flow and Heat transfer are selected and used. Mathematical equations are used in those modules in order to solve problems. A Flow module is used for solving any fluid flow problems, pressure field calculations and mass flow calculations. It provides detailed information about the flow field such as vector plots, used to depict the magnitude and direction of the flow velocity. Streamlines traces can also be provided.

3.2.2.1 Flow module

The flow module is a main module which is used in most simulations. The solution of the velocity field by solving for the z, r and θ momentum equations in cylindrical Coordinate and pressure field by solving the pressure correction equation will be obtained by activating the flow module. Conservation of mass is implemented by the time rate of change of mass in a control volume.

3.2.2.2 Heat transfer module

Heat transfer analysis is performed by the heat transfer module which is an integral part of the CFD-ACE-Solver. This module is used for all situations where heat transfer processes may affect a significant impact on the final solution. Activating the heat transfer module implies the solution of the total enthalpy form of the energy equation.

1) Thermal Field Calculations

The heat transfer module is often used for determining the thermal field within a given geometry. The energy equation (total enthalpy) can be used to determine the heat transfer characteristics of system by solving in the heat transfer module.

Two types of wall boundary conditions are available for the heat transfer module. The first is for the boundary condition itself and the second is the ability to add a heat source to the cells adjacent to the wall boundary condition.

For the wall boundary condition, the heat transfer modules need to know the method to set the heat flux for each cell face on the boundary condition patch. There are various methods to specify the information and six methods are available. In this work, only the isothermal condition (constant temperature) and axi-symmetric condition (on the axis of symmetry) will be used.

3.2.2.3 Control Panel

All of the model's physical and numerical settings are made through this panel. The control panel consists of various panels such as problem type (PT), model option (MO), volume condition (VC) and boundary condition (BC). The control panel is designed to provide an environment for problem setup and this chapter will only show the information that is pertinent to the current simulation. Two significant panels within the control panel will be introduced.

1) Volume Condition (VC)

The volume condition panel is to set the material properties and source terms on a volume-by-volume basis. For this study, a 2D grid system is used with every structured face as a separate volume condition. Volume conditions must be activated before volume conditions are set.

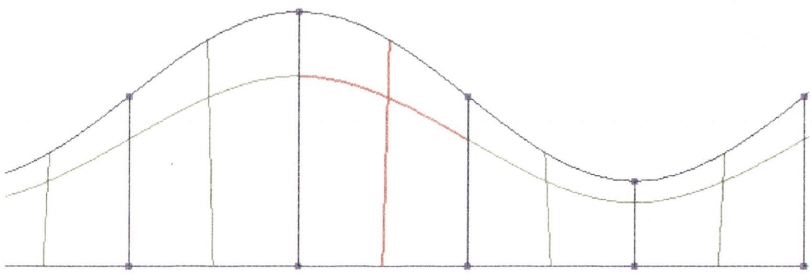

Figure 3.3 Example of structured face and an activated volume condition (red)

Fluid properties are set in this panel. Fluid properties have been selected corresponding to oil fluid properties which are adopted from Frene [7]. The properties are assumed as following.

Density	$\rho = 860\, kg / m^3$
Specific heat capacity	$c = 2000\ J/(Kg \cdot °C)$
Thermal conductivity	$k = 0.13W /(m \cdot °C)$
Dynamic viscosity	μ =0.0397 $Kg/(m \cdot s)$

(a)

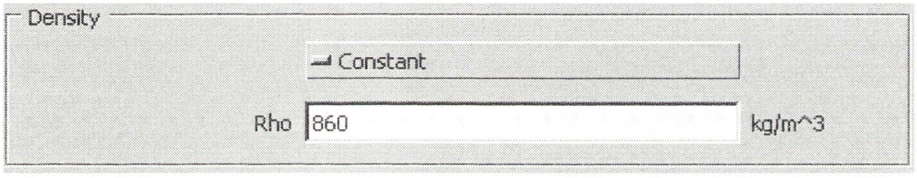

(b)

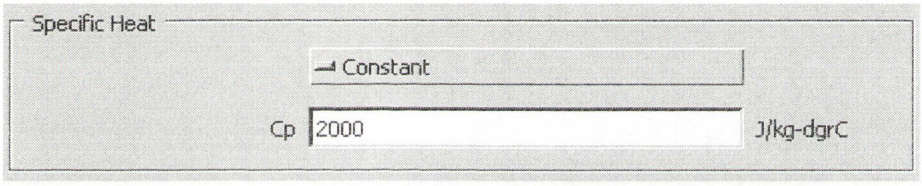

(c)

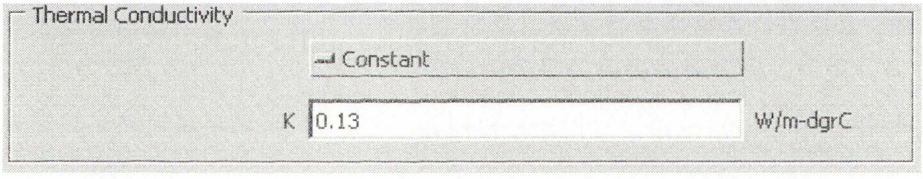

Figure 3.4 Input for density (a), specific heat capacity (b) and thermal conductivity (c)

In this work, the value of the Reynolds number is defined in the condition of Newtonian (n=1) and isothermal flow ($a_1 = 0\,°C^{-1}$).

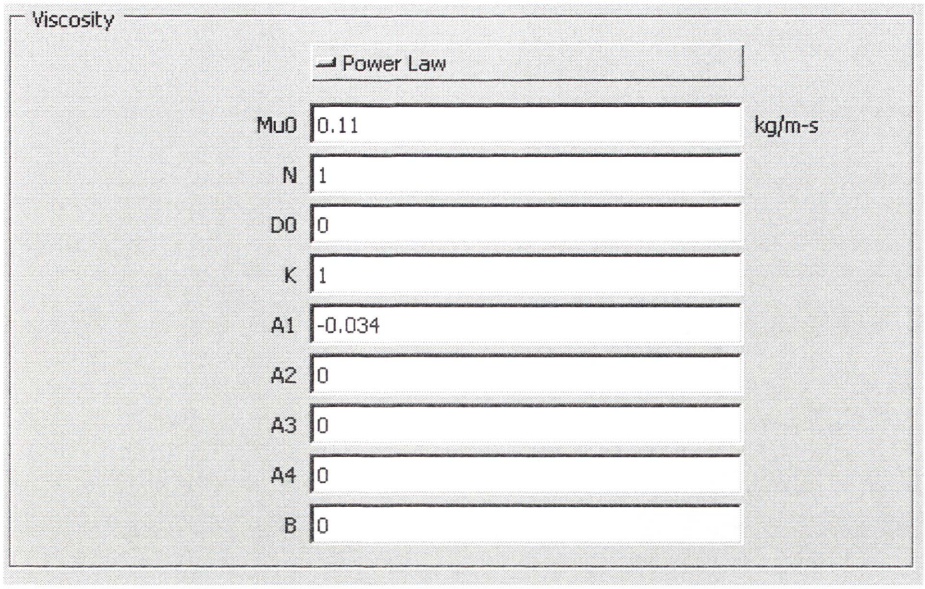

Figure 3.5 Example of inputs for viscosity properties (where Mu0 is the zero shear rate viscosity (μ_0), N is power-law index (n), K is the flow consistency index, A1 is exponential coefficient of temperature dependent viscosity (a_1) and A2, A3,A4 and B are set as zero in this work.

2) Boundary Condition (BC)

The inlet subtype allows specifying the velocity direction, temperature, pressure and the total mass flow rate to be applied over the entire boundary patch. The computational boundary conditions are set in this panel. In this research, every structured edge is a separate boundary condition.

When the boundary condition (BC) is selected, the boundary condition panel containing BC Type and BC Setting appears.

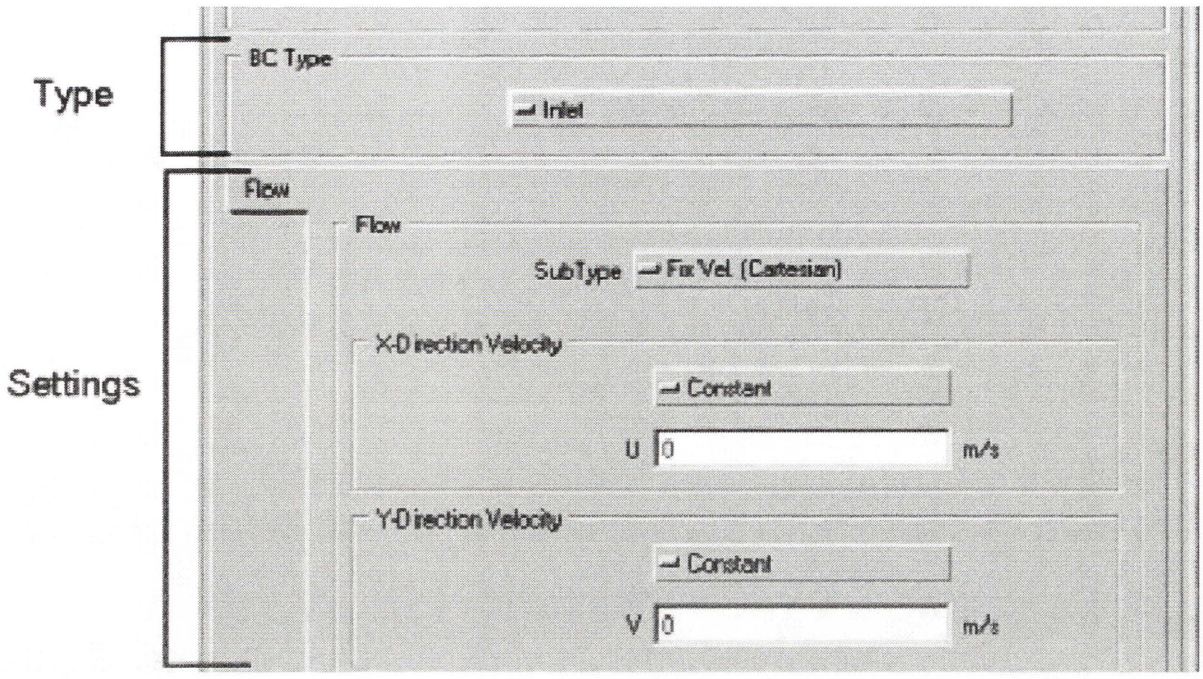

Figure 3.6 Illustration of BC type and BC settings inputs (in CFD-ACE terminology, X-direction and Y-direction are the axial (z) and radial (r) direction respectively in this work)

In the Figure 3.6, the type of boundary condition is determined in the BC type section. In this work, four types of boundary conditions, inlet, outlet, wall and symmetry were selected. In the boundary settings, values of velocity, pressure and temperature etc can be specified.

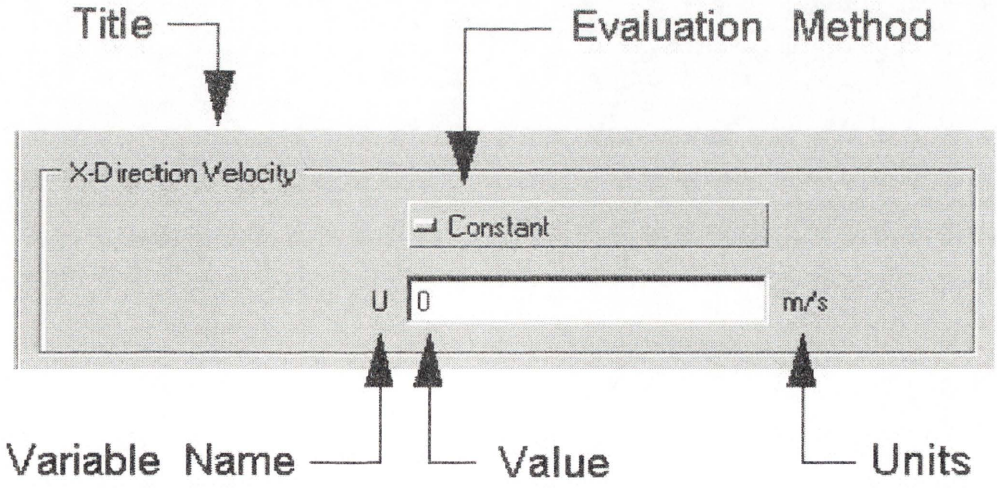

Figure 3.7 Boundary value regions (in CFD-ACE terminology, X-direction is the axial direction, z in this work)

Figure 3.7 shows the regions for applying boundary values. All of the boundary value regions contain a title that describes the boundary value. The constant option and the parametric option can be selected in evaluation method and the constant option ensures that every boundary face on the boundary condition patch will have the same constant values specified.

For applying equations of the boundary condition (2.20) for the wall, the parametric input panel will be utilized. The parametric input panel is to enter values for parameters which are utilized in several inputs for specification of variables such as sine, cosine, tan, time and coordinates etc.

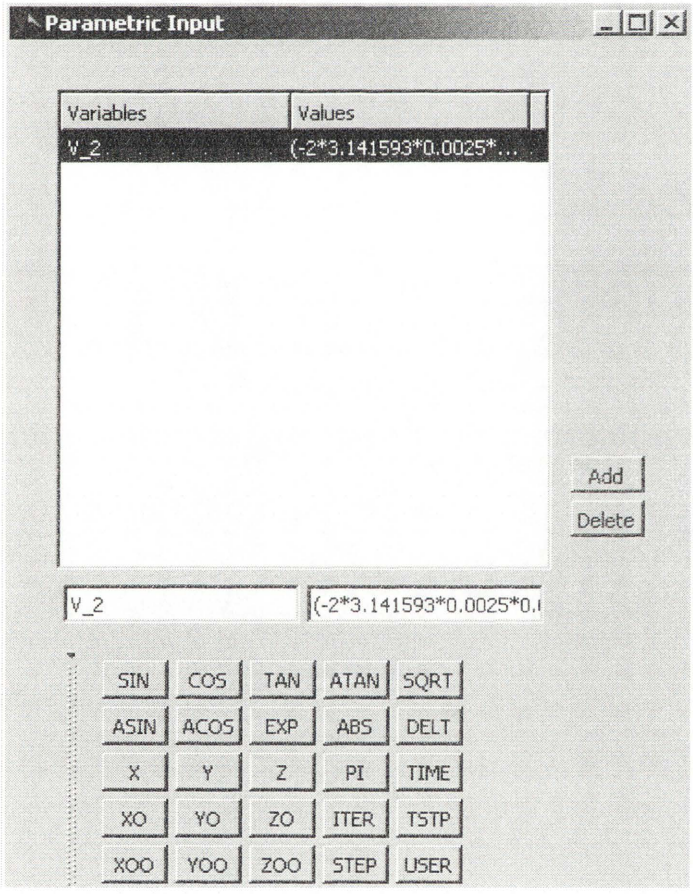

Figure 3.8 Input for the parametric input panel

Examples of boundary settings for inlet, outlet, wall and symmetry are shown in the Figure 3.9.

(a)

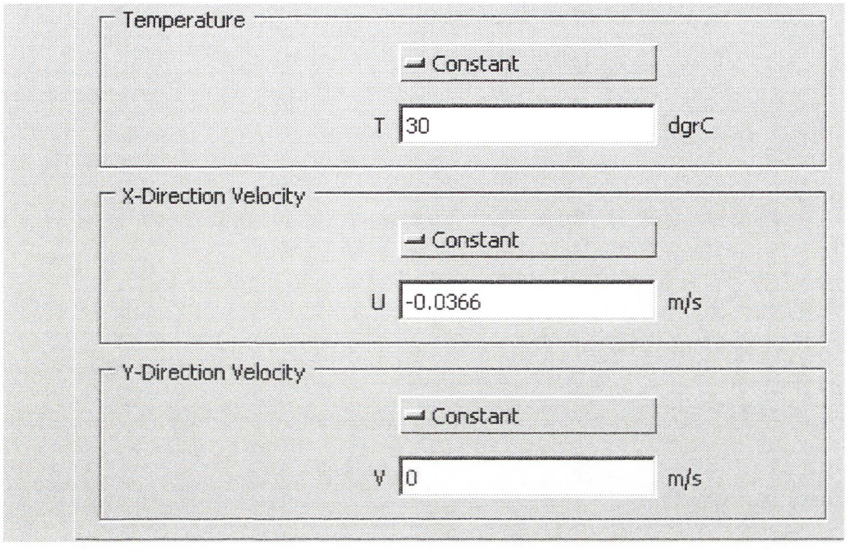

(b)

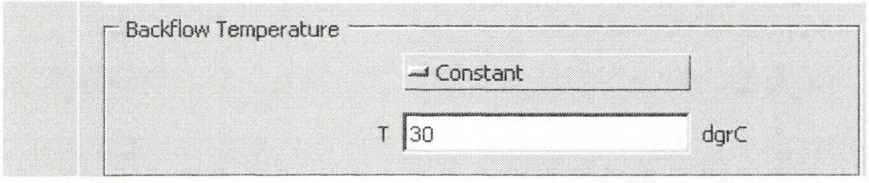

(c)

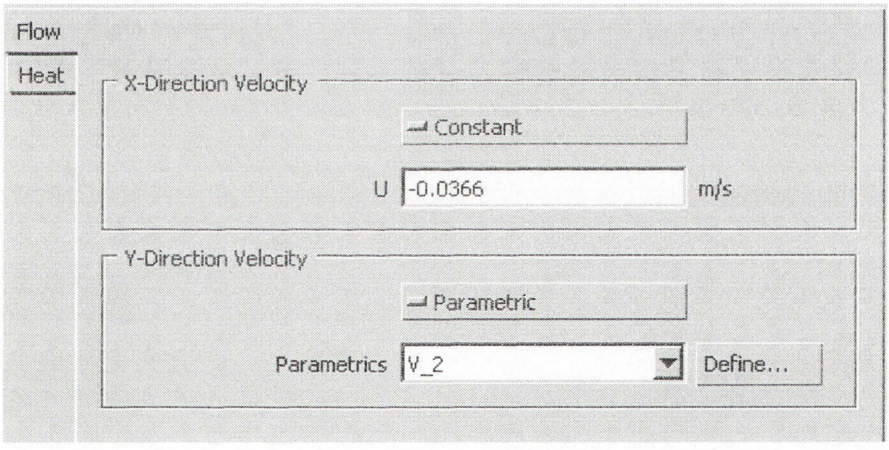

(d)

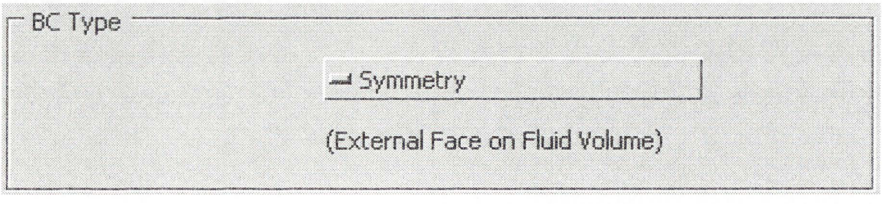

Figure 3.9 Inputs for (a) Inlet, (b) Outlet, (c) Wall and (d) Symmetry (in CFD-ACE terminology, X-direction and Y-direction are the axial (z) and radial (r) direction respectively in this work)

3.2.2.4 CFD-VIEW

CFD-VIEW is part of a suite of CFDRC (CFD Research Corporation) computer program that analyses computational fluid dynamics (CFD). One of the challenges in computational modelling is that each simulation generates a large volume of data that must be reduced to extract useful information that can be applied to engineering problems. To aid in the data reduction process, CFD-VIEW is the 3 D graphical post-processor.

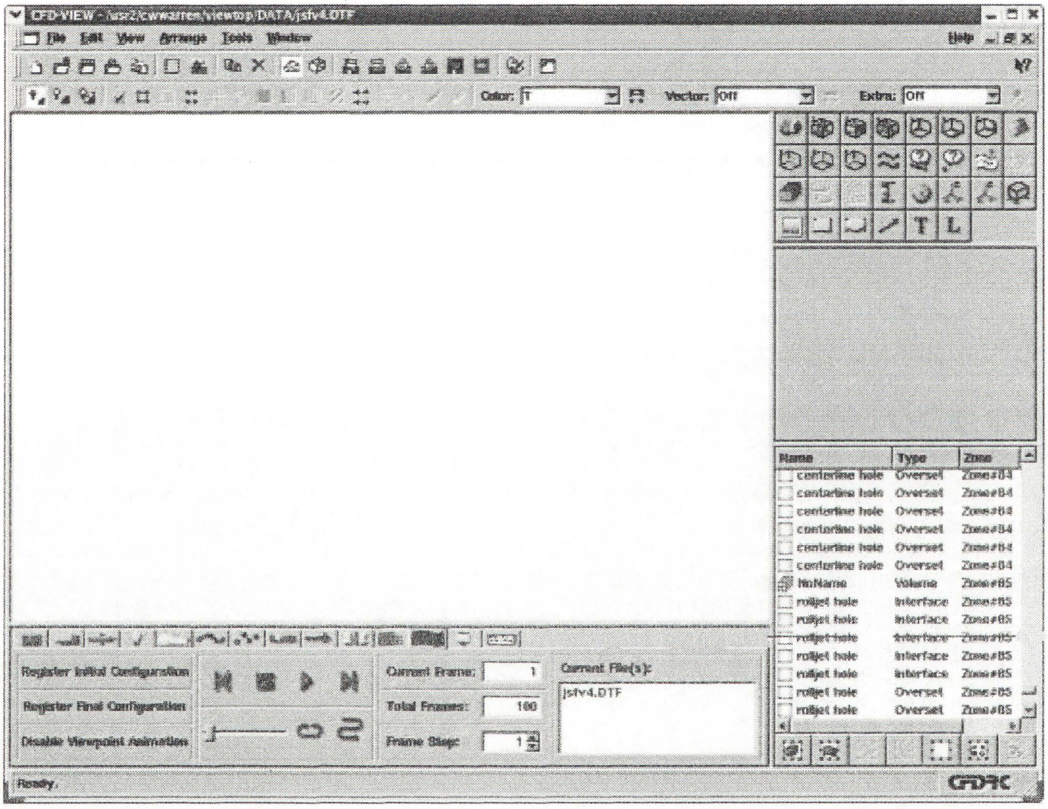

Figure 3.10 Window of CFD-VIEW

CFD-View supports the data format, the Data Transfer Facility (DTF) that is generated in CFD-ACE. DTF is a database mechanism that merges all of the codes in the CFD-ACE environment, including CFD-VIEW. The DTF allows simulation and problem data to be placed in a single file.

3.2.2.5 CFD-GEOM

CFD-GEOM is a comprehensive interactive geometry and grid generation system for computational fluid dynamics analysis. CFD-GEOM offers a fully integrated Non-Uniform Rational B-Spline (NURBS) geometry engine with multi-block structured, multi-domain unstructured, and multi-element hybrid grid systems. CFD-GEOM is designed for fast intuitive geometry and grid creation.

3.3 Grid Convergence.

This process, grid convergence, is essential for identifying appropriate quantity of grid points in a model in CFD. Grid points are utilised in generating meshes in a model. A best model will be obtained from this process.

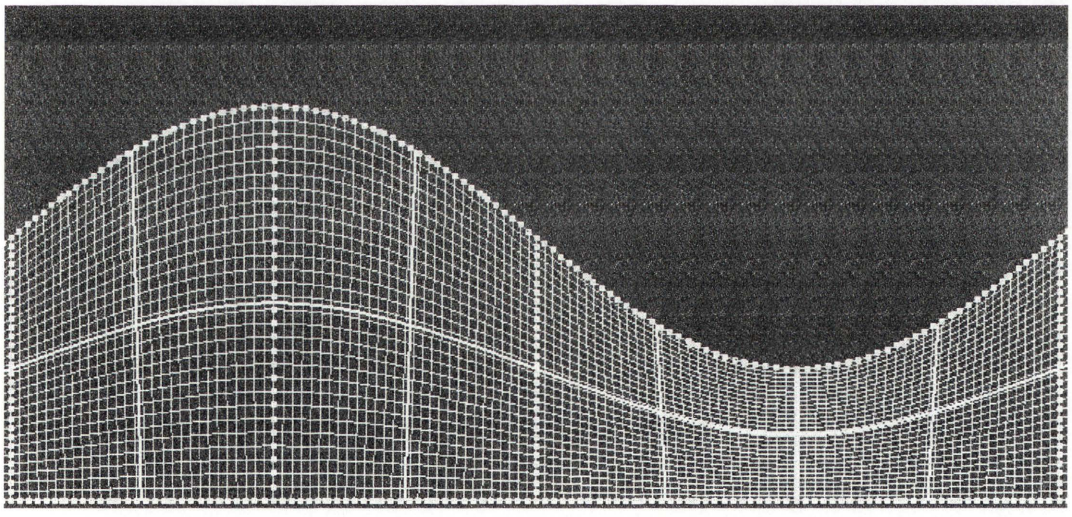

Figure 3.11 Grid points and meshes in a CFD model.

A various number of grid points are applied onto the models. Theses models are simulated with the same volume conditions, boundary conditions and geometry. Then pressure change per wavelength and velocity are collected in every model.

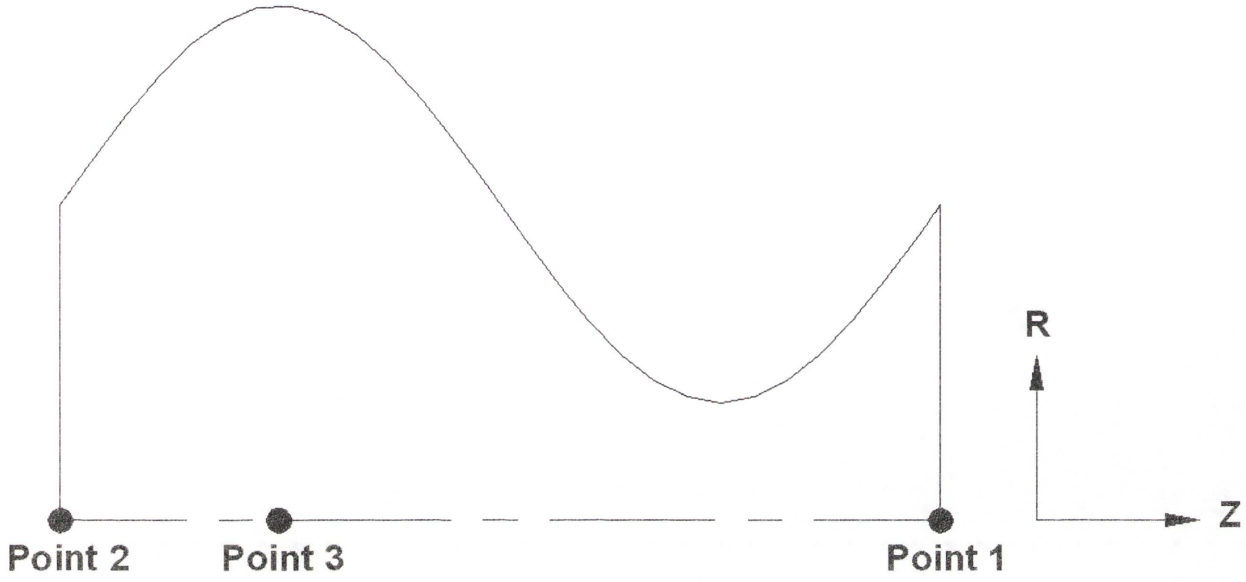

Figure 3.12 Arrangement of points to measure pressure change and velocity

Two points (1 and 2) are placed at each end of a cycle in order to obtain a value of pressure change. Point 3 is placed in order to obtain a value of the velocity at the centre axis of the crest section. The values of pressure change and velocity in each model are compared to ascertain grid convergence.

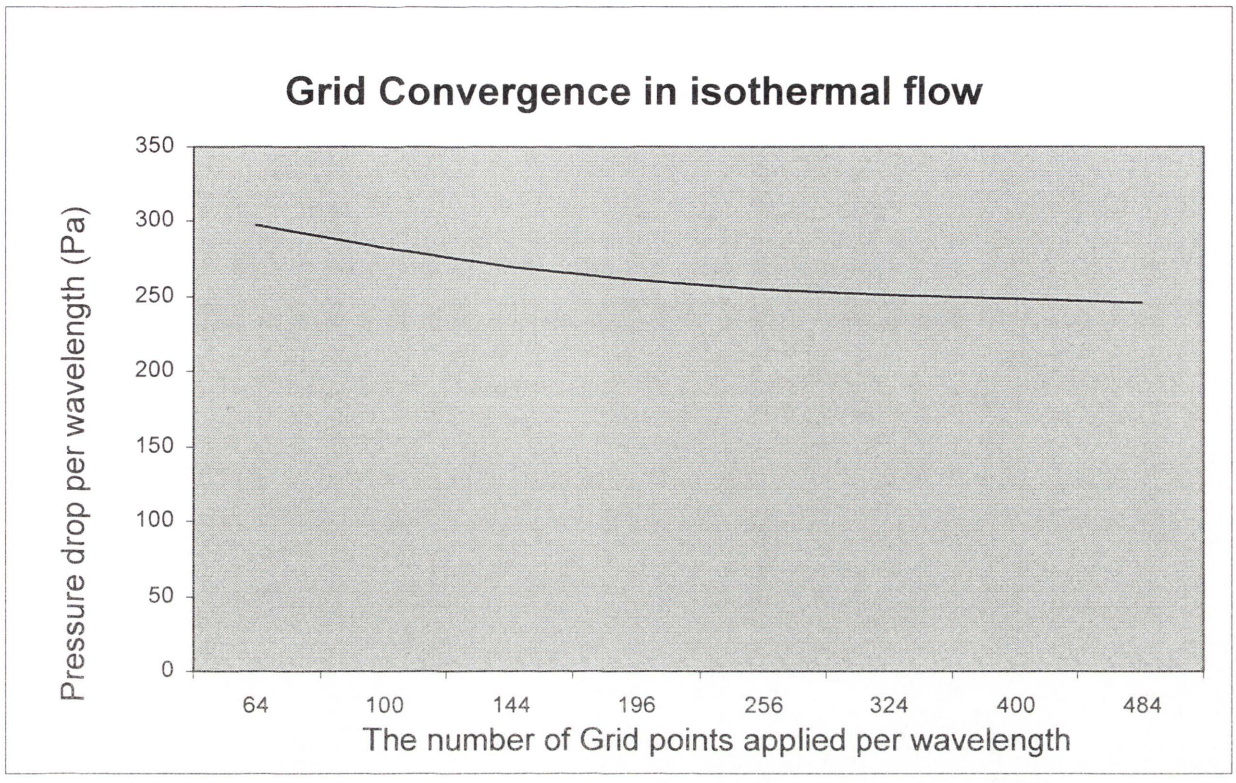

Figure 3.13 Comparison of pressure drop (Pa) per wavelength with the number of grids applied in a wave cycle (for Newtonian and isothermal flow; Re=1)

Figure 3.13 shows the comparison of pressure drop (Pa) per wavelength in conditions of Newtonian and isothermal flow. The pressure drop remains nearly constant in range of 324 – 484 of grids.

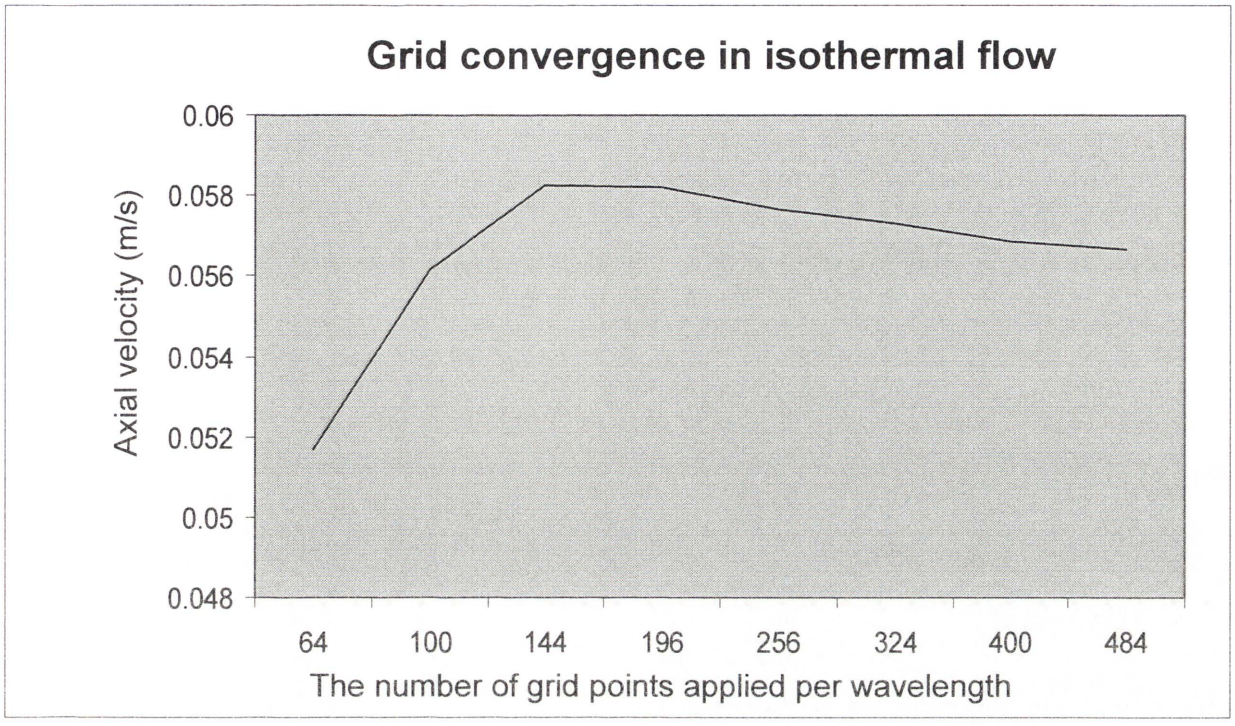

Figure 3.14 Comparison of axial velocity (m/s) at point 3 of Figure 3.12 with the number of grids applied in a wave cycle (for Newtonian fluid and isothermal flow; Re=1)

As it can be seen in Figure 3.14, the velocity profile stays almost unchanged with 400 or more grid points used. It is revealed that the model with 400 or 484 grids is adequate to produce appropriate results in these conditions, Newtonian fluid and isothermal flow.

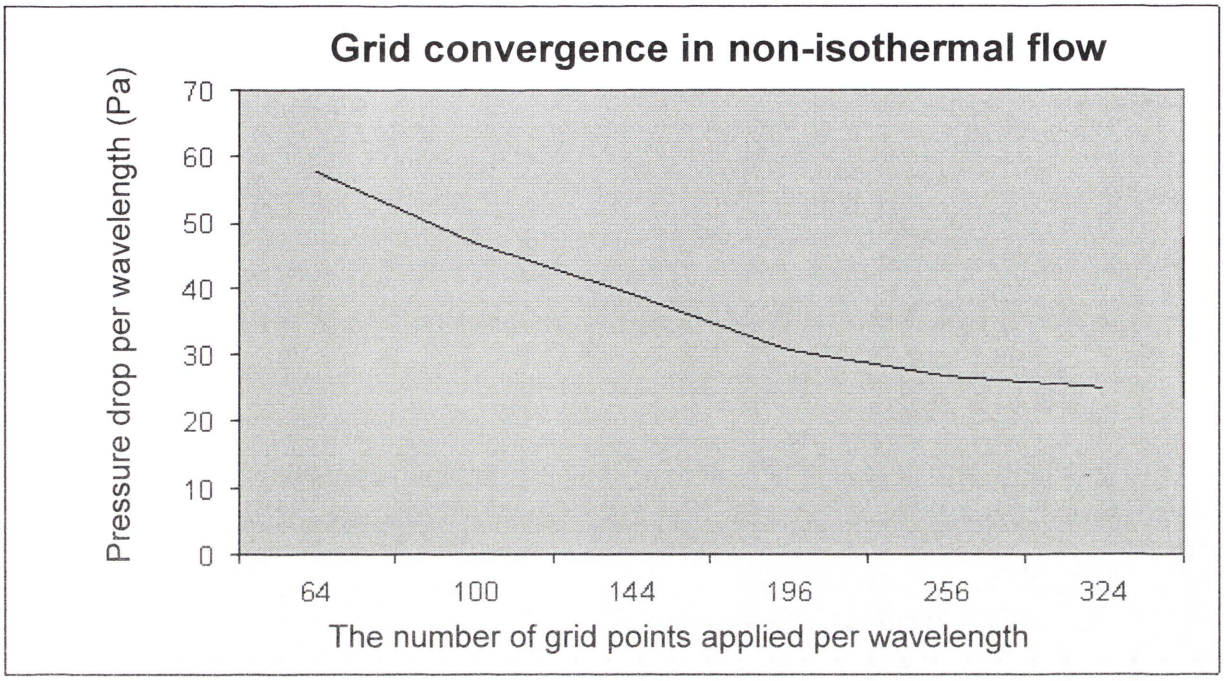

Figure 3.15 Comparison of pressure drop (Pa) per wavelength with the number of grids applied in a wave cycle (for Newtonian fluid and non-isothermal flow; Re=1)

In Figure 3.15, the pressure drop profile decreases significantly in the range of grids between 64 and 196. However, pressure drop is converged at approximately 24 (Pa) in the range of grids between 256 and 324.

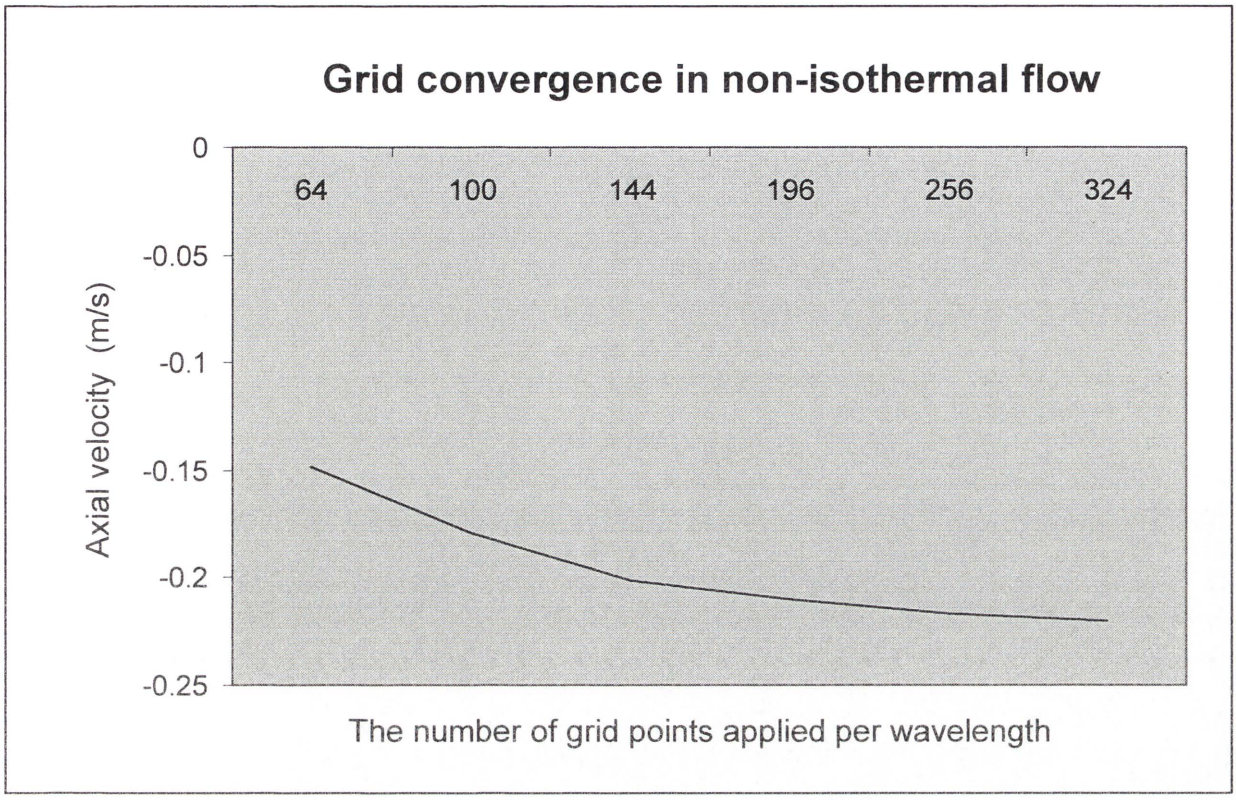

Figure 3.16 Comparison of velocity (m/s) at point 3 of Figure 3.12 with the number of grids applied in a wave cycle (for Newtonian fluid and non-isothermal flow; Re=1)

The velocity profile stays virtually unchanged in the range of grids between 256 and 324. An appropriate model is built by applying 324 grid points per a wave cycle in these conditions, Newtonian fluid and non-isothermal flow.

Temperature change per wave cycle in the condition of non-isothermal flow is to be insignificant in this study. However, the pressure drop per wave cycle and velocity are affected by the effect of temperature. It is revealed that even though temperature was not itself changed significantly but it still affects the other factors.

CHAPTER 4

ISOTHERMAL FLOW

4.1 Introduction

Peristaltic flow has been previously investigated and the study of peristaltic flow has been developed during the past few decades. The initial step in this study is to produce an isothermal flow model that is comparable to this previous work. This will provide a benchmark that future results can be compared to. The results shown in this chapter give comparison between these previous works and the newly generated computational model.

The following discusses various flow properties and how they compare with previous works. These include velocity profiles, streamline patterns and the Reynolds number.

4.2 The max and min axial velocity in simulation results

A CFD model was produced with an axi-symmetric tube using variables of $\alpha = 0.01, \mathrm{Re} = 0.01$ and varying amplitude ratio (ϕ). This was done in order to provide a comparison with data produced by Shapiro et al [18] and Xiao et al [23]. The following section demonstrates the similarities of maximum and minimum velocities.

4.2.1 Results

Comparison of maximum and minimum velocity

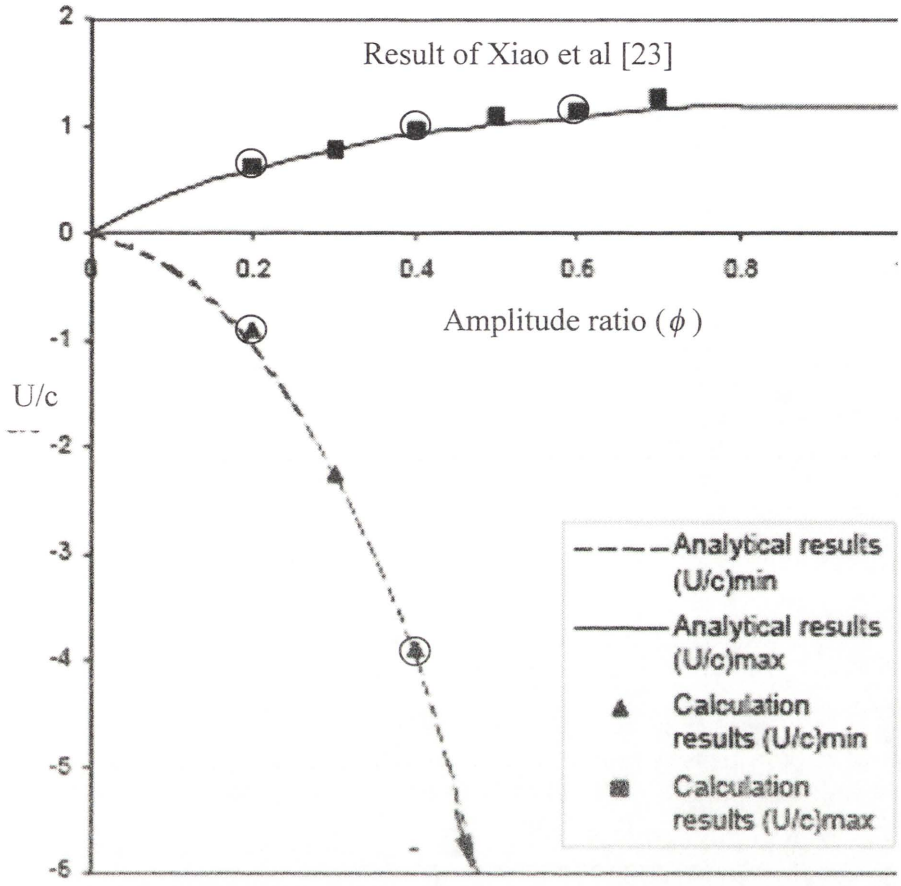

Figure 4.1 The comparison of the max and min axial velocity in simulation result with α=0.01 and the Reynolds number = 0.01 from the results of Xiao et al [23] and of Shapiro et al [9] (■ and ▲, compute results of Xiao, lines (solid and dashed) from Shapiro, as presented in Xiao' work, ○ from this work).

For verifying the mechanism, a few standard tests are simulated. An initial test is set at the Reynolds number =0.01 and wave number (α=0.01) with various values of amplitude ratio.

The new computational models was generated with α =0.01 verse ϕ =0.2, 0.4 and 0.6. The wave speed (c) was defined by the Reynolds number with mean distance (h) and kinematic viscosity (ν) and wave number.

Here h = 0.0004167 m

ν =0.000127906 m^2/s (when a_1 is uniform as 0)

c =-0.307 m/s (for the Reynolds number = 0.01)

		Results of Xiao et al [23]	Present work	Relative difference [%]
Maximum Velocity (U/c)				
α =0.01	ϕ =0.2	0.66	0.64	3.03 %
	ϕ =0.4	0.92	0.94	2.17 %
	ϕ =0.6	1.27	1.31	3.15 %
Minimum Velocity (U/c)				
α =0.01	ϕ =0.2	-0.96	-0.94	2.08 %
	ϕ =0.4	-3.91	-3.45	11.76 %

Table 4.1 Comparison of Xiao's results (maximum and minimum velocity) and the present work for Re = 0.01 and $\bar{Q}/\pi ch^2 = 0$ ($\bar{Q}/\pi ch^2$ = the dimensionless time-average flow rate for axi-symmetric flow)

For maximum velocity, the present computational model produced 0.65, 0.94 and 1.31 at amplitude ratio 0.2, 0.4 and 0.6 respectively and minimum velocity were obtained as -0.94 and -3.45 at amplitude ratio 0.2 and 0.4 respectively.

To compare the present work with the result of Xiao et al [23], approximate values of maximum and minimum velocities at the result of Xiao et al [23] were required.

As the result of Xiao et al [23] for maximum axial velocity in Figure 4.1 was enlarged, the corresponding results produced by Xiao et al [23] at ϕ =0.2, 0.4 and 0.6 can be read off to be 0.66, 0.92 and 1.27 respectively. (On the other hand, we obtained 0.65, 0.94 and 1.31 at ϕ =0.2, 0.4 and 0.6 respectively)

With enlarging the results of Xiao et al [23] for minimum axial velocity in Figure 4.1, the corresponding results can be read off to be -0.96 and -3.91 at ϕ =0.2 and 0.4 respectively. (whereas here we obtained -0.94 and -3.45)

It can be seen clearly that the results produced by the new computational model are comparable with the results produced by Xiao et al [23] and Shapiro et al [18]. The maximum and minimum velocities show identical trends and magnitudes.

The effect of the Reynolds number on the dimensionless velocity $\left(U/c\right)_{\max}$

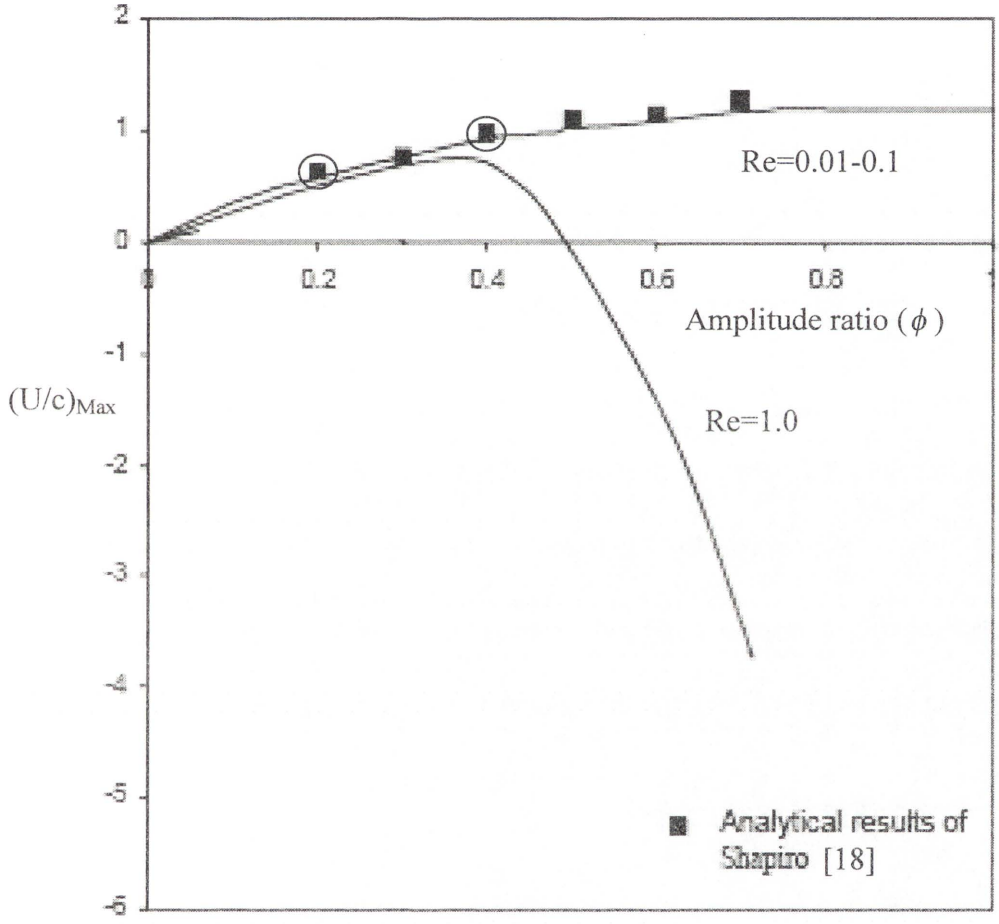

Figure 4.2 The effect of the Reynolds number on the maximum U velocity (U/c) of axis for α =0.01, $\bar{Q}/\pi ch^2 = 0$ and different values of amplitude ratio from the results of Xiao et al [23] (◯the results from this work).

The effect of the Reynolds number is considered. Xiao et al [23] proved the effect of the Reynolds number with for α =0.01 and different values of amplitude ratio as Figure 4.2.

As the flow and boundary conditions are considered, the maximum axial velocity (U/c) at $\phi = 0.2$ and $\phi = 0.4$ with Re=0.1 is obtained as the value of 0.652 and 0.945.

		Results of Xiao et al [23]	Present work	Relative difference [%]
Maximum Velocity (U/c)				
α =0.01	ϕ =0.2	0.66	0.65	1.52 %
	ϕ =0.4	0.92	0.95	3.26 %

Table 4.2 Comparison of Xiao's results and the present work for α =0.01 verse ϕ =0.2, 0.4 and 0.6 with Reynolds number = 0.1 and $\bar{\ell} = 0$

With enlarging Figure 4.2, the corresponding result from Xiao et al [23] at ϕ =0.2 and 0.4 can be read off to be 0.66 and 0.92 respectively, whereas here we obtained 0.652 and 0.945. The agreement is therefore good.

The Figure 4.2 and the results from this work show a fairly good agreement with the numerical results of Xiao et al [23], corresponding to $\alpha = 0.01$, zero flow rate.

4.3 The effect of the Reynolds number on the streamline pattern

The next step was to compare the effect of the Reynolds number on a model corresponding to $\phi = 0.7$, $\alpha = 0.01$. The Reynolds number is defined as $\mathrm{Re} = (\frac{ch}{v})\alpha$ (Shapiro et al [16]). It represents the ratio of inertial and viscous terms when peristalsis acts as a pump.

Streamlines are plotted with different value of the Reynolds number in order to compare the results of Xiao et al [23].

The results obtained are compared with the results of Takabatake et al [20] and Xiao et al [23]. This is a standard test problem simulated for the effect of the Reynolds number on the streamline patterns in the wave frame.

4.3.1 Results

The comparison of numerical results

Results of Xiao et al [23] (Wave Frame) Present work

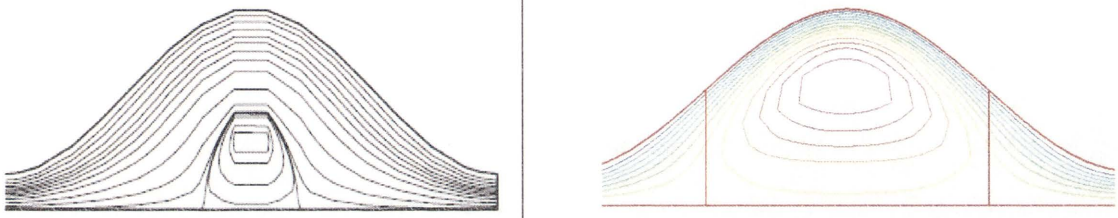

Re = 0.01

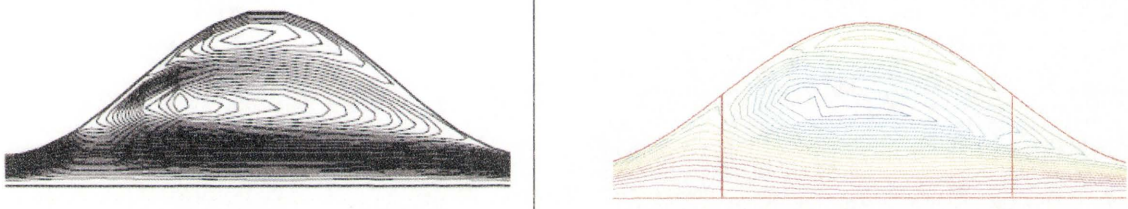

Re = 10

Figure 4.3 The comparison of the effect of the Reynolds number on the streamline patterns in the wave frame for $\alpha = 0.01$, $\phi = 0.7$ and $\bar{Q}/\pi c h^2 = 0$

With the Reynolds number at 0.01, both results have a circulation at the middle of crest. The arrangement of streamlines in the upper side of circulation is denser in both results. However, in the present work, a circulation stays higher and is wider in comparison with the result of Xiao et al [23]. It can be explained that a less quantity of mesh was possibly utilised in the results of Xiao because the streamline in the results of Xiao is angular.

With the Reynolds number at 10, new circulation occurs on the top of the crest section and is squeezed from the wall and the other circulation at the bottom. The two circulations are created and pressed on to the left side of wall.

Figure 4.3 demonstrates a good comparison between the new computational model and previous data. It suggests that in the case of changing the Reynolds number the results from the new model is supported.

4.4 The effect of the Reynolds number on the streamline patterns for $\frac{\bar{Q}}{\pi c h^2} = 0.6$

In the paper, 'Peristaltic pumping in circular cylindrical tubes: a numerical study of fluid transport and its efficiency' J. Fluid Mech [9], the trapping phenomenon is described with a wide range of the Reynolds numbers. Trapping phenomenon was theoretically studied by Jaffrin et al [14] in a two-dimensional channel flow. Takabatake and Mori [20] studied the flow pattern when the trapping occurred at finite Reynolds numbers. The dimensionless time-average flow rate ($\frac{\bar{Q}}{\pi c h^2}$) for axi-symmetric flow was defined in their paper where $\bar{Q}$ is the time-mean rate of volume flow. This $\frac{\bar{Q}}{\pi c h^2}$ indicates the dimensionless mean-volume flow per unit area.

The next model that will be produced shall incorporate this new form of inlet boundary condition. It shall display a variable inlet flow. A comparison shall be made with this new model.

4.4.1 Modification of Inlet condition for the case of $\frac{\bar{Q}}{\pi c h^2} = 0.6$

To apply a same condition ($\frac{\bar{Q}}{\pi c h^2} = 0.6$) into CFD-ACE, the parametric option in CFD-ACE on the inlet is used.

Firstly, the flow rate, q in wave frame is identified.

The rate of fluid flow in the laboratory frame is given by (Hayat et al [4]),

$$\bar{Q} = \int_0^h U(Z,R,t)dY \tag{4.1}$$

Where h is the position of the channel wall,

The rate of fluid flow in the wave frame is given by

$$q = \int_0^h u(z,r)dy \tag{4.2}$$

With the help of Transformation formula (2.16), the rate of fluid flow in the laboratory frame for the 2-dimensional model will be

$$\bar{Q} = q + ch \tag{4.3}$$

The dimensionless time-average flow rate $\bar{\ell}$, in the laboratory fame for axi-symmetric channel is defined as follows (from Xiao et al [23])

$$\frac{\bar{Q}}{\pi h^2 c} = \frac{q}{ch^2\pi} + (1 + 0.5 \times \phi^2) \tag{4.4}$$

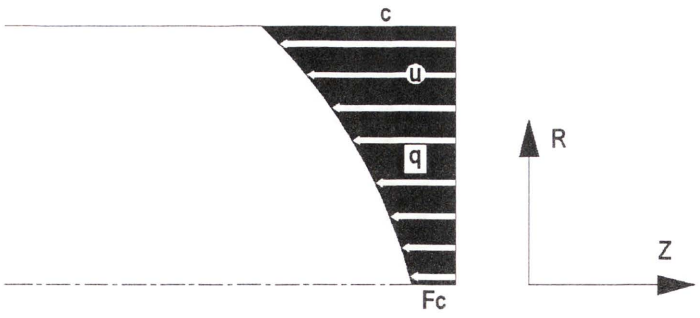

Figure 4.4 The flow rate q and u profile

The flow rate q is shown in the Figure 4.4. The flow rate q will be utilised as follows :

$$\frac{\bar{Q}}{\pi h^2 c} = \frac{q}{ch^2\pi} + (1 + 0.5\phi^2) \tag{4.5}$$

$$\frac{q}{\pi h^2 c} = \frac{\bar{Q}}{\pi h^2 c} - (1 + 0.5\phi^2) \tag{4.6}$$

To apply same applications into the inlet, the value of q is needed. The value of $\frac{\bar{Q}}{\pi h^2 c}$ is indicated as 0.6 and the amplitude ratio is 0.7 in this case.

Therefore,

$$\frac{q}{\pi h^2 c} = 0.60 - (1 + 0.5 * 0.7^2) \Rightarrow q = -0.645 \times \pi \times 0.041667^2 \times 3 \text{ when } h = 0.041667m, c = 3m/s$$

(Condition for boundary)

$$\therefore q = -0.011\ {}^{m^3}/_{s} \tag{4.7}$$

As it can be seen in Figure 4.4, a velocity profile varies in a quadratic across the inlet area. It will be expressed as follows

$$u = ar^2 + b \tag{4.8}$$

When r = 0, u would be Fc (Referred to Figure 4.4)

$$b = Fc \quad \therefore u = ar^2 + Fc$$

When r =h, u would be c

$$c = ah^2 + Fc$$

$$\therefore a = \frac{c - Fc}{h^2} \tag{4.9}$$

In this occasion, h and c is given by 0.041667 m and c is - 3 m/s respectively.(c is a condition for inlet) Therefore, the invariable a will be defined as $a = 1727.97(1 - F)$.

The u profile varies in a quadratic. The flow rate q will be obtained from the following equation.

$$q = \int_0^h 2\pi r u \, dr \tag{4.10}$$

$$q = \int_0^h \left[10857.17(F-1)r^3 - 18.85Fr\right] dr \tag{4.11}$$

$$q = \left[\frac{1}{4}10857.17(F-1)r^4 - 18.85Fr^2\right]_0^{0.041667} \tag{4.12}$$

$$q = \left[\frac{1}{4}10857.17(F-1)0.041667^4 - \frac{18.85}{2}F0.041667^2\right] \tag{4.13}$$

As the value of q (4.6) implies to (4.12), the value of F will be obtained as follows

$$-0.011 = \left[0.008181361(F-1) - 0.01636F\right]$$

$$F = 0.3446$$

The formula of u velocity profile in inlet can be defined as below.

$$u = -1132.513r^2 - 1.0338 \tag{4.14}$$

When $c = -3m/s$ (Condition for inlet)

$$h = 0.041667m$$

When the u velocity profile (4.14) is applied, the result of the dimensionless time-average flow rate $\frac{\bar{Q}}{\pi c h^2}$ is gained.

4.4.2 Results

The comparison of numerical results

Results of Xiao et al [23] (Wave Frame) Present work

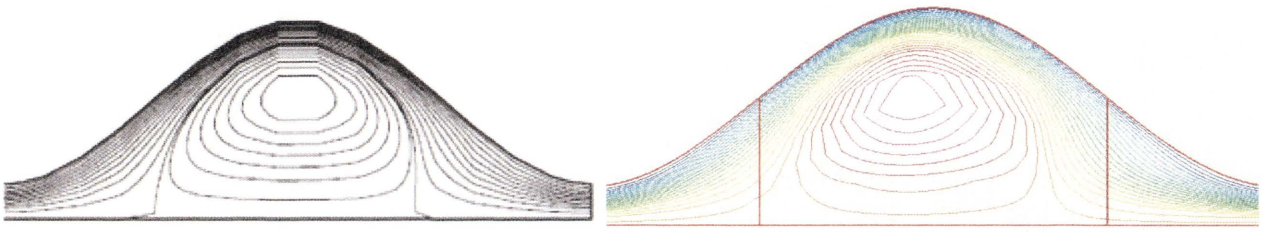

Re = 1

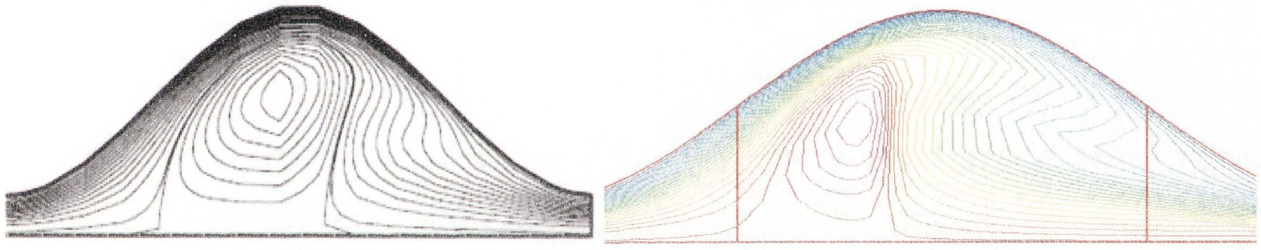

Re = 2

Figure 4.5 The effect of the Reynolds number on the streamline patterns in the wave frame for

$$\alpha = 0.01, \phi = 0.7, \frac{\bar{Q}}{\pi c h^2} = 0.6$$

The effect of the Reynolds number (Re) on streamline patterns is shown in Figure 4.5. As Re increases from 1 to 2, the trapping phenomenon, shown as enclosed streamlines, is seen to be displaced downstream in the wave frame, here on the left side of the plot. This works results are closing aligned with those of Xiao et al [23].

4.5 Summary of isothermal flow

Maximum and minimum axial velocities are demonstrated in section 4.1. Streamline patterns with the effect of the Reynolds number are presented in section 4.3. Finally in this section 4.4, the dimensionless time-average flow rate is used and the streamline patterns are plotted. All results from figure 4.1, 4.2, 4.3 and 4.5 suggest that the applications in CFD-ACE are reasonable. Therefore, it is suggested that the boundary conditions, volume conditions and calculations in CFD-ACE can be assumed to be reasonable results.

CHAPTER 5

NON-ISOTHERMAL FLOW

5.1 Introduction

The purpose of the previous chapter was to create an isothermal CFD model that replicated models from previous studies. This process enabled the creation of a benchmark by which variables required in the modelling process could be verified. As the data proved comparable, items such as boundary and volume conditions were identified. The newly created isothermal models could now be utilised in non-isothermal applications.

Many variables are considered in order to study the effect of temperature on peristaltic flow in this chapter.

1) The case for Newtonian fluid, with a wide range of Reynolds numbers, is used for demonstrating the effect of temperature on peristaltic flow. Pressure drop, temperature change and velocity profiles are used in investigating this effect.

2) The cases for non-Newtonian fluid, shear thinning and shear thickening fluids are considered in investigating the effect of temperature. This fluid condition is determined by the value of the power-law index (n). The power-law index (n) has a strong relationship with shear rate in power-law fluid.

3) The effect of temperature is influenced by the exponential coefficient a_1 of viscosity. Thus, the effect of a_1 on peristaltic flow in Newtonian fluids is investigated in this chapter. Three different values of a_1 are utilised.

4) Numerical results for vorticity are obtained for Newtonian and non-Newtonian fluids. Results were also obtained for isothermal and non-isothermal flow. Each of these figures is compared in order to define the difference. Vorticity has a strong relationship with viscosity that is affected by temperature.

5) New models were produced with changing a length of h to create different geometries. (h: the mean distance of the wall from the symmetric axis). The isothermal flow model firstly shows the effect of geometry upon peristaltic flow and the condition for non-isothermal flow will be added on the isothermal flow model in order to show the effect of temperature. The effect of temperature upon different geometries is investigated by comparable results produced by the isothermal flow models. The temperature effect will be shown in different geometries by streamline patterns, pressure drop and velocity.

5.2 Effect of temperature in Newtonian flow for the case when $\alpha = 0.25,\ \phi = 0.5$ over a wide range of Reynolds number

The effect of temperature on peristaltic flow is demonstrated for Newtonian fluid over a wide range of Reynolds numbers (1-1000) when $\alpha = 0.25,\ \phi = 0.5$. Pressure drop, temperature change and variations of velocity are shown to demonstrate this effect. Flow patterns will be presented later, in the section dealing with power-law fluid. The dimensionless time-average flow rate in non-isothermal flow are investigated in this section.

For isothermal flow, $a_1 = 0\ °C^{-1}$ is utilised to produce a result. There is a change in flow patterns but without any change in viscosity. This is so because under the condition of isothermal flow, viscosity would stay unchanged.

In the case of non-isothermal flow ($a_1 = -0.034\ °C^{-1}$), there is a change in flow patterns but with change in viscosity because viscosity is expected to change in non-isothermal flow as can be seen from Equation (2.7) below.

Pressure drop and temperature change are presented in Table 5.1 to show viscosity changes under non-isothermal flow.

A power-law module (2.7) for fluid viscosity is used with an exponential dependence on temperature for non-isothermal flow.

$$\text{Viscosity} = K\mu_0 e^{a_1 T}\left[\max(\dot{\gamma}, \dot{\gamma}_0)\right]^{n-1} \tag{2.7}$$

Where :

T : temperature ($°C$).

μ_0 : 0.11 ($kg{\cdot}m^{-1}{\cdot}s^{-1}$).

n : power-law index is 1

a_1 : the exponential coefficient of viscosity is -0.034 $^{\circ}C^{-1}$

Two points are placed at each end side of the wave length as the inlet and outlet. The points 0 and 1 are placed along the central axis to measure pressure values. The other points, 2 and 3, are placed on the wall to measure temperature change (Figure 5.1).

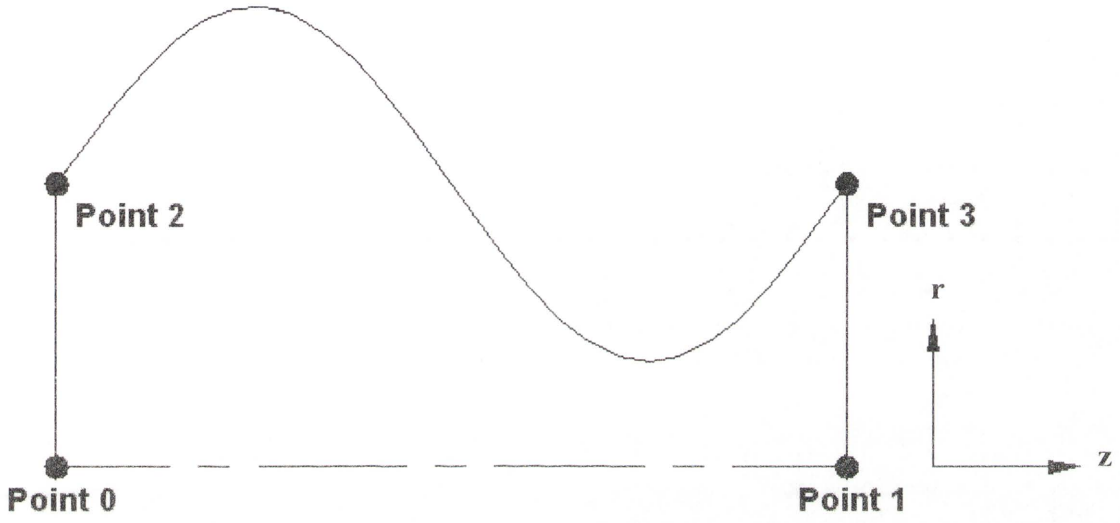

Figure 5.1 Arrangement of measurement points

Values of temperature change and pressure drop per wavelength (Table 5.1 and Figure 5.2) demonstrate the viscosity change in peristaltic flow with non-isothermal flow.

The variations of velocity are shown in Figures 5.3 and 5.4 to present the effect of temperature on axial velocity (U/c)

Where U : axial velocity in laboratory frame (m/s)

c : wave speed (m/s)

5.2.1 Results

The effect of temperature on pressure drop and velocity variation in peristaltic flow

Isothermal flow

	$\alpha = 0.25,\ \phi = 0.5,\ a_1 = 0\ ^\circ C^{-1}\ \ \bar{Q}/\pi ch^2 = 0$						
	Re=1	Re=5	Re=10	Re=50	Re=100	Re=500	Re=1000
$\Delta P = P_{\lambda in\_1} - P_{\lambda out\_0}$ (Pa)	255.12	2133.7	6305.2	105884	388450	8771800	34320000
$\Delta T = T_{\lambda out} - T_{\lambda in}\ (^\circ C)$	-0.001	-0.004	-0.008	-0.044	-0.095	-1.314	-3.191

Non-isothermal flow

	$\alpha = 0.25,\ \phi = 0.5,\ a_1 = -0.034\ ^\circ C^{-1}\ \ \bar{Q}/\pi ch^2 = 0$						
	Re=1	Re=5	Re=10	Re=50	Re=100	Re=500	Re=1000
$\Delta P = P_{\lambda in\_1} - P_{\lambda out\_0}$ (Pa)	26.707	617.67	2054.7	61318	245170	6127100	24508000
$\Delta T = T_{\lambda out} - T_{\lambda in}\ (^\circ C)$	0	0	0	0	0	0	-0.001

Table 5.1 Pressure drop (ΔP) and Temperature change (ΔT) per wavelength along the flow direction with Newtonian fluid

Table 5.1 shows temperature change and pressure drop in isothermal flow ($a_1 = 0\,^\circ C^{-1}$) and non-isothermal flow ($a_1 = -0.034\,^\circ C^{-1}$) for a wide range of Reynolds numbers. This table shall demonstrate viscosity change in non-isothermal flow.

With isothermal flow ($a_1 = 0\,^\circ C^{-1}$), a value of temperature change is found for all values of the Reynolds number and the value of temperature change increases as the Reynolds number increases. The values of pressure drop are higher in comparison with the condition of non-isothermal flow.

However, with non-isothermal flow ($a_1 = -0.034\,°C^{-1}$), temperature change is not found in a range of Reynolds numbers (1-500) then a small temperature change is found at Re = 1000. The values of the pressure drop stays lower in comparison with isothermal flow.

The variation of pressure drop in isothermal and non-isothermal flow is plotted in Figure 5.2.

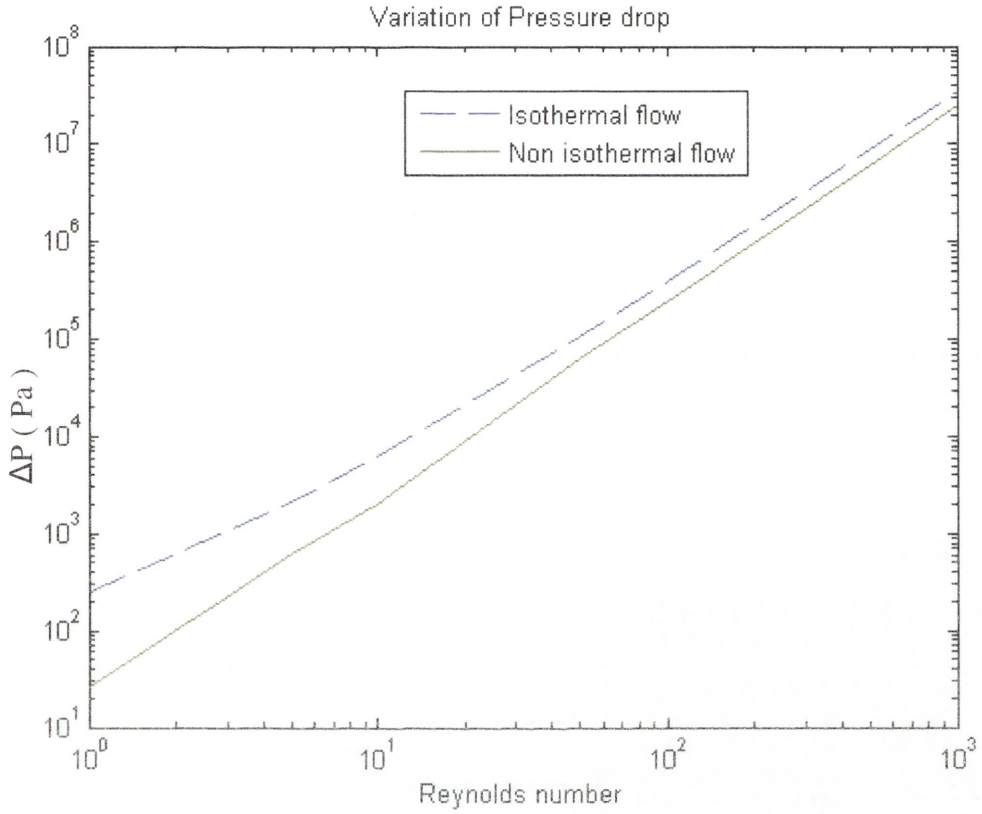

Figure 5.2 Variation of Pressure drop when isothermal flow ($a_1 = 0\,°C^{-1}$) and non-isothermal flow ($a_1 = -0.034\,°C^{-1}$) in a wide range of Reynolds number (ΔP over wavelength: λ =0.02m)

With isothermal flow ($a_1 = 0\,°C^{-1}$), in Figure 5.2, the change in the pressure drop stays higher in comparison with non-isothermal flow for all values of the Reynolds number because under the condition of isothermal flow, viscosity is constant. Therefore, shear stress is higher at the region adjacent to the wall in comparison with non-isothermal flow.

On the other hand, with non-isothermal flow ($a_1 = -0.034\,°C^{-1}$), the change in the pressure is lower because viscosity decreases by the action of viscous heating around the wall. Shear stress decreases at the region adjacent to the wall with decreasing viscosity. Low wall shear stress yields less resistance to the flow, that results in a lower pressure drop.

It can be explained that temperature change is utilised to reduce viscosity under the condition of non-isothermal flow. Therefore, as viscosity decreases, pressure drop decreases in this condition.

Figures 5.3 and 5.4 shows the effect of temperature on velocity on the crest and trough section respectively. These figures will indicate how velocity will be changed in non-isothermal flow model.

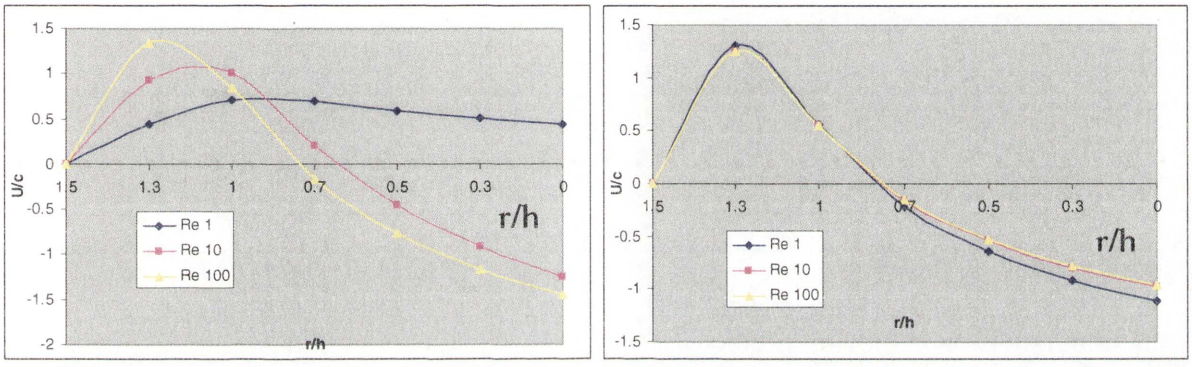

Figure 5.3 Velocity profile on the crest section in $a_1 = 0\ ^{\circ}C^{-1}$ (left) and $a_1 = -0.034\ ^{\circ}C^{-1}$ (right)

Figure 5.3 shows the variation of the velocity profile (the laboratory frame U/c) along the central axis at the crest section with Reynolds number (Re)= 1-100.

With isothermal flow, the velocity profiles vary at the cross section of the crest with Reynolds number 1 – 100. As the Reynolds number increases, the velocity profiles change and the maximum velocity becomes higher and moves to the wall ($r/h = 1.5$).

With non-isothermal flow, the velocity profiles become a similar profile of Re=100. As the Reynolds number increases, the velocity profiles are unchanged and the maximum velocity stays unchanged and does not move.

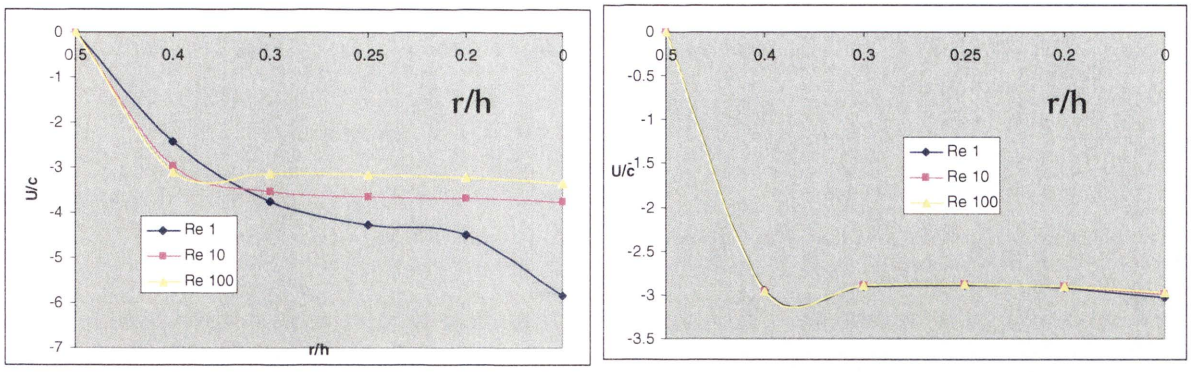

Figure 5.4 Velocity profile on the trough section in $a_1 = 0\ ^{\circ}C^{-1}$ (left) and $a_1 = -0.034\ ^{\circ}C^{-1}$ (right)

In isothermal flow, as the Reynolds number increases, each model produces different velocity profiles. An increase in the flow rate (c: the wave speed) yields an increase in the Reynolds number, ($\mathrm{Re} = \left(\frac{hc}{v}\right)\alpha$). As increases occur in the Reynolds number, the flow patterns also change. This case shows the effect of the Reynolds number in isothermal flow.

On the other hand, in non-isothermal flow, as the Reynolds number increases, velocity profiles stay virtually unchanged and the effect of the Reynolds number is not shown.

It can be concluded that temperature has influenced the flow property for viscosity and any change in viscosity reduced the effect of Reynolds number on peristatic flow in the both crest and trough section.

The effect of temperature on the dimensionless time-average rate of volume flow

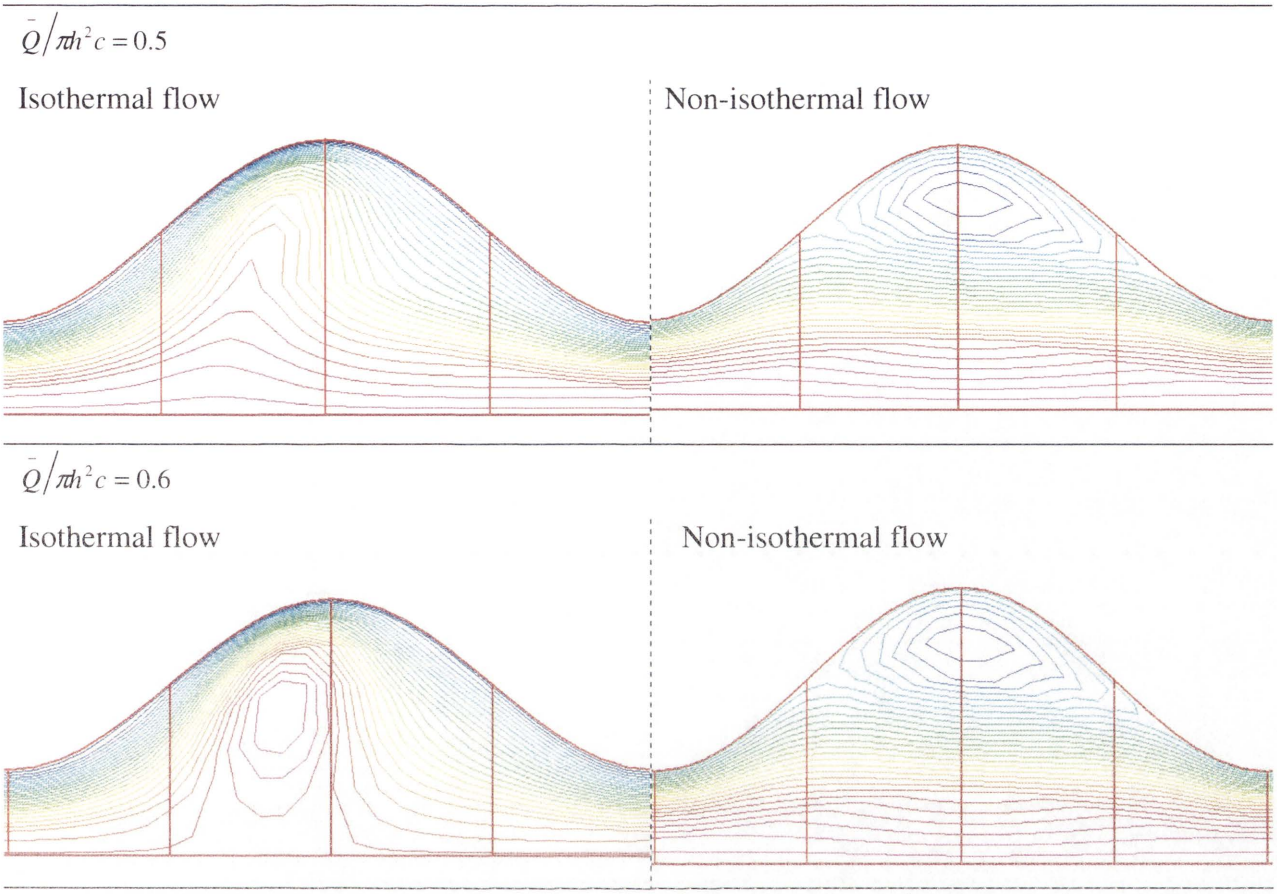

Figure 5.5 Comparison of the streamline patterns with different value of $\bar{Q}/\pi h^2 c$ for the case when $a_1 = 0$ °C^{-1} (left) and $a_1 = -0.034$ °C^{-1} (right) in Re=10

The dimensionless time-average flow rate is one of the important parameters to control peristaltic flow. In chapter 4, a model was produced demonstrating the dimensionless time-average rate of volume flow $\bar{Q}/\pi h^2 c$. In this section, the condition of non-isothermal flow (a_1 =-0.034 °C^{-1}) is employed to show the effect of temperature on this model when $\bar{Q}/\pi h^2 c = 0.5, 0.6$.

With isothermal flow (a_1 =0 °C^{-1}), Figure 5.5 shows streamline patterns with different values of dimensionless time-average rate of volume flow $\bar{Q}/\pi h^2 c$ for the case Re=10. The streamline pattern is similar with the results of Takabatake et al [20] and Xiao et al [23]. As the value of dimensionless time-average rate of volume flow $\bar{Q}/\pi h^2 c$ increases, the streamline pattern is changed in the case of isothermal flow (a_1 =0 °C^{-1}).

With non-isothermal flow (a_1 =-0.034 $^{\circ}C^{-1}$), the streamline patterns is changed by the effect of temperature. However, as the value of dimensionless time-average rate of volume flow increases, the streamline patterns stay unchanged. A circulation is located at the middle of the crest and seen to settle on the upper side of crest.

It is revealed that allowing for temperature effect (with a_1 =-0.034 $^{\circ}C^{-1}$) significantly altered the flow pattern in comparison with isothermal case. On the other hand, allowing for temperature effect also reduces significantly (here, virtually removes) the dependence of the flow pattern on flow rate.

5.3 The effect of temperature on power-law fluids.

Hayat et al [5] studied peristaltic flow for power-law fluids in 2006. They used two dimensional models which are formulated based upon the fundamental equations of mass conservation and momentum.

In this present work, an axi-symmetric flow model of power-law type for non-isothermal and non-Newtonian fluids is used. Thus, an additional balance-of-energy equation with the constitutive equation for power-law fluids will be employed.

Isothermal situations will be considered while the power-law index (n) is varied to cover the range of fluid property for shear thinning ($n < 1$), through Newtonian fluid (n=1) to shear thickening ($n > 1$). This would show the influence on the items of interest like flow patterns and pressure variation. Then the condition of non-isothermal flow is added on the models to show the effect of temperature.

Figures 5.6, 5.7 and 5.8 show the effect of temperature on flow patterns with three values of the power-law index (0.5, 1 and 2) for isothermal and non-isothermal conditions. The figures reveal that temperature variations cause changes in viscosity as well as flow patterns.

5.3.1 Results

The effect of temperature on streamline pattern in shear thinning fluid (n=0.5)

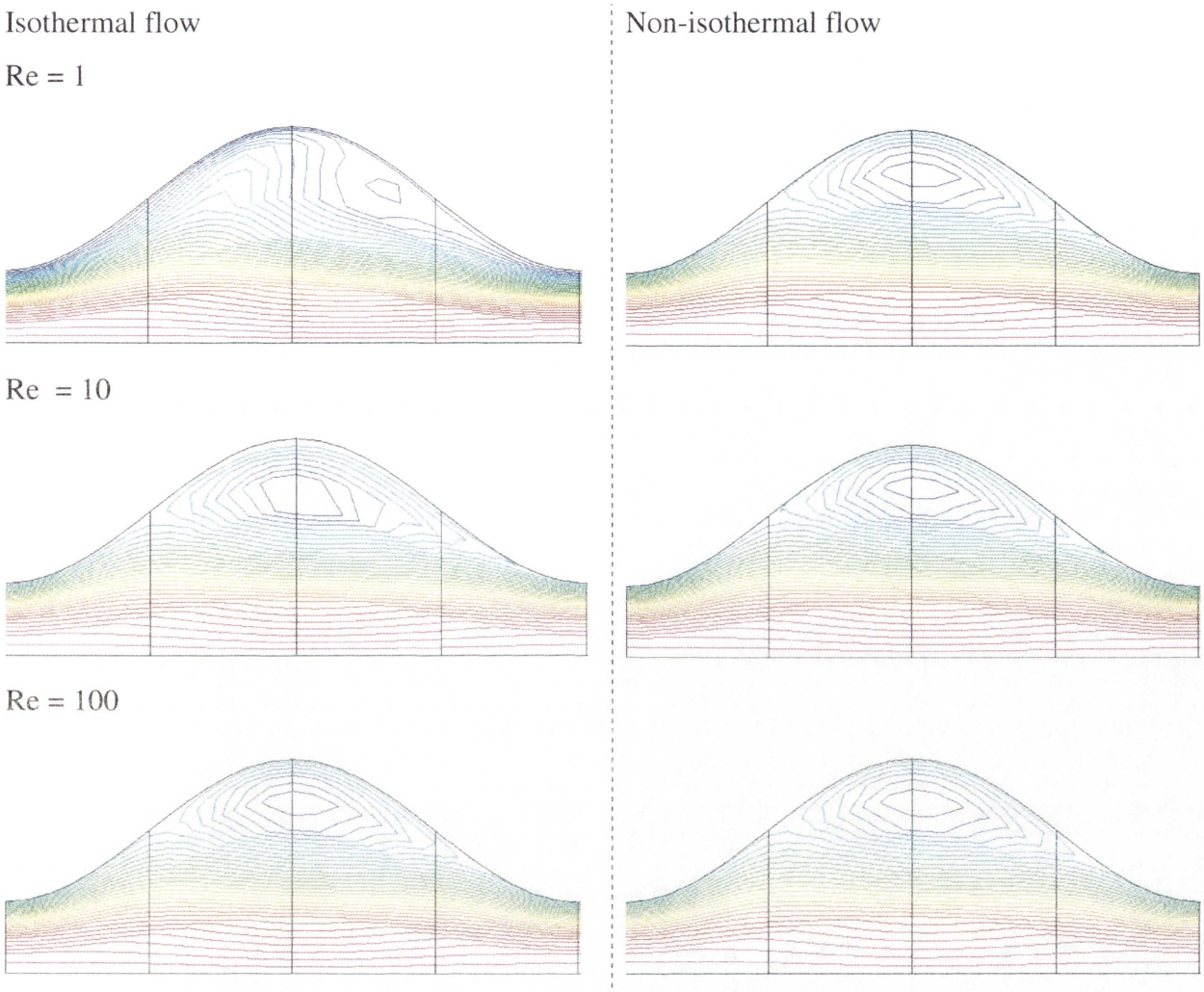

Figure 5.6 Comparison of the variation of streamline in shear thinning fluid (in the wave frame) for the case when $a_1 = 0\ ^{\circ}C^{-1}$ (left) and $a_1 = -0.034\ ^{\circ}C^{-1}$ (right) with $\bar{Q}/\pi ch^2 = 0$

Figure 5.6 shows streamline patterns (in wave frame) in a shear thinning fluid for different values of the Reynolds number.

In isothermal flow, as the Reynolds number increases from 1 to 10, the flow pattern is changed. As the Reynolds number increases further from 10 to 100, the flow pattern is also changed but

this further change is only a slight change. With the power-law index ($n < 1$), viscosity becomes smaller as shear rate increases. The flow patterns stay unchanged when the Reynolds number is high.

In non-isothermal flow, as the Reynolds number increases, flow patterns are virtually unchanged. Viscosity stays lower because the condition of non-isothermal flow is employed. Low viscosity effect leads to small change in flow patterns.

The effect of temperature on streamline pattern in Newtonian fluid (n = 1)

Isothermal flow

Re = 1

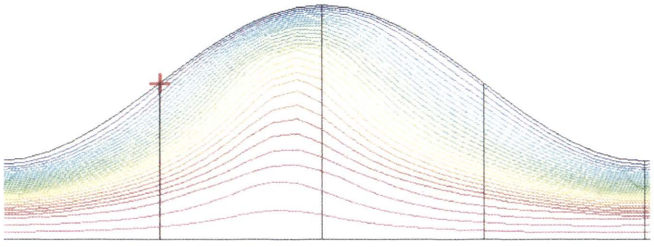

Re = 10

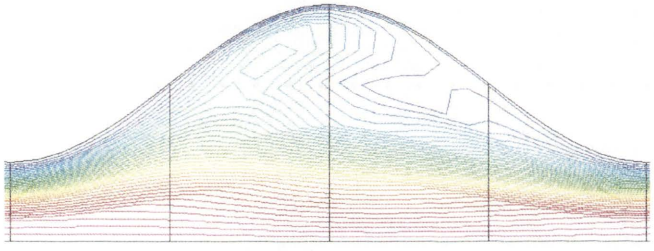

Re = 100

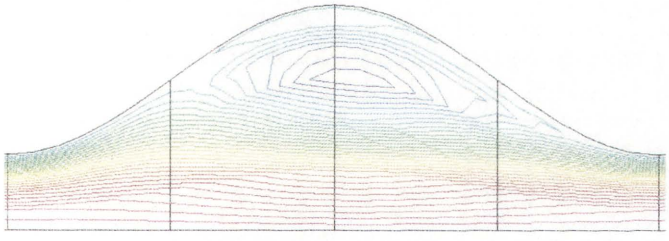

Re=1000

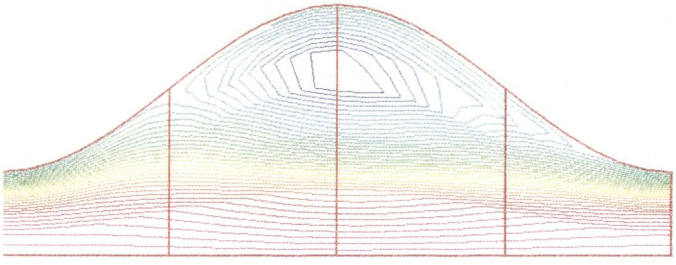

Non-isothermal flow

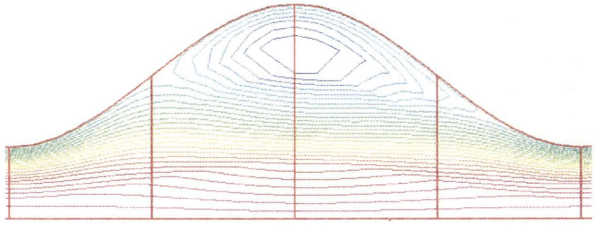

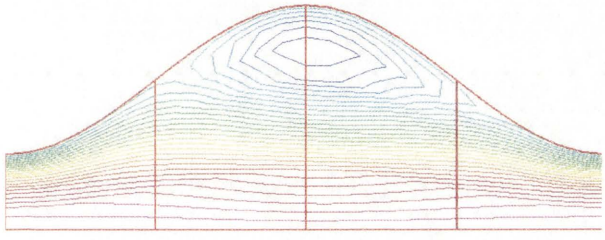

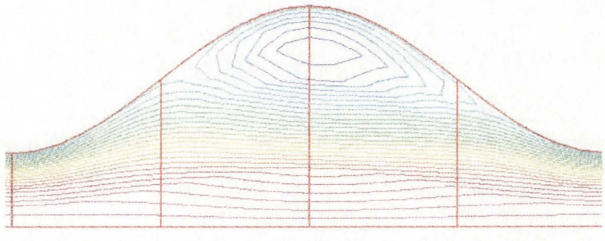

Re=1000

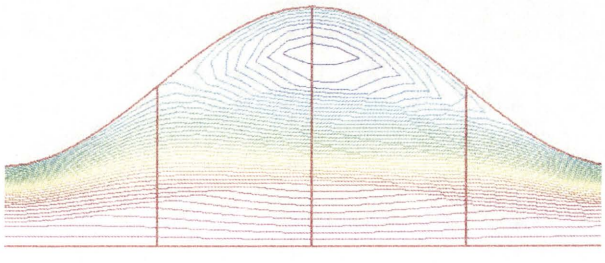

Figure 5.7 Comparison of the variation of streamline in Newtonian fluid (in the wave frame) for the case when $a_1 = 0$ °C^{-1} (left) and $a_1 = -0.034$ °C^{-1} (right) with $\bar{Q}/\pi ch^2 = 0$

In this case, for a Newtonian fluid, the effect of temperature is shown by streamline patterns (wave frame) along a range of Reynolds numbers (1-1000). With isothermal flow, no recirculation is presented at the low Reynolds number Re=1. As Re increases to 10, then to 100, a recirculation region is seen to develop and grow. Furthermore, this recirculation moves upstream against the flow direction (in wave frame). As Re increases further from 100 to 1000, the side of the recirculation increases slightly but its location tends to settle at about the crest section.

With non-isothermal case, on the other hand, the flow pattern does not change significantly as the Reynolds number increases. Specifically, a recirculation develops very early at the low Re=1 but both the recirculation's shape and location, which is at the crest section, stay virtually unchanged as Re increases to the quite high value of 1000.

The effect of temperature on streamline pattern in shear thickening fluid (n=2)

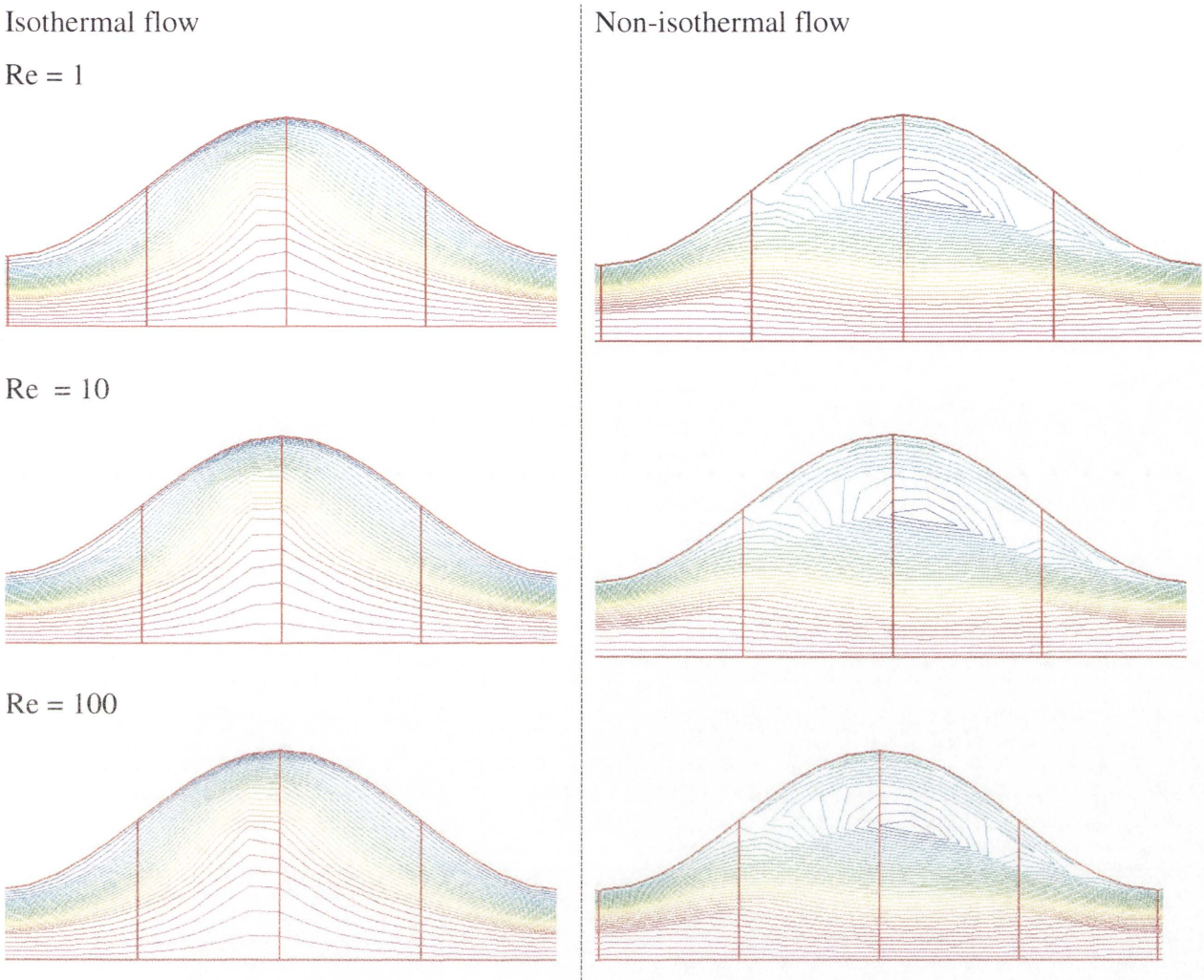

Figure 5.8 Comparison of the variation of streamline in shear thickening fluid (in the wave frame) for the case when $a_1 = 0\ ^{\circ}C^{-1}$ (left) and $a_1 = -0.034\ ^{\circ}C^{-1}$ (right) with $\bar{Q}/\pi ch^2 = 0$

Figure 5.8 show streamline patterns in a shear thickening fluid ($n > 1$) for isothermal and non-isothermal flow. Generally, under this condition of shear thickening fluid, an increase in flow rates yields increases in the shear stress and viscosity is expected to increase by an increase in the shear stress. Therefore, as the value of the Reynolds number (flow rate) increases, the also viscosity increases.

According to the definition of the Reynolds number, $\mathrm{Re} = \left(\frac{hc}{v}\right)\alpha$, the Reynolds number can not be changed because viscosity (v) increases with an increase in a value of c (the wave speed m/s).

With isothermal flow, as the Reynolds number increases, the flow pattern is unchanged. No circulation is found for all values of the Reynolds number.

With non-isothermal flow, the flow pattern is changed with decreasing viscosity. A large circulation is located at the middle of crest and smaller circulation is located and deformed to the top of crest. However, as the Reynolds number increases, the flow patterns stay virtually unchanged.

It is concluded that temperature change yields decreasing viscosity in non-isothermal flow. However, as the Reynolds number increases, viscosity increases significantly. Therefore, the flow patterns are not changed by the Reynolds number even if the effect of temperature yields decrease in viscosity.

Pressure drop and temperature change in power-law index (n) for isothermal and non-isothermal flow

Pressure drop and temperature change are shown in Table 5.2 for the cases of non-Newtonian and Newtonian fluids when Re=1. The Table 5.2 and Figure 5.9 show the change in the pressure drop for power-law index (n) with the conditions of non-isothermal and isothermal flow.

		$n=0.5$	$n=1$	$n=2$
$a_1=-0.034\ ^{\circ}C^{-1}$	$\Delta P=P_{\lambda in\_1}-P_{\lambda out\_0}(Pa)$	20.617	21.408	62.124
	$\Delta T=T_{\lambda out}-T_{\lambda in}(^{\circ}C)$	0	0	0

		$n=0.5$	$n=1$	$n=2$
$a_1=0\ ^{\circ}C^{-1}$	$\Delta P=P_{\lambda in\_1}-P_{\lambda out\_0}(Pa)$	41.612	255.124	24868.4
	$\Delta T=T_{\lambda out}-T_{\lambda in}(^{\circ}C)$	0	0.001	0.092

Table 5.2 Comparison of Pressure drop(ΔP) and Temperature change (ΔT) along flow direction in Newtonian and non-Newtonian fluid for the case of Re=1 with $\bar{Q}/\pi ch^2=0$

In the case for a shear thinning fluid, Δp is 20.617 Pa for a_1=-0.034 $^{\circ}C^{-1}$ and 41.612 Pa for $a_1=0$ $^{\circ}C^{-1}$ The difference is 20.995 Pa.

In the case for a Newtonian fluid, Δp is 21.408 (Pa) for a_1=-0.034 $^{\circ}C^{-1}$ and 255.124 Pa for $a_1=0$ $^{\circ}C^{-1}$. The difference is 233.716 Pa.

In the case for a shear thickening fluid, Δp is 62.124 Pa for a_1=-0.034 $^{\circ}C^{-1}$and 24868.4 Pa for $a_1=0$ $^{\circ}C^{-1}$. The difference is 24806.276 Pa.

An increase in power-law index (n) yields an increase in the value of the pressure drop in both isothermal and non-isothermal flow. However, with non-isothermal flow, the pressure drop decreases with decreasing viscosity in these three cases (shear thinning, Newtonian and shear thickening).

Temperature change is not shown in the case for shear thinning fluid ($n < 1$) because in this condition, shear stress could be significantly small so that this fluid property can not yield a decrease in viscosity around the wall for isothermal and non-isothermal flow.

Therefore, the case for a shear thinning fluid has significantly similar values of the pressure drop for isothermal and non-isothermal flow in comparison to the other cases, Newtonian and shear thickening fluid.

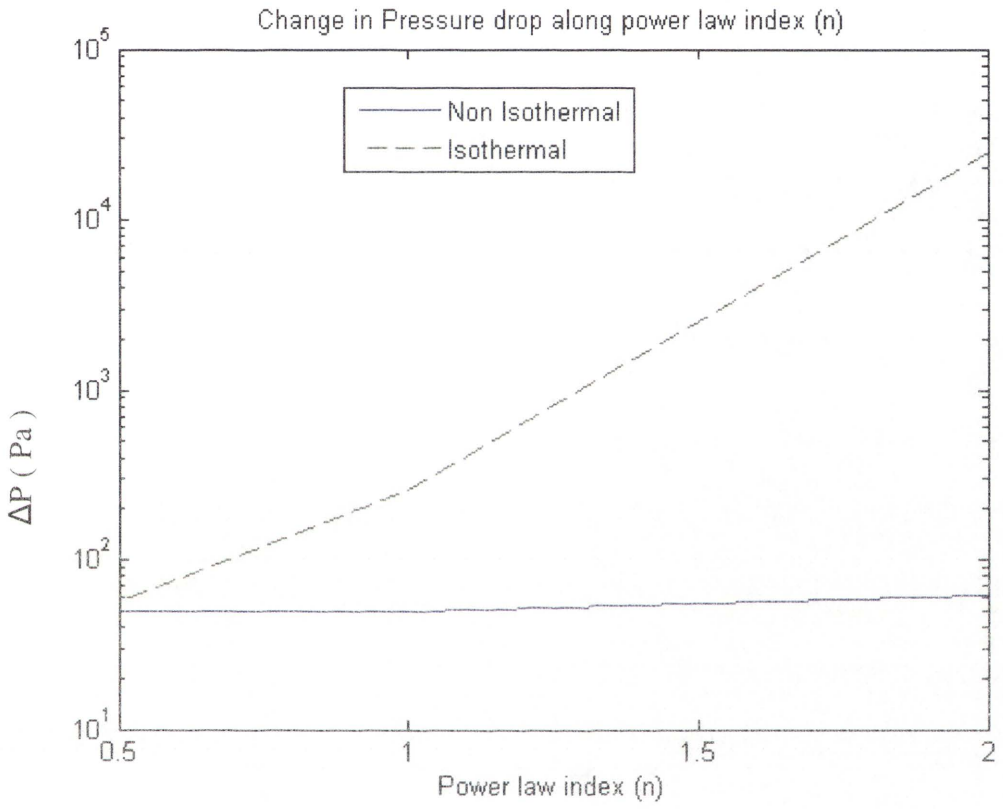

Figure 5.9 Change in Pressure drop (Pa) along Power-law index when Re=1 (ΔP Over Wavelength: λ =0.02m)

As Hayat et al [5] studied in 2006, ΔP per wavelength increases as the power-law index increases in isothermal flow. It can be seen in Figure 5.9, that in an isothermal flow, as an the power-law index increases, ΔP per wavelength also increases.

However, the change in the pressure drop against the power-law index is reduced by the effect of temperature in non-isothermal flow. According to Figure 5.9, the slope for isothermal flow is sharp but the slope for non-isothermal flow is gentle. Specially, with shear thickening fluid, the pressure drop is dramatically reduced by the effect of temperature.

5.4 The effect of exponential coefficient a_1 of viscosity on peristaltic flow for Newtonian fluid.

In the previous section, the effect of temperature on velocity field with Newtonian and non-Newtonian fluids is investigated when $a_1 = -0.034\ ^{\circ}C^{-1}$. In this section, three different values (0 , -0.02 and -0.04 $^{\circ}C^{-1}$) are utilised to investigate the influence of a_1 with a Newtonian fluid by plotting streamline patterns, velocity profiles and the pressure drop..

The effective viscosity is defined as:

$$\mu_{eff} = K\mu_0 e^{a_1 T}\left[\frac{\partial u}{\partial r} + \frac{\partial v}{\partial z}\right]^{n-1} \tag{2.7}$$

All terms are defined in previous chapters.

In the case of a Newtonian fluid (n=1), the effective viscosity (2.7) is reduced to $\mu_{eff} = K\mu_0 e^{a_1 T}$. The effective viscosity (2.7) would decrease with increase in absolute values of a_1 as a_1 is negative in this work. This change in viscosity would be expected to change the flow patterns.

5.4.1 Results

Streamline patterns and velocity variations for different values of a_1 when Re=1

Wave frame

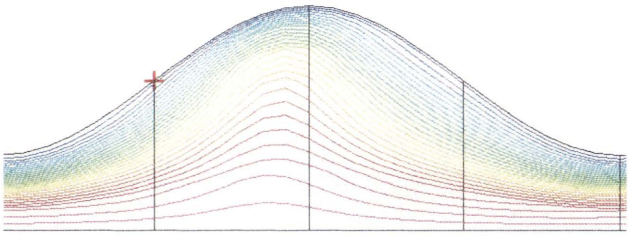

$a_1 = 0\ ^{\circ}\mathrm{C}^{-1}$

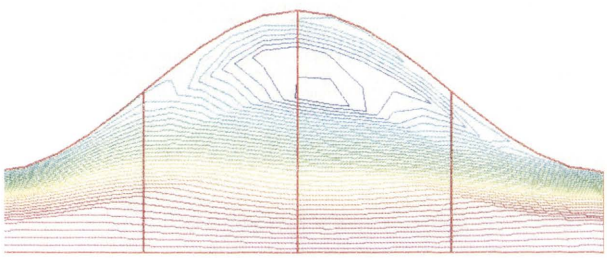

$a_1 = -0.02\ ^{\circ}\mathrm{C}^{-1}$

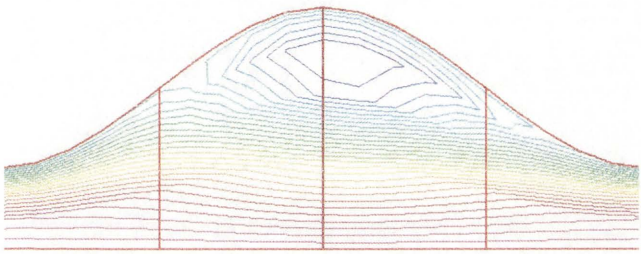

$a_1 = -0.04\ ^{\circ}\mathrm{C}^{-1}$

Figure 5.10 Comparison of streamline in different values of $a_1 = 0\ ^{\circ}\mathrm{C}^{-1}$ (Top), $a_1 = -0.02\ ^{\circ}\mathrm{C}^{-1}$ (Left) and $a_1 = -0.04\ ^{\circ}\mathrm{C}^{-1}$ (Right) with Re=1 and $\bar{Q}/\pi ch^2 = 0$

Figure 5.10 presents streamline patterns produced by three different values of exponential coefficient a_1 of viscosity.

As an absolute value of a_1 increases, a circulation develops with decreasing viscosity. The isothermal flow ($a_1 = 0\ ^{\circ}\mathrm{C}^{-1}$) produces no circulation at the crest section. However, as an absolute value of a_1 increases from 0 to -0.04 $^{\circ}\mathrm{C}^{-1}$, the circulation develops and the circulation at the middle of crest grows. In the cases for $a_1 = -0.02\ ^{\circ}\mathrm{C}^{-1}$ and $a_1 = -0.04\ ^{\circ}\mathrm{C}^{-1}$., the circulation is shown at the middle of crest. This fact indicates an increase in an absolute value of a_1 yields decrease in viscosity.

Figure 5.11 and 5.12 shows the variation of the velocity profile along the dimensionless mean distance (r/h) of wall in the crest and trough section respectively. These velocity variations will prove the effect of a_1 on velocity. The region where the effect of a_1 is strong can be indicated.

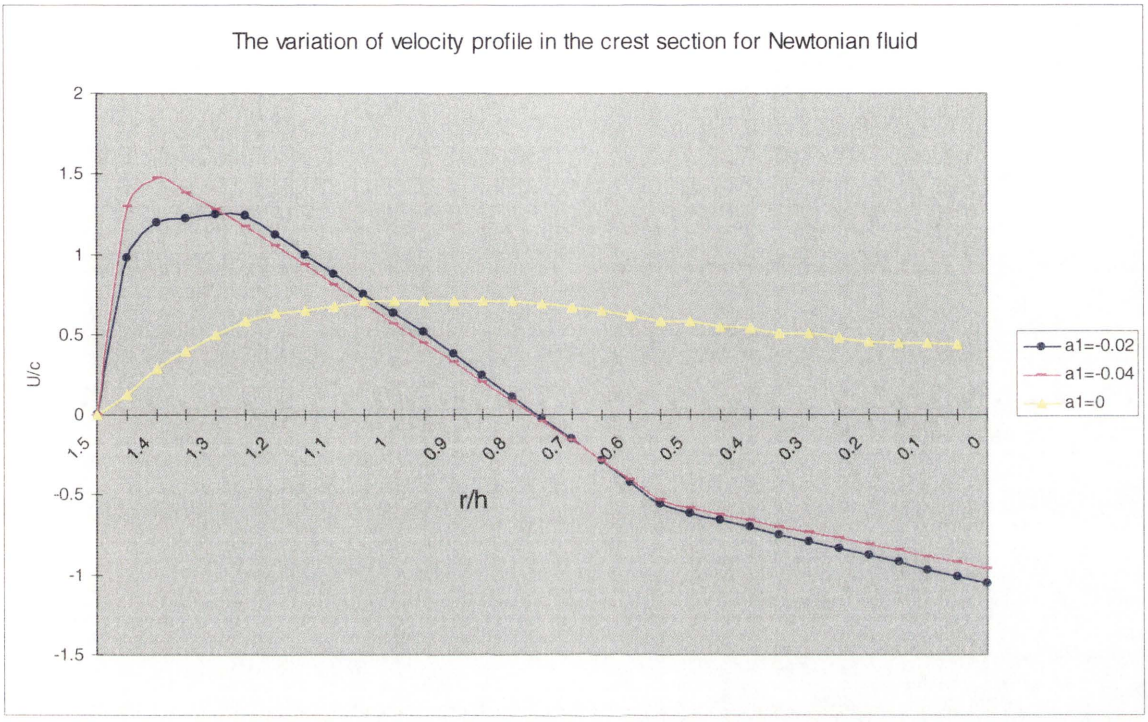

Figure 5.11 the variation of velocity profile in the crest section with different values of a_1 when Re=1

As an absolute value of a_1 increases from 0 to -0.02 $°C^{-1}$ then -0.02 $°C^{-1}$ to -0.04 $°C^{-1}$, the velocity at the region adjacent to the wall ($r/h = 1.5$) becomes higher.

This result proves that as an absolute value of a_1 increases, viscosity decreases. Furthermore, this phenomenon is strong at the region adjacent to the wall ($r/h = 1.5$).

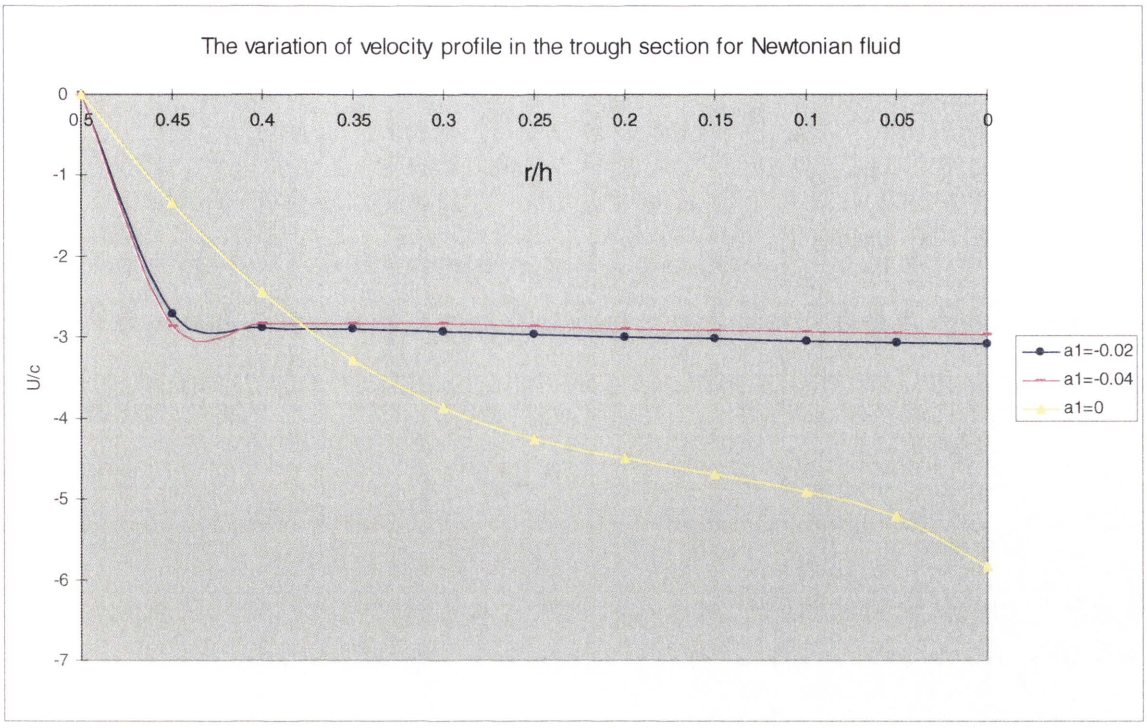

Figure 5.12 the variation of velocity profile in the trough section with different values of a_1 when Re=1

In Figure 5.12, under the condition of non-isothermal flow ($a_1 = -0.02$ and $a_1 = -0.04$ °C^{-1}), the velocity profiles dramatically increase at around wall ($r/h > 0.4$) because of decreasing viscosity. Since the velocity profile is fully developed, velocity is constant in the range ($r/h < 0.4$).

On the other hand, in isothermal flow ($a_1 = 0$ °C^{-1}), a whole cross section is affected by wall motion. Therefore, the velocity is changed along whole cross section.

It can be explained that as an absolute value of a_1 increases, viscosity becomes lower near the wall. This low viscosity enables the change in velocity.

	$a_1 = 0$	$a_1 = -0.02\ ^{\circ}C^{-1}$	$a_1 = -0.04\ ^{\circ}C^{-1}$
$\Delta P = P_{\lambda in\_1} - P_{\lambda out\_0}\,(Pa)$	255.12	44.558	39.33

Table 5.3 Comparison of Pressure drop(ΔP) in a wavelength between $a_1 = -0.02\ ^{\circ}C^{-1}$ and $a_1 = -0.04\ ^{\circ}C^{-1}$ with Newtonian fluid for the case of Re=1 with $\bar{Q}/\pi ch^2 = 0$

The Table 5.3 shows the pressure drop per wavelength for cases of $a_1 = 0$, $a_1 = -0.02\ ^{\circ}C^{-1}$ and $a_1 = -0.04\ ^{\circ}C^{-1}$. As it can be seen, as absolute value of a_1 increases, pressure drop decreases with decreasing viscosity.

5.5 Vorticity patterns and pressure contour in non-isothermal flow with Newtonian fluid and shear thinning fluid when Re=1

In fluid dynamics, vorticity can be defined as the rotation of the fluid velocity. It is also considered as the circulation per unit area at a point in a fluid flow field.

To prove vorticity patterns in non-isothermal flow, isothermal flow shall be compared because viscosity is unchanged; however, it is changed in the condition of a non-isothermal flow. As the power-law index (n) has a strong relationship with viscosity, vorticity patterns in Newtonian ($n=1$) versus shear thinning fluids ($n<1$) shall be shown.

This is shown through vorticity patterns and pressure distribution in Newtonian and shear thinning fluids. As viscosity decreases by the effect of temperature, higher values of vorticity would be expected at the region adjacent to the wall in non-isothermal flow.

According to Equation 2.6, in shear thinning fluid, as the shear stress is significantly small, a change in viscosity is not expected. Therefore, vorticity would be expected to stay unchanged.

5.5.1 Results

Vorticity contour and vorticity variations for Newtonian and shear thinning fluids when Re=1

Figure 5.12 and Figure 5.13 show the vorticity patterns for Newtonian and shear thinning fluids respectively. Figures 5.14 and 5.15 present vorticity profiles at the central axis of the crest and trough section respectively. By these figures, the region where vorticity is mostly shown can be investigated for both cases, isothermal and non-isothermal flow.

Wave frame

$n=1$ (Newtonian fluid)

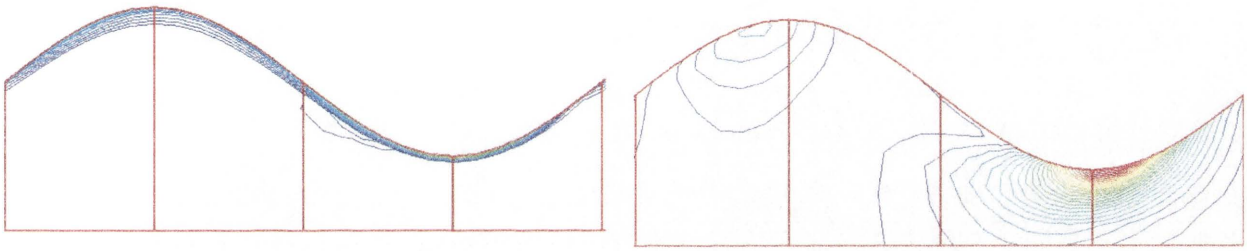

$a_1 = -0.034\ ^{\circ}\mathrm{C}^{-1}$ (Non-isothermal flow) $a_1 = 0\ ^{\circ}\mathrm{C}^{-1}$ (Isothermal flow)

Figure 5.13 Comparison of the variation of vorticity in non-isothermal and isothermal flow with Newtonian fluid when Re=1 with $\bar{Q}/\pi c h^2 = 0$

As obtained in the previous section, the effect of a_1 is strong at the region adjacent to the wall. With isothermal flow ($a_1 = -0.034\,^{\circ}\mathrm{C}^{-1}$), as it can be seen in Figure 5.13, the change in vorticity is found mostly at the region adjacent to wall.

On the other hand, with isothermal flow ($a_1 = 0\,^{\circ}\mathrm{C}^{-1}$), vorticity is mostly found around the region of the trough section. Vorticity can be detected also at the crest section but it is very small.

In the Figure 5.14, vorticity patterns in non-isothermal and isothermal flow are plotted with shear thinning fluid.

Wave frame

n=0.5 (shear thinning fluid)

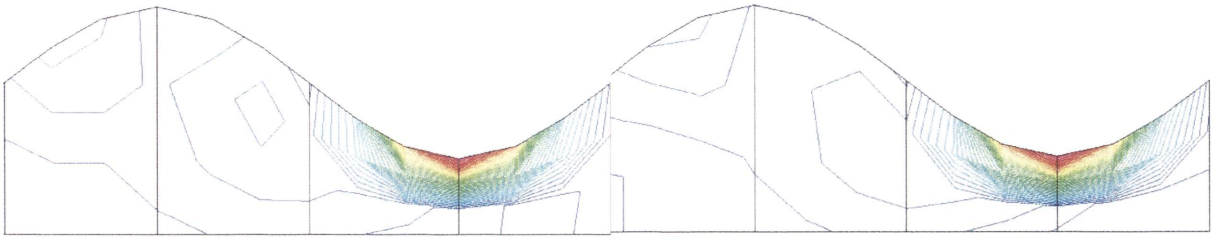

Non-isothermal flow $a_1 = -0.034\ ^{\circ}C^{-1}$ Isothermal flow $a_1 = 0\ ^{\circ}C^{-1}$

Figure 5.14 Comparison of the variation of vorticity for shear thinning fluid when Re=1 with $\bar{Q}/\pi c h^2 = 0$

Vorticity patterns stay unchanged even if the condition of non-isothermal flow ($a_1 = -0.034\ ^{\circ}C^{-1}$) is employed; this agrees with the expectation as viscous effect becomes smaller with shear thinning fluids. Therefore, this result agrees with the result in Figure 5.6 which shows streamline patterns for a shear thinning fluid.

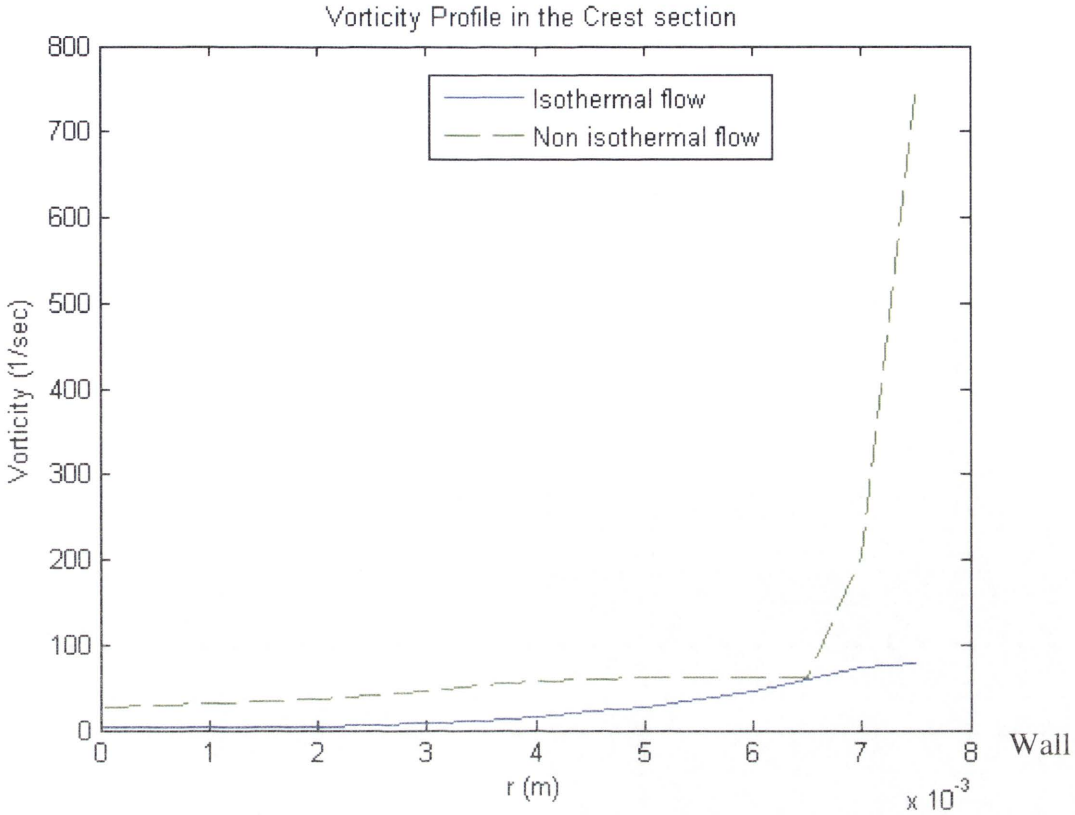

Figure 5.15 The comparison of vorticity profile between isothermal and non-isothermal flow in the crest section with Newtonian fluid when Re=1 (r: radial direction)

Figure 5.15 shows the vorticity profile at the central axis of the crest section for isothermal and non-isothermal flow. With isothermal flow, vorticity increases slowly across the whole cross section. On the other hand, vorticity increases dramatically at the region adjacent to the wall ($r \rangle 6.5\times10^{-3}\ m$).

This phenomenon demonstrates that viscosity for non-isothermal flow around the wall is much smaller in comparison with that for isothermal flow.

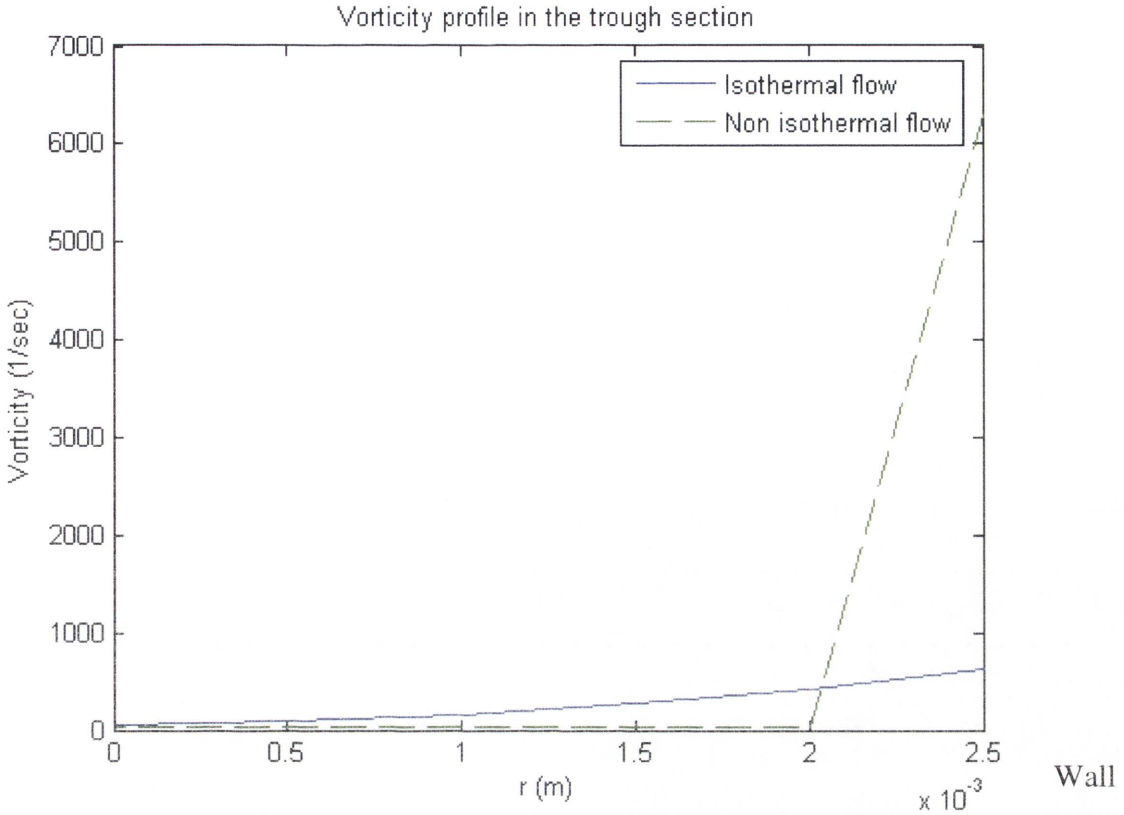

Figure 5.16 The comparison of vorticity profile between isothermal and non-isothermal flow in the trough section with the condition of Newtonian fluid when Re=1 (r: radial direction)

Vorticity profiles in Figure 5.16 are similar to the results in Figure 5.15. The vorticity increases considerably at the region ($r = 2\times10^{-3}\ m$) with non-isothermal flow. On the other hand, vorticity increases slightly in isothermal flow.

Pressure contour for Newtonian and shear thinning fluid when Re=1

Pressure contour

n=0.5 (shear thinning fluid)

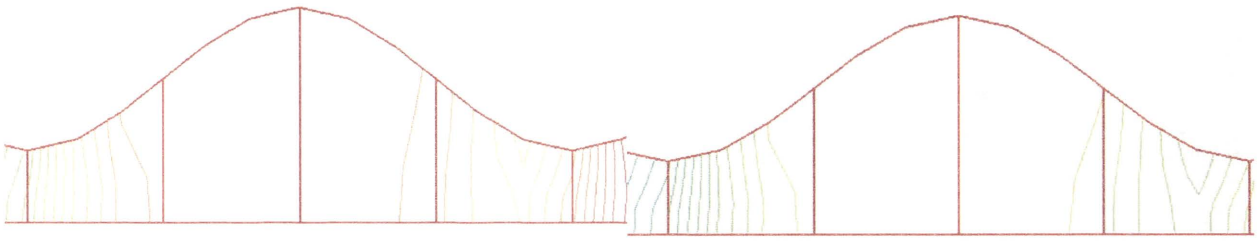

Isothermal flow $a_1 = 0\ ^{\circ}C^{-1}$ Non-isothermal $a_1 = -0.034\ ^{\circ}C^{-1}$

n=1 (Newtonian fluid)

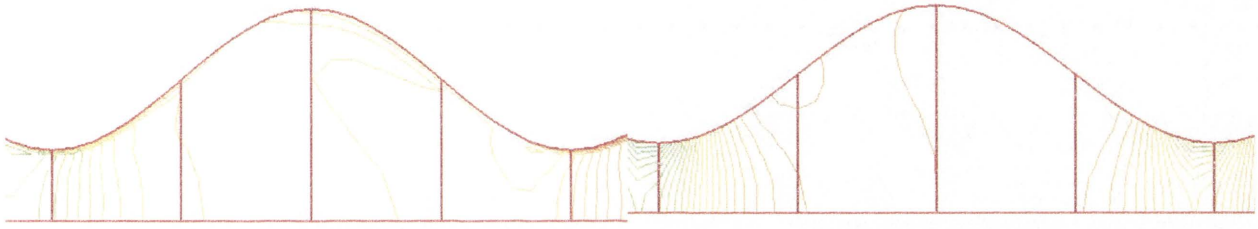

Isothermal flow $a_1 = 0\ ^{\circ}C^{-1}$ Non-isothermal $a_1 = -0.034\ ^{\circ}C^{-1}$

Figure 5.17 Pressure contour for the condition of isothermal and non-isothermal flow with $\bar{Q}/\pi ch^2 = 0$

With regards to Table 5.2, the effect of temperature has not occurred in the conditions for a shear thinning fluid. Therefore, in Figure 5.17, pressure contours and colour for a shear thinning fluid is not changed when the condition of non-isothermal flow is employed.

In the case for a Newtonian fluid (n=1), colour for pressure contour in non-isothermal flow is changed when the condition of non-isothermal flow is employed.

5.6 The effect of temperature on different geometries with non-isothermal flow in Newtonian fluid.

In the previous sections, the effects of temperature on peristaltic flow with various conditions in the same geometry corresponding to $\alpha = 0.25$, $\phi = 0.5$ were investigated. Kyozo et al [11] studied the effect of the amplitude ratio ($\phi = \frac{\varepsilon}{h}$) and wave number ($\alpha = \frac{h}{\lambda}$) on peristaltic isothermal flow. The intent of the investigation in this section is to study the effect of temperature on different geometries that affect peristaltic flow.

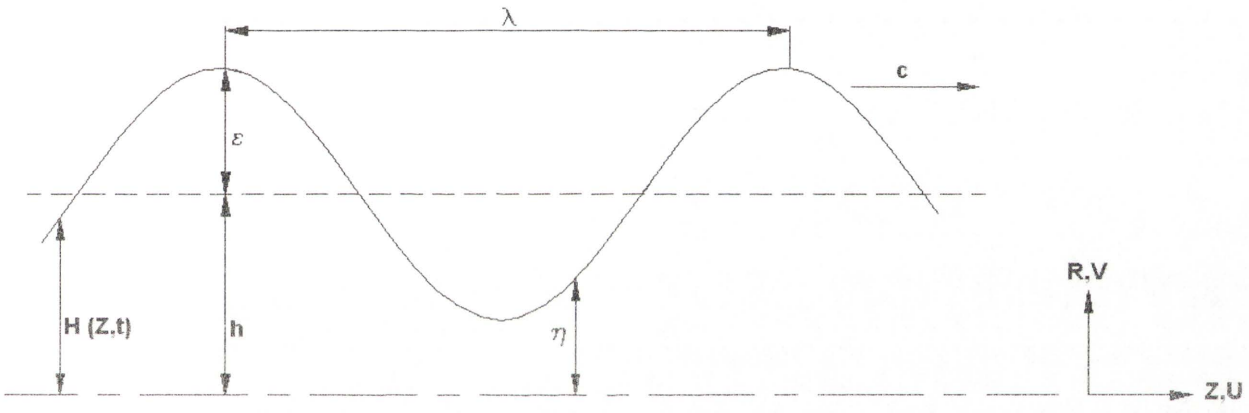

Figure 5.18 Configuration of peristaltic flow in two-dimensional axi-symmetric tube

Figure 5.18 shows the configuration of peristaltic flow. The variable, h (the mean distance of the wall from the symmetric axis) is varied to show the effect of the geometry in isothermal flow.

Utilising the three values of h 0.0045m, 0.004m and 0.0035m, the corresponding wave numbers are 0.225, 0.2 and 0.175. With same h values, amplitude ratios are 0.556, 0.625 and 0.714 respectively.

In an isothermal flow, in Figures 5.19, 5.20, 5.21 and 5.23, the effect of the geometry is shown by their velocity profiles, the streamline pattern and the pressure drop.

In a non-isothermal flow in Figures 5.19, 5.20, 5.22 and 5.23, the effect of temperature on different geometries is also presented.

5.6.1 Results

The streamline patterns in different geometries for isothermal and non-isothermal flow when Re=10 (with Newtonian fluid, n=1)

Isothermal flow	Non-isothermal flow
Wave number($\frac{h}{\lambda}$)=0.225, Amplitude ratio($\frac{\varepsilon}{h}$)=0.556	(h=0.0045 m)
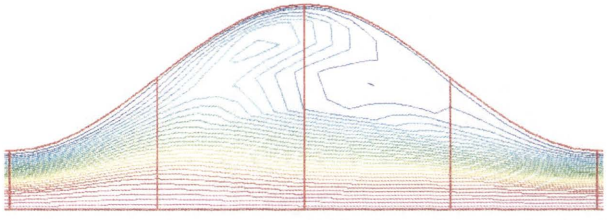	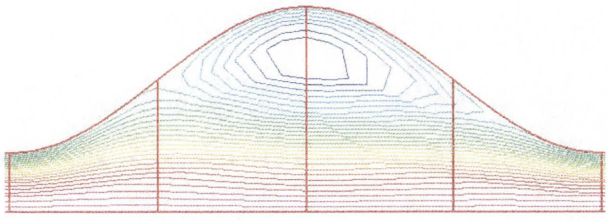
Wave number($\frac{h}{\lambda}$)=0.2, Amplitude ratio($\frac{\varepsilon}{h}$)=0.625	(h=0.004 m)
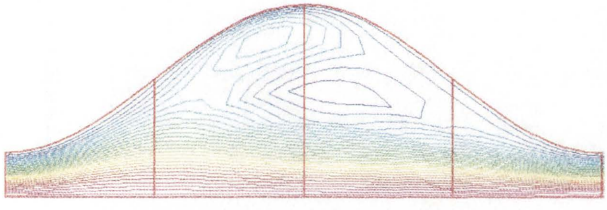	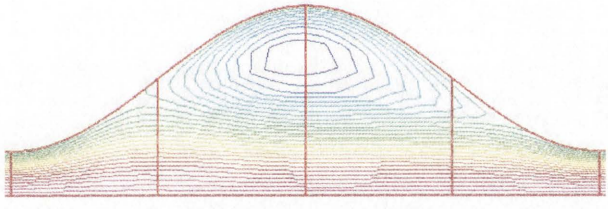
Wave number($\frac{h}{\lambda}$)=0.175, Amplitude ratio($\frac{\varepsilon}{h}$)=0.714	(h=0.0035 m)
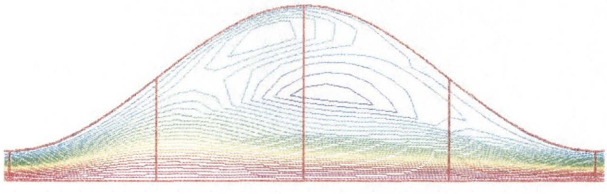	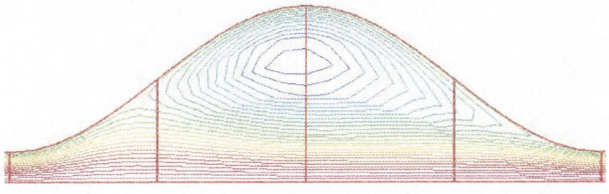

Figure 5.19 Comparison of the variation of streamline in different geometry (in the wave frame) for the case when $a_1 = 0\ ^{\circ}C^{-1}$ (left) and $a_1 = -0.034\ ^{\circ}C^{-1}$ (right) with $\bar{Q}/\pi ch^2 = 0$

In the case of an isothermal flow, the decrease in the value of h yields a change in streamline patterns. While the value of h decreases 0.0045 m to 0.004 m, two circulations are clearly developed and visualised by the effect of geometry then the circulations' location and shape stay unchanged as the value of h decreases 0.004 m to 0.0035 m.

With non-isothermal flow, the decrease in the value of h does not change streamline patterns. A circulation's location tends to settle at the crest section and the flow pattern is slightly changed but the change is considerably small.

The pressure drop and velocity profiles in different geometries for isothermal and non-isothermal flow

Figure 5.20 shows the pressure drop in isothermal flow and non-isothermal flow with different geometries.

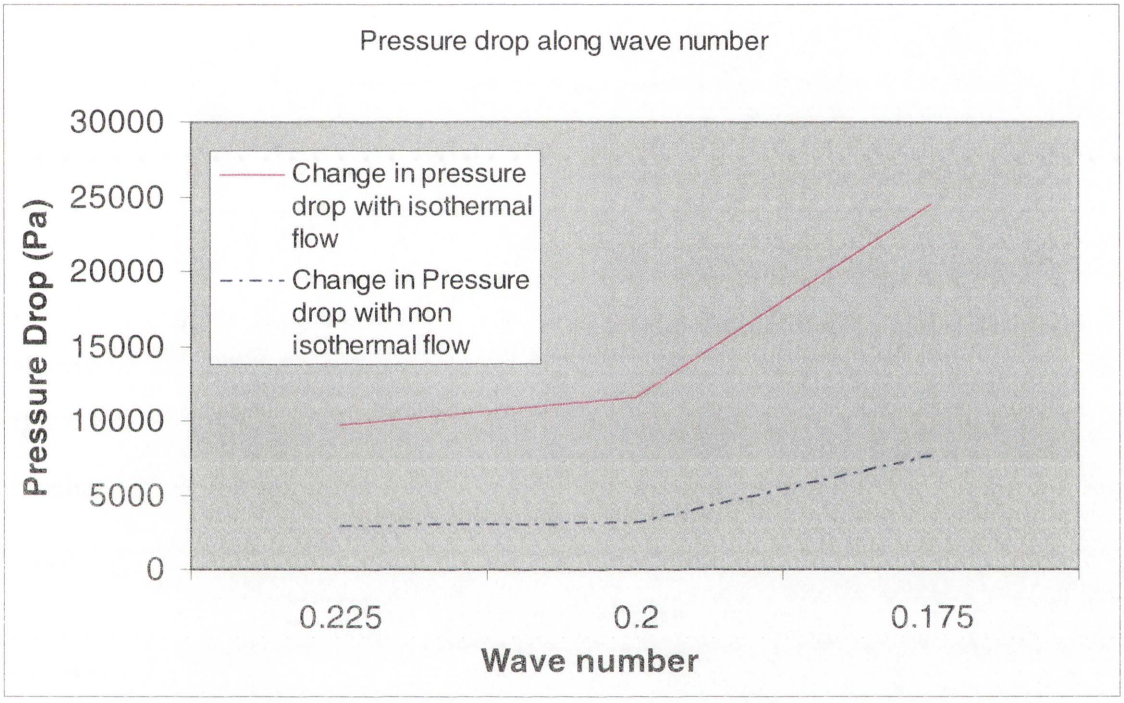

Figure 5.20 Change in pressure drop per wavelength in the three different geometries with the case of isothermal and non-isothermal flow when n=1 (Newtonian fluid)

As it can be seen in Figure 5.20, the decrease in the value of h yields the increase in the pressure drop in isothermal and non-isothermal flow. However, the values of the pressure drop in isothermal flow stay higher for all wave numbers. In non-isothermal flow, the values of the pressure drop have reduced with decreasing viscosity.

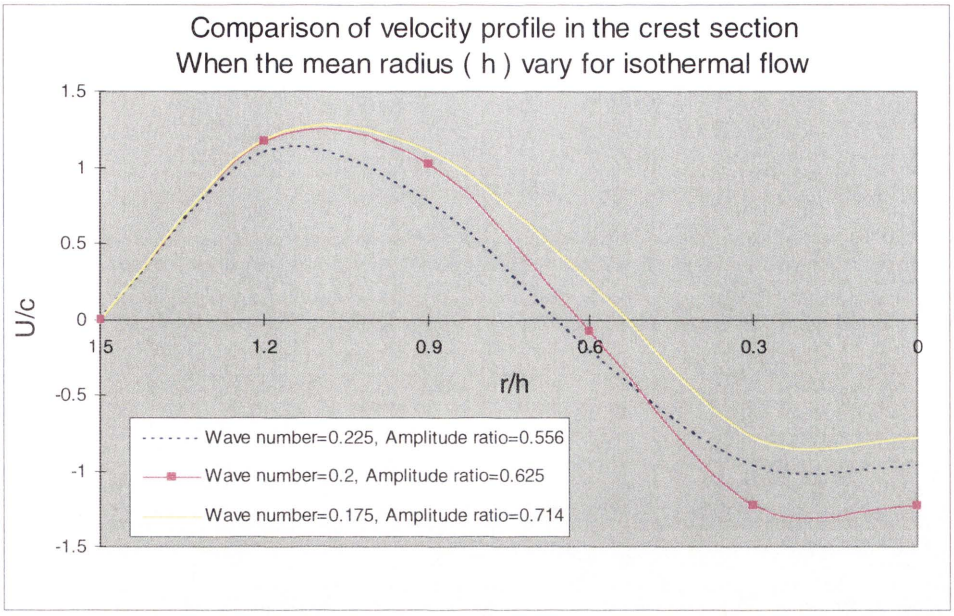

Figure 5.21 Comparison of velocity profile in the three geometries with the case of isothermal flow in the crest section (Newtonian fluid)

In Figures 5.21 and 5.22, with the effect of wave number (α) on the velocity on the axis, the velocity decreases when the wave number (α) increases from 0.175 to 0.225 at the crest section. Figure 5.23 indicates that as the wave number increases from 0.175 to 0.225, the absolute value of velocity (U/c) increases at the trough section. These results concur with the results from Takabatake et al [19].

For isothermal flow, as h varies resulting in changing wave number and amplitude ratio, the profile (U/c) at the crest section is essentially unchanged near the wall ($r/h \rangle 1.2$) in the figure 5.20.

Figure 5.22 for non-isothermal flow shows substantial variation of U/c in this section.

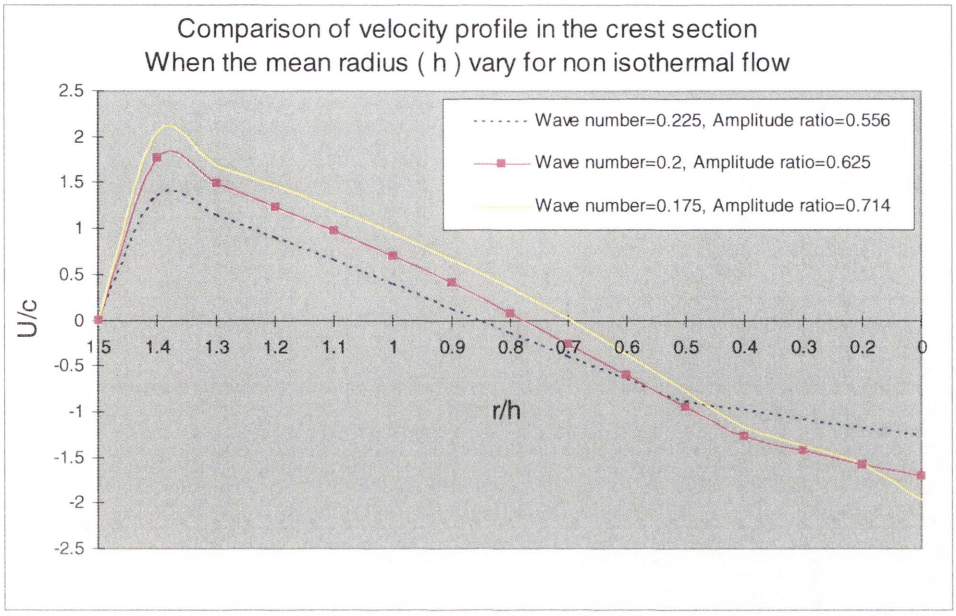

Figure 5.22 Comparison of velocity profile in the three geometries with the case of non-isothermal flow in the crest section (Newtonian flow)

Velocity profiles vary in the whole region because viscosity decreases significantly near the wall ($r/h > 1.4$).

The maximum velocity for the isothermal case is found at about $r/h = 1.1$. Whereas for the non-isothermal case, the maximum velocity occurs at about $r/h = 1.4$. It can be concluded that the boundary layer near the wall could be developed earlier ($r/h \rangle 1.4$) because viscosity decreases by the effect of temperature.

It can be explained that with decreasing viscosity, the velocity at the region adjacent to wall is influenced and velocity profiles vary by the effect of temperature.

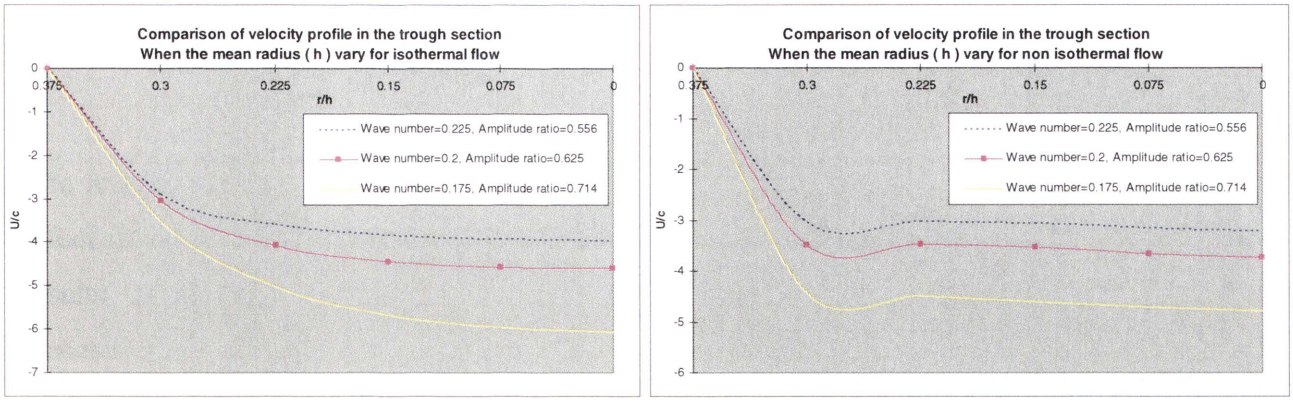

Figure 5.23 Comparison of velocity profile in the three geometries with the cases of isothermal flow (left) and non-isothermal flow (right) in the trough section (Newtonian flow)

In Figure 5.23, under the conditions of a non-isothermal flow, the maximum velocity in each model is found at the region adjacent to the wall. Velocity is virtually unchanged since the maximum velocity occurs.

On the other hand, in an isothermal flow, the velocity in each model increases constantly. Therefore, the velocity increases until the central axis (r/h=0).

5.6 Summary of non-isothermal flow

The results in Figure 5.2 indicate that a pressure drop was influenced by thermal effects. The effect of temperature on the velocity field with a Newtonian fluid was demonstrated with the results of Figures 5.3 and 5.4. It is concluded that temperature change yields decreasing viscosities under the condition of non-isothermal flow. Therefore, the pressure drop decreases.

The dimensionless time-average flow with non-isothermal flow was investigated and the results were plotted in Figure 5.5. The result shows the effects of the dimensionless time-average flow was reduced by the effect of temperature.

In this research, the effect of temperature on non Newtonian fluids is investigated. It is observed that the effect of temperature on peristaltic flow reduces the pressure drop in wavelength in the cases of shear thickening and Newtonian fluids. However, under the condition of a shear thinning fluid, the effect of temperature was not shown. In a non-Newtonian fluid, as with shear thinning and shear thickening fluids, the effect of Reynolds number is not shown in isothermal and non-isothermal flow.

The effect of a_1 on peristaltic flow was investigated. As the absolute value of a_1 increases, viscosity decreases and the result in Figures 5.11 and 5.12 showed that this effect was stronger at the region adjacent to the wall.

Vorticity patterns and pressure distributions are plotted in Figures 5.13, 5.14 and 5.15. Vorticity is powerful in the conditions that viscosities is low. Figures 5.15 and 5.16 demonstrate the existence of a relationship between viscosity and vorticity. The effect of temperature for the vorticity on peristaltic flow is powerful at the region adjacent to wall as the viscosity decreases.

Figure 5.19 showed the variation of streamline patterns produced by isothermal and non-isothermal flow models to show the effect of temperature on different geometries. The streamline patterns were produced firstly by isothermal flow to show the effect of geometry. A non-isothermal flow model produced streamline patterns to show the effect of temperature in different geometries. The results in Figure 5.19 indicated that the effect of temperature reduced the effect of geometry for streamline patterns and the pressure drop. Figures 5.20, 5.21 and 5.22

showed the effect of temperature influenced velocities at the region adjacent to the wall in different geometries.

CHAPTER 6

CONCLUSION AND RECOMMENDATION

6.1 Conclusion.

Peristaltic flow and its parameters have been studied by a number of authors for quite some time (Shapiro et al [18]). The peristaltic flow with power-law fluids has been investigated more recently, for example, by Hayat and Ali [5] in 2006. However, the peristaltic flow under non-isothermal conditions has not been investigated until present work, especially for non-Newtonian fluid of the power-law type.

This work presents axi-symmetric peristaltic flow in circular tubes with the effect of temperature in various conditions to provide a possible use in industry. Numerical results in this research are used for an investigation of the effect of temperature on peristaltic flow. Comparison with isothermal flow has been made.

The computational fluid Dynamic (CFD) software package CFD-ACE of the ESI group has been used for the numerical solution. The coupled system of non-linear governing equations to be solved are those of conservation of mass, momentum and energy. Constitutive relation appropriate for non-isothermal, power-law fluids has been used.

Incompressible fluid flow in axi-symmetric configuration has been assumed. The software package solves for the main parameters consisting of 2 velocity components (in axial and radial direction respectively), pressure and temperature, iteratively.

An isothermal flow model is produced and results are compared to previous work in the literature. In the case of isothermal flow, velocity profiles and streamline patterns on peristaltic flow are shown to agree well with previous studies (Xiao et al [23], Shapiro et al [18] and Takabatake et at [20]). It is shown in this work that non-isothermal flow can be very different to isothermal flow (Xiao et al [23]).

The comparison of the maximum and minimum axial velocity (U/c) at the Reynolds number = 0.01 is presented. The new computation model is in agreement with the results produced by Xiao et al [23] and Shapiro et al [18]. The effect of Reynolds number (Re=0.01-0.1) on the maximum U velocity (U/c) is considered to show a fairly good agreement with Xiao et al [23].

The new computational model produced in this research achieved a good agreement with the results of Xiao et al [23]. This is revealed by comparing the effect of the Reynolds number on the streamline patterns in wave frame at $\alpha = 0.01$ $\phi = 0.7$ and $\frac{\bar{Q}}{\pi c h^2}$ =0.

The dimensionless time-average flow rate ($\frac{\bar{Q}}{\pi c h^2}$) was considered in order to prove validation of the computation model produced in this study. Again, the results produced by present computational model are in good agreement with the results of Takabatake et al [20] and Xiao et al [23].

Thus, it can be concluded that the present computational results of peristaltic flow are trust-worthy and reliable.

After this confidence has been established, non-isothermal peristaltic flow is considered.

Firstly, the effect of temperature on the U velocity profiles in the case for Newtonian fluid is examined. The obtained figures show that temperature reduces viscosity, as expected. Velocity profile $\left(U/_c\right)$ in central axis at crest and trough sections is also presented to show effect of temperature on the flow field.

The effect of temperature on pressure drop per wavelength is investigated. Pressure drop is shown with respect to change in Reynolds number. As the value of Reynolds number increases, the change in pressure drop increases. It is shown that with non-isothermal flow, change in pressure drop with respect to Reynolds number becomes smaller.

In the case for isothermal flow, the forms of velocity profiles $\left(U/_c\right)$ vary with different values of Reynolds number. On the other hand, for the case of non-isothermal flow, the velocity profiles become nearly a single curve for all Reynolds-number values up to Re=100.

It is concluded that under the condition of non-isothermal flow, viscosity decreases by the action of viscous heating around wall. As a result, the decrease in viscosity causes decrease in

shear stress which yields less pressure drop. The decreasing viscosity reduced the effect of the Reynolds number.

The following results can be drawn about the effect of temperature on streamline patterns in peristaltic flow with three different conditions which are shear thinning, Newtonian, and shear thickening fluid.

1) The case for shear thinning fluid seems to be not influenced by temperature. Streamline patterns were transformed by temperature when Reynolds number =1. The effect of temperature was insignificant with Reynolds number 10 and 100. When Reynolds number increases from 1 to 10, the streamline pattern was changed in the case for isothermal flow. However, the effect of Reynolds number was negligible in the case for non-isothermal flow.

2) In this case for Newtonian fluid, the effect of temperature is stronger than in the case for shear thinning fluid. Streamline patterns were dramatically transformed by temperature with increasing Reynolds number 1-100. The effect of Reynolds number is strong for isothermal flow but the effect is reduced by temperature. The streamline patterns were changed with increase of Reynolds number in the case for isothermal flow. The case for non-isothermal flow shows a single form of the streamline pattern as Reynolds number varies.

3) The streamline patterns for shear thickening fluid are influenced by temperature but they are not significantly influenced by Reynolds number (in both isothermal and non-isothermal flow). In the range of Reynolds number 1-100, the streamline patterns are changed by temperature. However, the streamline patterns were virtually unchanged with increase of Reynolds number.

It can be revealed that under the condition of shear thinning fluid, shear stress is significantly small as a result of viscosity decreasing with shear rate. Therefore, viscosity stays low even if the condition of non-isothermal flow is employed.

With isothermal shear-thickening fluid, as the wave speed increases, higher shear rate is expected. This results in the viscosity becoming higher. However, since the Reynolds number is defined as

$\mathrm{Re} = \left(\frac{hc}{v}\right)\alpha$, where v being the kinematic viscosity and c the wave speed

the increasing values of both c and v thus tend to cancel out, resulting in the effective value of Re changing very little. This results in Re (as defined above) having little influence on the flow field. This applies to both isothermal and non-isothermal flows. On the other hand, temperature affect viscosity without the compensating effect in the Re expression. As a result, a_1 has been shown to affect the flow pattern significantly.

Therefore, the effect of Reynolds number was not shown in both isothermal and non-isothermal flow. When non-isothermal flow is employed, flow patterns were changed with decreasing viscosity. However, as Reynolds number increases, flow patterns stay unchanged in this condition of shear thickening fluid.

It was observed that a higher absolute value of coefficient a_1 has a larger influence on velocity at the region adjacent to wall. Therefore, as an absolute value of exponential coefficient a_1 of viscosity increases, viscosity decreases.

Effect of temperature on vorticity distribution has also been presented. Under the condition of non-isothermal flow, vorticity is mostly shown at the region adjacent to wall because viscosity is low by the effect of temperature in Newtonian fluid. Vorticity distribution in shear thinning fluid is also presented. In this case, vorticity patterns stayed unchanged because shear rate stays very low; in other word, temperature plays an insignificant role in flow of shear-thinning fluids considered here.

The effect of temperature on different geometry is shown by streamline patterns, pressure drop and velocity profile. With isothermal flow, as values of h decrease, the profile (U/c) at the crest section is essentially unchanged near the wall ($r/h \rangle 1.2$). On the other hand, with non-isothermal flow, velocity profiles vary in the whole region because viscosity decreases

6.2 Recommendation

The non-isothermal flow model with various conditions is considered in investigating the effect of temperature and the results fairly meet the objectives. However, there are still many ways for this study could be extended.

This study utilised the method for steady flow which is the flow travels to negative x-direction in the wave frame. Even though this method has been developed and its applications are verified by many studies since 1969, it would be quite revealing if the results are presented in the laboratory frame, and thus unsteady flow configuration, as well. This, however, is only a mathematical change of reference frames.

In this work, investigation was performed by many different conditions. A wide value of amplitude ratios and wave numbers would be recommended for the next development.

Three values of power-law index (n = 0.5, 1, 2) and two values of exponential coefficient a_1 of viscosity ($a_1 = -0.02$ and $a_1 = -0.04$ $^{\circ}C^{-1}$) are utilised in this work A higher quantity of power-law index and exponential coefficient a_1 of viscosity would be desirable.

Only one type of fluid properties is used and investigated for proving the effect of temperature on peristaltic flow. The fluid properties are very important to determine fluid behaviour. Therefore, many different fluid properties should be utilised to prove the possible use in industry.

Other ranges of values of parameter like amplitude ratio, flow rate, Reynolds number would provide a wider coverage of useful configurations. Furthermore, viscoelastic fluids and multi-phase fluids (for example, mixture of solid and liquids) would provide extension of this work to many other practical applications.

REFERENCES

[1] Bayliss,W.M. and Starling,E. H., 1899. The movements and innervation of the small intestine. *the journal of Physiology.*, vol 24, pp 99-143

[2] Brown, T.D. and Hung,T.K., 1977. Computational and experimental investigations of two-dimensional nonlinear peristaltic flow. *J. Fluid Mech.*, vol 83, pp 249-272

[3] Hayat,T., Wang,Y., Siddiqui,A.M and Hutter, K., 2003. Peristaltic motion of a Johnson-Segalman fluid in a planar channel. *Mathematical Problems in Engineering.*, no 1-2, pp1-23

[4] Hayat,T., Wang,Y., Hutter, K., Asghar,S. and Siddiaui,A.M., 2004. Peristaltic transport of an oldroyd-b fluid in a planar channel. *Mathematical Problems in Engineering.*, vol 4, pp 347-376

[5] Hayat,T. and Ali,N., 2006. On mechanism of peristaltic flows for power-law fluids. *Physica A.*, vol 371, pp 188-194

[6] Huynh,B.P., 1998. A numerical investigation of non-isothermal extrusion through annular dies. *Int J. Engng Sci.*, vol 36, no 2, pp 171-188

[7] Huynh,B.P., 2005. Numerical Study of Slider Bearings with Limited Corrugation. *Journal of Tribology.*, vol 127, no 3, pp 582-595

[8] Jaffrin, M. Y., 1973. Internal and streamline curvature effects on peristaltic pump. *Int. J. Eng. Sci.*, vol 11, pp 681-699

[9] Jaffrin,M.Y. and Shapiro,A.H., 1971. Peristaltic pumping *Annual Review of Fluid Mechanics.*, vol 3, pp 13-37

[10] Kyozo,A., Tatsuo,K. and Masaki,K., 1981. Streamlines and Path line in peristaltic flows at high Reynolds numbers. *Bulletin*, vol 24, no 192, pp 948-955

[11] Kyozo,A and Takabatake,S., 1982. Numerical Analysis of Two-Dimensional Peristaltic Flow. *Bulletin of the JSME.*, vol 25, no 205, pp 1061-1069

[12] Mishra,M. and Rao,A.R., 2003. Peristaltic transport of a Newtonian fluid in an asymmetric channel. *Z. Angew. Math. Phys.*, vol 54, no 3, pp 532-550

[13] Pozrikids., 1987. A study of peristaltic flow. *J. Fluid Mech.*, vol 180, pp 515-527

[14] Rao,A.R. and Usha,S., 1995. Peristaltic transport of two immiscible viscous fluids in a circular tube. *Math. Problems Eng.*, no 298, pp 271-285

[15] Radhakrishnamacharya,G., 1982. Long wavelength approximation to peristaltic motion of a power-law fluid. *Rheol. Acta.*, vol 21, pp 30-35

[16] Rathish, B.V. and Naidu, K.B., 1995. A Numerical study of peristaltic flows. *Comput. Fluids.*, vol 24, no 2, pp 161-176

[17] Srinivasacharya,D., Mishra,M. and Rao,A.R., 2003. Peristaltic pumping of a micropolar fluid in a tube. *Acta Mech.*, vol 161, no 3-4, pp 165-178

[18] Shapiro,A.H., Jaffrin,M.Y. and Weinberg,S.L., 1969. Peristaltic pumping with low wavelength at low Reynolds number. *J., Fluid Mech.*, vol 37, pp 799-825

[19] Takabatake,S. and Ayukawa,K., 1982. Numerical study of two-dimensional peristaltic flows. *J. Fluid Mech.*, vol 122, pp 439-465

[20] Takabatake,S. and Ayukawa,K., and Mori, A., 1988. Peristaltic pumping in circular cylindrical tubes ; a numerical study of fluid transport and its efficiency. *J. Fluid Mech.,* vol 193, pp 267-283

[21] Tong,P. and Vauter,D., 1972. An Analysis of Peristaltic pumping. *J. Appl. Mech.*, vol 39, pp 857-862

[22] Weinberg,S.L., Ckstein,E. and Shapiro,A.H., 1971. An experimental study of peristaltic pumping. *J. Fluid. Mech.,* vol 49, part 3, pp 461-479

[23] Xiao,Q. and Damodaran,M., 2002. A Numerical Investigation of Peristaltic Waves in Circular Tubes. *International Journal of Computational Fluid Dynamics.,* vol 16, Issue 3, pp 201-216

[24] Yin,F. and Fung,Y.C., 1969. Peristaltic Waves in Circular Cylindrical Tubes. *Trans. ASME J. appl. Mech.,* vol 36, pp 579-587

[25] Pock,Y.K., 2000. Navier-Stokes equation. Korea University.

http://www.peaceone.net/basic/transport/00700%20navier%20stokes.html

APPENDIX

Part 1. Conservation of mass (Continuity equation) referred from [25]

The conservation of mass is a basic principle of science and engineering. The continuity equation expresses the basic principle in a particularly convenient form for the analysis of materials processing operations.

The conservation of mass can be derived from this expression.

Rate of change of mass in ΔV =Rate of mass convected into ΔV – Rate of mass convected out of ΔV

Expressed mathematically this is

$$\Delta x\Delta y\Delta z\frac{\partial \rho}{\partial t}=\Delta y\Delta z\left[(\rho v_x)\Big|_x-(\rho v_x)\Big|_{x+\Delta x}\right]+\Delta x\Delta z\left[(\rho v_y)\Big|_y-(\rho v_y)\Big|_{y+\Delta y}\right]$$
$$+\Delta x\Delta y\left[(\rho v_z)\Big|_z-(\rho v_z)\Big|_{z+\Delta z}\right] \tag{2-1}$$

Lead to $$\frac{\partial \rho}{\partial t}=-\left[\frac{\partial}{\partial x}(\rho v_x)+\frac{\partial}{\partial y}(\rho v_y)+\frac{\partial}{\partial z}(\rho v_z)\right] \tag{2-2}$$

It will be expressed more succinctly as

$$\frac{\partial \rho}{\partial t}=-\nabla\bullet(\rho v), \tag{2-3}$$

where v is velocity vector.

Part 2. Conservation of momentum (Navier-Stokes equation)

Navier-stokes equation is derived from the equation below

$$\sum \vec{F} = \int_A \rho \vec{v}(\vec{v}.\vec{n})dA + \frac{\partial}{\partial t}\int_V \rho \vec{v}dV \tag{1-1}$$

The each side of equations above is divided by a stationary differential volume element.

$$\lim_{\Delta x\Delta y\Delta z \to 0} \frac{\sum \vec{F}}{\Delta x\Delta y\Delta z} = \frac{\int_A \rho \vec{v}(\vec{v}.\vec{n})dA}{\Delta x\Delta y\Delta z} + \frac{\frac{\partial}{\partial t}\int_V \rho \vec{v}\,dV}{\Delta x\Delta y\Delta z} \tag{1-2}$$

Total Forces, according to coordinate X,Y and Z are derived as below.

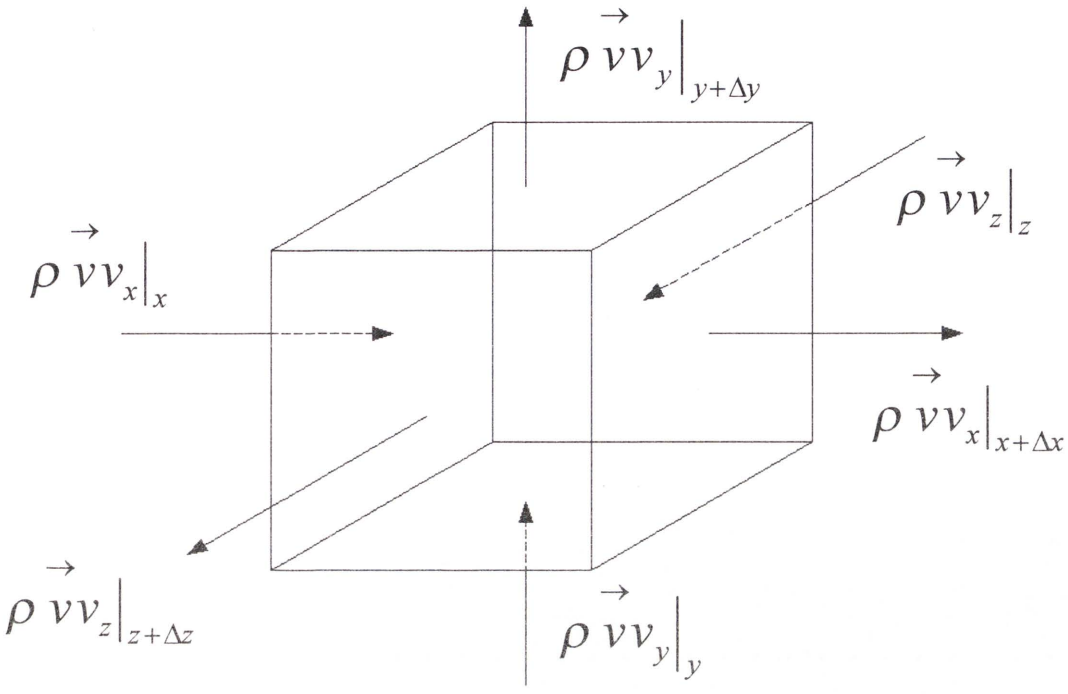

Figure 6.1 Diagram of flux in volume

$$\sum F_x = (\sigma_{xx}|-\sigma_{xx}|_{x+\Delta x})\Delta y\Delta z + (\tau_{yx}|_y - \tau_{yx}|_{y+\Delta y})\Delta x\Delta z + (\tau_{zx}|_z - \tau_{zx}|_{z+\Delta z})\Delta x\Delta y$$
$$+ (P|_x - P|_{x+\Delta x})\Delta y\Delta z + g_x\rho\Delta x\Delta y\Delta z$$

(1-3)

$$\sum F_y = (\sigma_{yy}|-\sigma_{yy}|_{y+\Delta y})\Delta x\Delta z + (\tau_{xy}|_x - \tau_{xy}|_{x+\Delta x})\Delta y\Delta z + (\tau_{zy}|_z - \tau_{zy}|_{z+\Delta z})\Delta x\Delta y$$
$$+ (P|_y - P|_{y+\Delta y})\Delta x\Delta z + g_y\rho\Delta x\Delta y\Delta z$$

(1-4)

$$\sum F_z = (\sigma_{zz}|-\sigma_{zz}|_{z+\Delta z})\Delta x\Delta y + (\tau_{xz}|_x - \tau_{xz}|_{x+\Delta x})\Delta y\Delta z + (\tau_{yz}|_y - \tau y_{yz}|_{y+\Delta y})\Delta x\Delta z$$
$$+ (P|_z - P|_{z+\Delta z})\Delta x\Delta y + g_z\rho\Delta x\Delta y\Delta z$$

(1-5)

$$\lim_{\Delta x\Delta y\Delta z\to 0}\frac{\sum F_x}{\Delta x\Delta y\Delta z}=-\frac{\partial\sigma_{xx}}{\partial x}-\frac{\partial\tau_{yx}}{\partial y}-\frac{\partial\tau_{zx}}{\partial z}-\frac{\partial P}{\partial x}+g_x\rho \tag{1-6}$$

$$\lim_{\Delta x\Delta y\Delta z\to 0}\frac{\sum F_y}{\Delta x\Delta y\Delta z}=-\frac{\partial\sigma_{yy}}{\partial y}-\frac{\partial\tau_{xy}}{\partial x}-\frac{\partial\tau_{zy}}{\partial z}-\frac{\partial P}{\partial y}+g_y\rho \tag{1-7}$$

$$\lim_{\Delta x\Delta y\Delta z\to 0}\frac{\sum F_z}{\Delta x\Delta y\Delta z}=-\frac{\partial\sigma_{zz}}{\partial z}-\frac{\partial\tau_{xz}}{\partial x}-\frac{\partial\tau_{yz}}{\partial y}-\frac{\partial P}{\partial z}+g_z\rho \tag{1-8}$$

The momentum flux is described as below

$$\lim_{\Delta x\Delta y\Delta z\to 0}\frac{\int\rho\vec{v}(\vec{v}.\vec{n})dA}{\Delta x\Delta y\Delta z}= \tag{1-9}$$

$$\lim_{\Delta x\Delta y\Delta z\to 0}\left[\frac{(\rho\vec{v}v_x\Big|_{x+\Delta x}-\rho\vec{v}v_x\Big|_x)\Delta y\Delta z}{\Delta x\Delta y\Delta z}+\frac{(\rho\vec{v}v_y\Big|_{y+\Delta y}-\rho\vec{v}v_y\Big|_y)\Delta x\Delta z}{\Delta x\Delta y\Delta z}+\frac{(\rho\vec{v}v_z\Big|_{z+\Delta z}-\rho\vec{v}v_z\Big|_z)\Delta x\Delta y}{\Delta x\Delta y\Delta z}\right] \tag{1-9}$$

$$=\left[\frac{\partial}{\partial x}(\rho\vec{v}v_x)+\frac{\partial}{\partial y}(\rho\vec{v}v_y)+\frac{\partial}{\partial z}(\rho\vec{v}v_z)\right] \tag{1-10}$$

$$= \vec{v}\left[\frac{\partial}{\partial x}(\rho v_x)+\frac{\partial}{\partial y}(\rho v_y)+\frac{\partial}{\partial z}(\rho v_z)\right]+\rho\left[v_x\frac{\partial \vec{v}}{\partial x}+v_y\frac{\partial \vec{v}}{\partial y}+v_z\frac{\partial \vec{v}}{\partial z}\right]$$

(1-11)

As a concerning the continuity equation, the equation 3 would be reduced as (4)

$$\frac{\partial P}{\partial t} = -\left[\frac{\partial}{\partial x}(\rho v_x)+\frac{\partial}{\partial y}(\rho v_y)+\frac{\partial}{\partial z}(\rho v_z)\right] \quad \text{..... Continuity equation}$$

$$= -\vec{v}\frac{\partial P}{\partial t}+\rho\left[v_x\frac{\partial \vec{v}}{\partial x}+v_y\frac{\partial \vec{v}}{\partial y}+v_z\frac{\partial \vec{v}}{\partial z}\right] \qquad (1\text{-}12)$$

$$\lim_{\Delta x\Delta y\Delta z\to 0}\frac{\int\rho\vec{v}(\vec{v}.\vec{n})dA}{\Delta x\Delta y\Delta z} = -\vec{v}\frac{\partial P}{\partial t}+\rho\left[v_x\frac{\partial \vec{v}}{\partial x}+v_y\frac{\partial \vec{v}}{\partial y}+v_z\frac{\partial \vec{v}}{\partial z}\right] \qquad (1\text{-}13)$$

$$\lim_{\Delta x\Delta y\Delta z\to 0}\frac{\frac{\partial}{\partial t}\int_V\rho\vec{v}\,dV}{\Delta x\Delta y\Delta z} = \frac{\frac{\partial}{\partial t}\rho\vec{v}\,\Delta x\Delta y\Delta z}{\Delta x\Delta y\Delta z} = \frac{\partial}{\partial t}\rho\vec{v} = \rho\frac{\partial \vec{v}}{\partial t}+\vec{v}\frac{\partial\rho}{\partial t}$$

(1-14)

$$\lim_{\Delta x\Delta y\Delta z\to 0}\frac{\sum \vec{F}}{\Delta x\Delta y\Delta z}=\begin{Bmatrix}\left(-\frac{\partial\sigma_{xx}}{\partial x}-\frac{\partial\tau_{yx}}{\partial y}-\frac{\partial\tau_{zx}}{\partial z}-\frac{\partial P}{\partial x}+g_x\rho\right)\\ \left(-\frac{\partial\sigma_{yy}}{\partial y}-\frac{\partial\tau_{xy}}{\partial x}-\frac{\partial\tau_{zy}}{\partial z}-\frac{\partial P}{\partial y}+g_y\rho\right)\\ \left(-\frac{\partial\sigma_{zz}}{\partial z}-\frac{\partial\tau_{xz}}{\partial x}-\frac{\partial\tau_{yz}}{\partial y}-\frac{\partial P}{\partial z}+g_z\rho\right)\end{Bmatrix} \quad (1\text{-}15)$$

$$\lim_{\Delta x\Delta y\Delta z\to 0}\frac{\int\rho\vec{v}(\vec{v}.\vec{n})dA}{\Delta x\Delta y\Delta z}=-\vec{v}\frac{\partial P}{\partial t}+\rho\left[v_x\frac{\partial\vec{v}}{\partial x}+v_y\frac{\partial\vec{v}}{\partial y}+v_z\frac{\partial\vec{v}}{\partial z}\right] \quad (1\text{-}16)$$

$$\lim_{\Delta x\Delta y\Delta z\to 0}\frac{\frac{\partial}{\partial t}\int_V\rho\vec{v}\,dV}{\Delta x\Delta y\Delta z}=\rho\frac{\partial\vec{v}}{\partial t}+\vec{v}\frac{\partial\rho}{\partial t} \quad (1\text{-}17)$$

$$\lim_{\Delta x\Delta y\Delta z\to 0}\frac{\sum\vec{F}}{\Delta x\Delta y\Delta z}=\lim_{\Delta x\Delta y\Delta z\to 0}\frac{\int_s\rho\vec{v}(\vec{v}.\vec{n})dA}{\Delta x\Delta y\Delta z}+\lim_{\Delta x\Delta y\Delta z\to 0}\frac{\frac{\partial}{\partial t}\int_V\rho\vec{v}\,dV}{\Delta x\Delta y\Delta z} \quad (1\text{-}18)$$

The Stokes viscosity law would apply into the Navier-Stoke equation above and the equation will be transformed as

$$\rho\frac{Dv_x}{Dt}=\rho g_x-\frac{\partial p}{\partial x}-\frac{\partial}{\partial x}\left(\frac{2}{3}\mu\nabla\vec{v}\right)+\nabla\left(\mu\frac{\partial\vec{v}}{\partial x}\right)+\nabla(\mu\nabla v_x) \quad (1\text{-}19)$$

$$\rho\frac{Dv_y}{Dt}=\rho g_y-\frac{\partial p}{\partial y}-\frac{\partial}{\partial y}(\frac{2}{3}\mu\nabla\vec{v})+\nabla(\mu\frac{\partial\vec{v}}{\partial y})+\nabla(\mu\nabla v_y) \quad (1\text{-}20)$$

$$\rho\frac{Dv_z}{Dt}=\rho g_z-\frac{\partial p}{\partial z}-\frac{\partial}{\partial z}(\frac{2}{3}\mu\nabla\vec{v})+\nabla(\mu\frac{\partial\vec{v}}{\partial z})+\nabla(\mu\nabla v_z) \quad (1\text{-}21)$$

In compressible flow, as $\nabla\vec{v}=0$, the equation (1-21) will be reduced as

$$\rho\frac{D\vec{v}}{Dt}=-\nabla p+\mu\nabla^2\vec{v}+\rho\vec{g} \quad (1\text{-}22)$$

Part 3. Conservation of energy

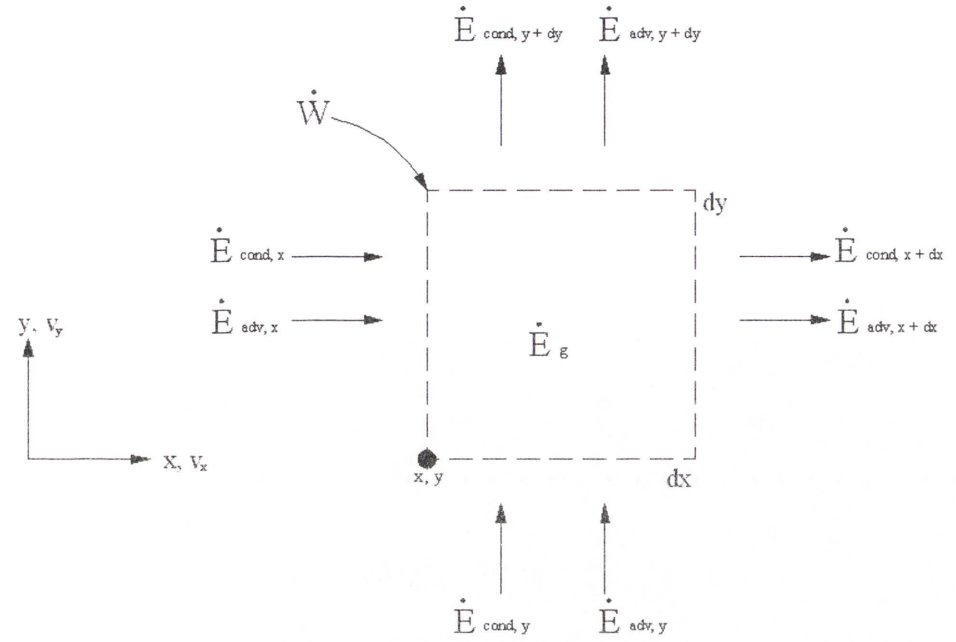

Figure 6.2 Differential control volume (dx • dy) for energy conservation in two-dimensional flow of a viscous fluid with heat transfer.

If potential energy effects are treated as work done by the body forces, the energy per unit mass of the fluid includes the thermal internal energy e and the kinetic energy, $V^2/2$, where $V^2 = v_x^{\ 2} + v_y^{\ 2}$. Accordingly, thermal and kinetic energy are advected with the bulk fluid motion across the control surfaces, and for the x-direction, the net rate at which this energy enters the control volume is

$$\dot{E}_{adv,x} - \dot{E}_{adv,x+dx} = \rho v_x\left(e + \frac{V^2}{2}\right)dy - \left\{\rho v_x\left(e + \frac{V^2}{2}\right) + \frac{\partial}{\partial x}\left[\rho v_x\left(e + \frac{V^2}{2}\right)\right]dx\right\}dy$$

$$= -\frac{\partial}{\partial x}\left[\rho v_x\left(e + \frac{V^2}{2}\right)\right]dxdy \qquad (1\text{-}23)$$

Energy is also transferred across the control surface by molecular processes. There may be two contributions: that due to conduction and energy transfer due to the diffusion of species A and B. However, it is only in chemically reacting flows that species diffusion strongly influences

thermal conditions. Hence the effect is neglected in this development. For the conduction process, the net transfer of energy into the control volume is

$$\dot{E}_{cond,x} - \dot{E}_{cond,x+dx} = -\left(k\frac{\partial T}{\partial x}\right)dy - \left[-k\frac{\partial T}{\partial x} - \frac{\partial}{\partial x}\left(k\frac{\partial T}{\partial x}\right)dx\right]dy$$

$$= \frac{\partial}{\partial x}\left(k\frac{\partial T}{\partial x}\right)dxdy \qquad (1\text{-}24)$$

Where;

X and Y : the x and y component of body force per unit volume of fluid respectively

ρ : the density of fluid

k : thermal conductivity

T : temperature

Energy may also be transferred to and from the fluid in the control volume by work interactions involving the body and surface forces. The net rate at which work is done on the fluid by forces in the x-direction may be expressed as

$$\dot{W}_{net} = (Xv_x)dxdy + \frac{\partial}{\partial x}[(\sigma_{xx} - P)v_x]dxdy + \frac{\partial}{\partial y}(\tau_{yx}v_x)dxdy \qquad (1\text{-}25)$$

The first term on the right-hand side of Equation (1-25) represents the work done by the body force, and the remaining terms account for the net work done by the pressure and viscous forces.

Using Equations (1-23) through (1-25), as well as analogous equations for the y-direction, the energy conservation requirement may be expressed as

$$-\frac{\partial}{\partial x}\left[\rho v_x\left(e + \frac{V^2}{2}\right)\right] - \frac{\partial}{\partial y}\left[\rho v_y\left(e + \frac{V^2}{2}\right)\right] + \frac{\partial}{\partial x}\left(k\frac{\partial T}{\partial x}\right) + \frac{\partial}{\partial y}\left(k\frac{\partial T}{\partial y}\right) + (Xv_x + Yv_y)$$

$$-\frac{\partial}{\partial x}(Pv_x) - \frac{\partial}{\partial y}(Pv_y) + \frac{\partial}{\partial x}(\sigma_{xx}v_x + \tau_{xy}v_y) + \frac{\partial}{\partial y}(\tau_{yx}v_x + \sigma_{yy}v_y) + \dot{q} = 0 \qquad (1\text{-}26)$$

Where $\dot{q}$ is the rate at which thermal energy is generated per unit volume. This expression provides a general form of the energy conservation requirement for flow of a viscous fluid with heat transfer.

Because Equation (1-26) represents conservation of kinetic and thermal internal energy, it is rarely used in solving heat transfer problems. Instead, a more convenient form, which is termed the thermal energy equation, is obtained by the continuity equation by u, v respectively and subtracting the results from Equation 1-26. After considerable manipulation, it follows that [2]

$$\rho v_x \frac{\partial e}{\partial x} + \rho v_y \frac{\partial e}{\partial y} = \frac{\partial}{\partial x}\left(k\frac{\partial T}{\partial x}\right) + \frac{\partial}{\partial y}\left(k\frac{\partial T}{\partial y}\right) - p\left(\frac{\partial v_x}{\partial x} + \frac{\partial v_y}{\partial y}\right) + \mu\Phi + \dot{q} \qquad (1\text{-}27)$$

where the term, $p(\partial u/\partial x + \partial v/\partial y)$, represents a reversible conversion between mechanical work and thermal energy, and $\mu\Phi$, the viscous dissipation, is defined as

$$\mu\Phi = \mu\left\{\left(\frac{\partial v_x}{\partial y} + \frac{\partial v_y}{\partial x}\right)^2 + 2\left[\left(\frac{\partial v_x}{\partial x}\right)^2 + \left(\frac{\partial v_y}{\partial y}\right)^2\right] - \frac{2}{3}\left(\frac{\partial v_x}{\partial x} + \frac{\partial v_y}{\partial y}\right)^2\right\} \qquad (1\text{-}28)$$

The first term on the right-hand side of Equation (1-28) originates from the viscous shear stresses, and the remaining terms arise from the viscous normal stresses. Collectively, the terms account for the rate at which mechanical work is irreversibly converted to thermal energy due to viscous effects in the fluid.

If the fluid is incompressible, Equations (1-27) and (1-28) may be simplified by substituting continuity equation ($\nabla \vec{v} = 0$). Moreover, with $de = C_v dT$ and $C_v = C_p$ for an incompressible fluid, the thermal energy equation may then be expressed as

$$\rho C_p\left(v_x\frac{\partial T}{\partial x} + v_y\frac{\partial T}{\partial y}\right) = \frac{\partial}{\partial x}\left(k\frac{\partial T}{\partial x}\right) + \frac{\partial}{\partial y}\left(k\frac{\partial T}{\partial y}\right) + \mu\left\{\left(\frac{\partial v_x}{\partial y} + \frac{\partial v_y}{\partial x}\right)^2 + 2\left[\left(\frac{\partial v_x}{\partial x}\right)^2 + \left(\frac{\partial v_y}{\partial y}\right)^2\right]\right\} + \dot{q}$$